A Study of Multichannel Open Circuit Potentiometry in Biosensor Applications

Wong, Lai Chun Caleb

Award date:
2018

Awarding institution:
University of Bath

A Study of Multichannel Open Circuit Potentiometry in Biosensor Applications

Lai Chun Caleb Wong

A thesis submitted for the degree of Doctor of Philosophy

University of Bath

Department of Electronic and Electrical Engineering

June 2018

Contents

CONTENTS ..... **I**

LIST OF FIGURES ..... **V**

LIST OF PUBLICATIONS ..... **XI**

ABSTRACT ..... **XIII**

LIST OF ABBREVIATIONS ..... **XV**

CHAPTER 1. INTRODUCTION **1**

1.1 INTRODUCTION TO BIOSENSORS 1

1.1.1 Sensors Principles *1*

1.2 PRINCIPLES OF ELECTROCHEMISTRY 4

1.2.1 Electrochemical Interface (Electric Double Layer) *4*

1.2.1.1 Electric double layer models 6

1.2.1.1.1 Helmholtz 7

1.2.1.1.2 Gouy-Chapman 8

1.2.1.1.3 Gouy-Chapman-Stern 9

1.3 SELF-ASSEMBLED MONOLAYERS 11

1.4 LABEL-FREE DETECTION TECHNIQUES 13

1.4.1 Open Circuit Potential Measurement *15*

1.4.2 Electrochemical Impedance Spectroscopy *18*

1.4.3 Differential Pulse Voltammetry *19*

1.4.4 Localised Surface Plasmon Resonance *20*

1.5 GENERAL OVERVIEW OF THE THESIS 21

1.5.1 Outline of the Thesis *23*

REFERENCES 26

CHAPTER 2. OCP MEASUREMENT SYSTEM **31**

2.1 INTRODUCTION 31

2.1.1 Instrumentation Amplifier *32*

2.1.1.1 Fundamentals of an Instrumentation Amplifier 32

2.1.1.2 Instrumentation Amplifier – Texas Instruments INA116 34

2.1.1.3 Bill of Materials of INA116 Electronic Circuit 36

2.2 OCP MEASUREMENT SYSTEM DESIGN – ELECTRONICS 38

2.2.1 A Simultaneous Multichannel Design for Parallel Biosensing *39*

2.2.2 Specification of the electronic circuit *42*

2.3 OCP MEASUREMENT SYSTEM DESIGN – SOFTWARE 43

2.3.1 Data Acquisition – Client End *43*

2.3.1.1 Serial Peripheral Interface 44
2.3.1.2 Universal Serial Bus 47
2.3.2 Data Acquisition – Server End 48
2.4 SUMMARY 50
REFERENCES 51

CHAPTER 3. CHARACTERISATION OF THE OCP MEASUREMENT SYSTEM WITH THE DETECTION OF PROSTATE CANCER BIOMARKERS AS A CASE STUDY 53

3.1 BACKGROUND 54
3.2 EXPERIMENTAL PREPARATION AND CHARACTERISATION METHOD 55
3.2.1 Electrochemical Characterisation 55
3.2.2 Fabrication of PSA Aptasensor 57
3.2.3 Binding Studies 57
3.3 RESULTS AND DISCUSSION 58
3.3.1 Real-Time OCP Measurements 58
3.3.1.1 Stability of the System 58
3.3.1.2 Multichannel Approach 59
3.3.2 Analytical and Selectivity Performance 61
3.3.2.1 Dose-Response and Linear Dose-Response 61
3.3.2.2 Clinical level performance 63
3.4 SUMMARY 64
REFERENCES 66

CHAPTER 4. OCP DETECTION OF DNA – DNA INTERACTION WITH INTERCALATOR 69

4.1 INTRODUCTION 69
4.1.1 Intercalator - the Cobalt Complex $[Co(GA)_2(aqphen)]Cl$ 71
4.1.1.1 Synthesis and General Analysis of $[Co(GA)_2(aqphen)]Cl$ 73
4.2 DNA – DNA SYSTEM WITH INTERCALATOR 74
4.2.1 Experimental Preparation and Characterisation Methods 75
4.2.1.1 Materials 75
4.2.1.1.1 Oligonucleotides 75
4.2.1.2 Electrochemical Measurements 75
4.2.1.2.1 Open Circuit Potentiometry 75
4.2.1.2.2 Electrochemical Impedance Spectroscopy 76
4.2.1.3 Preparation of the DNA Self-Assembled Monolayer 77
4.2.1.4 DNA Hybridisation and $[Co(GA)_2(aqphen)]Cl$ Incubation 77
4.2.1.4.1 Open Circuit Potentiometry 77
4.2.1.4.2 Electrochemical Impedance Spectroscopy 78
4.2.2 Discussion on DNA Hybridisation with Cobalt Complex 78
4.2.2.1 Impedimetric Responses of the System with Electrochemical Impedance Spectroscopy 79

4.2.2.1.1 Impedimetric Response of DNA Hybridisation....79
4.2.2.1.2 Impedimetric Response of Cobalt Complex Attachment....80
4.2.2.1.3 Impedimetric Response of Intercalator on Bare Gold Surface....81
4.2.2.1.4 Fit and Simulation....83
4.2.2.2 Potentiometric Responses of the System with Open Circuit Potentiometry....85
4.2.2.2.1 Potentiometric Response of DNA Hybridisation....85
4.2.2.2.2 Potentiometric Response of Cobalt Complex Attachment....86
4.3 Summary....87
References....88

CHAPTER 5. OCP DETECTION OF PNA – DNA INTERACTION WITH GOLD NANOPARTICLES....91

5.1 Introduction....92
5.1.1 Gold Nanoparticles....94
5.2 PNA – DNA System with Gold Nanoparticles....95
5.2.1 Experimental Preparation and Characterisation Methods....96
5.2.1.1 Materials....96
5.2.1.1.1 Oligonucleotides....96
5.2.1.2 Preparation of 20 nm Positively Charged Gold Nanoparticles....96
5.2.1.3 Electrochemical Measurements....97
5.2.1.4 Preparation of the PNA Self-Assembled Monolayer....98
5.2.1.5 DNA Hybridisation and Gold Nanoparticles Incubation....99
5.2.1.5.1 Open Circuit Potentiometry....99
5.2.1.5.2 Electrochemical Impedance Spectroscopy....99
5.2.2 Discussion on PNA/DNA Hybridisation with Positively Charged Gold Nanoparticles... 99
5.2.2.1 Potentiometric responses of the system with Open Circuit Potentiometry....99
5.2.2.1.1 Potentiometric Response of PNA/DNA Hybridisation....99
5.2.2.1.2 Potentiometric Response of Positively Charged Gold Nanoparticle....102
5.2.2.2 Validation of the System with Impedimetric Response of the System....103
5.2.3 Discussion on DNA – DNA and PNA – DNA System....106
5.3 Summary....107
References....109

CHAPTER 6. OCP DETECTION OF PROTEIN PHOSPHORYLATION AND MULTIMODAL ELECTROCHEMICAL AND NANOPLASMONIC SENSING APPROACHES....111

6.1 Introduction....112
6.1.1 Protein Phosphorylation....114
6.1.2 Gold Nanoparticles and Ferrocene....115
6.2 Protein Phosphorylation System....116
6.2.1 Experimental Preparation and Characterisation Methods....117
6.2.1.1 Materials....117
6.2.1.2 Electrochemical Measurements....118

6.2.1.2.1 Open Circuit Potentiometry..... 118
6.2.1.2.2 Electrochemical Impedance Spectroscopy and Differential Pulse Voltammetry..... 118
6.2.1.2.3 Localised Surface Plasmon Resonance 119
6.2.1.3 Preparation of the MUA/MCH Self-Assembled Monolayer 119
6.2.1.4 Protein Phosphorylation with Attachment of Gold Nanoparticle and Ferrocene..... 120
6.2.2 Discussion on Protein Phosphorylation with Multimodal Sensing Approaches.....121
6.2.2.1 Potentiometric Responses of the System with Open Circuit Potentiometry 121
6.2.2.1.1 Potentiometric Response of Protein Phosphorylation 121
6.2.2.1.2 Potentiometric response of Gold Nanoparticles and Ferrocene Attachment 122
6.2.2.2 Validation of the System with Multimodal Biosensing Techniques..... 124
6.2.2.3 Plasmonic Response of the System with Localised Surface Plasmon Resonance 125
6.2.2.4 Impedimetric Response of the System with Electrochemical Impedance Spectroscopy 126
6.2.2.5 Amperometric Response of the system with Differential Pulse Voltammetry..... 127
6.3 Discussion on Multimodal Biosensing 127
6.4 Summary 128
References 130

CHAPTER 7. CONCLUSIONS.....133

7.1 Future Work 137
7.1.1 Cancer Biomarkers and Aptasensor 137
7.1.2 miRNA.....137
7.1.3 Semiconductor Design of the OCP Electronic System 138

APPENDIX.....141

List of Figures

FIGURE 1-1 SCHEMATIC LAYOUT OF A BIOSENSOR 2
FIGURE 1-2 ILLUSTRATION OF THE ELECTRIC DOUBLE LAYER. IHP IS INNER HELMHOLTZ PLANE; OHP IS OUTER HELMHOLTZ PLANE. 4
FIGURE 1-3. AN ELECTRONIC SCHEME EQUIVALENT TO THE ELECTROCHEMICAL CELL. C_D IS DIFFERENTIAL CAPACITY OF THE ELECTRIC DOUBLE LAYER; R_F IS RESISTANCE TO FARADAIC CURRENT AT THE ELECTRODE SURFACE. 5
FIGURE 1-4 SCHEMATICS OF THE ELECTRIC DOUBLE LAYER STRUCTURE SHOWING CHARGE DISTRIBUTION MODEL. (A) HELMHOLTZ MODEL. (ADAPTED FROM WANG AND PILON (2011)) 7
FIGURE 1-5 SCHEMATICS OF THE ELECTRIC DOUBLE LAYER STRUCTURE SHOWING COMPARISON OF DIFFERENT CHARGE DISTRIBUTION MODELS. (A) HELMHOLTZ MODEL, (B) GOUY-CHAPMAN MODEL. (ADAPTED FROM WANG AND PILON (2011)) 8
FIGURE 1-6 SCHEMATICS OF THE ELECTRIC DOUBLE LAYER STRUCTURE SHOWING COMPARISON OF DIFFERENT CHARGE DISTRIBUTION MODELS. (A) HELMHOLTZ MODEL, (B) GOUY-CHAPMAN MODEL, AND (C) GOUY-CHAPMAN-STERN MODEL. (ADAPTED FROM WANG AND PILON (2011)) 9
FIGURE 1-7 A TYPICAL OCP SIGNAL WITH BINDING AND SUBSEQUENT RINISING. INTERACTION OF STM^{Cys+}–PEP2 WITH RCDK2 PROBED BY OCP MEASUREMENTS. (ADAPTED FROM ESTRELA ET AL. (2008)) 16
FIGURE 1-8 SCHEMATIC OF THE BASIC DESIGN OF A SINGLE CHANNEL OCP MEASUREMENT SYSTEM. WE IS WORKING ELECTRODE; RE IS REFERENCE ELECTRODE; PT WIRE IS PLATINUM WIRE FOR GROUNDING. 17
FIGURE 1-9 RANDLES EQUIVALENT CIRCUIT. C_{DL} IS DOUBLE LAYER CAPACITANCE, R_{CT} IS CHARGE TRANSFER RESISTANCE, Z_W IS WARBURG EIMPEDANCE ELEMENT, AND R_U IS SOLUTION UNCOMPENSATED RESISTANCE. 18
FIGURE 1-10 DPV EXCITATION (LEFT) AND RESPONSE WAVEFORM (RIGHT). 19
FIGURE 1-11 MULTICHANNEL CHIP TO ILLUSTRATE MULTICHANNEL BASED OCP DETECTION SYSTEM. 22
FIGURE 2-1 BASIC SCHEMATIC OF AN INSTRUMENTATION AMPLIFIER. 33
FIGURE 2-2 BASIC CONNECTIONS OF THE INA116 INSTRUMENTATION AMPLIFIER. (ADAPTED FROM BURR-BROWN (1995)) 36
FIGURE 2-3 SCHEMATIC OF THE BASIC DESIGN OF A SINGLE CHANNEL OCP MEASUREMENT SYSTEM. WE IS THE WORKING ELECTRODE; RE IS THE REFERENCE ELECTRODE; THE PT WIRE IS GROUNDING THE SOLUTION. 38
FIGURE 2-4 SCHEMATIC OF THE MULTIPLEXED OCP DETECTION CIRCUIT CONSTRUCTED WITH FOUR INA116 INSTRUMENTATION AMPLIFIERS AND ONE MAX11040K ADC. 40
FIGURE 2-5 SIMPLIFIED SCHEMATIC OF THE MULTIPLEXED OCP DETECTION CIRCUIT CONSTRUCTED WITH CASCADED ADCS TO PROVIDE 32 CHANNELS. 41
FIGURE 2-6 ARDUINO SOFTWARE DESIGN ARCHITECTURE FOR THE TRANSMISSION OF OCP DIGITAL DATA. 43
FIGURE 2-7 SPI BUSSES TOPOLOGY WITH SPI MASTER CONNECTED TO A SINGLE SLAVE (POINT-TO-POINT TOPOLOGY). . 44
FIGURE 2-8 SPI PROTOCOL IS USED FOR THE COMMUNICATION BETWEEN ADC AND MICROCONTROLLER. 45
FIGURE 2-9 SPI BUSSES TOPOLOGY WITH SPI MASTER CONNECTED TO MULTIPLE SLAVES. 45
FIGURE 2-10 DAISY-CHAINING MULTIPLE MAX11040K (ADAPTED FROM MAXIM INTEGRATED PRODUCTS (2015)) . 46
FIGURE 2-11 USB PROTOCOL IS USED FOR THE COMMUNICATION BETWEEN MICROCONTROLLER AND PC. 47

FIGURE 2-12 FLOW DIAGRAM OF THE OCP MEASUREMENT SYSTEM SERVER END SOFTWARE. 49
FIGURE 3-1 (A) AN ILLUSTRATION OF THE WHOLE OCP SYSTEM SETUP, INCLUDING THE FABRICATED PSA APTASENSOR LOADED IN A FLOW CELL. (B) A PHOTO OF THE FLOW CELL AND CIRCUIT BOARD. 56
FIGURE 3-2 (LEFT) AN OPTIMISED INITIALISATION OCP SIGNAL OF THE CHANGE IN OCP *VS* TIME, WITH AN INJECTION OF BUFFER (BLANK SOLUTION). SHOWING THE OPTIMISED STABILITY AND NOISE. (RIGHT) AN UNOPTIMISED INITIALISATION OCP SIGNAL. SHOWING AN UNSUITABLE INITIALISATION SIGNAL TO START OCP DETECTION. 59
FIGURE 3-3 A TYPICAL OCP BEHAVIOUR OF THE APTASENSOR WITH THE RESPONSE OF CONSECUTIVE INJECTIONS OF DIFFERENT CONCENTRATIONS OF PSA (BLACK ARROWS) AND RINSING BUFFER (BLUE ARROWS) ON FOUR SEPARATE ELECTRODES OF THE ARRAY. THE NUMBERS NEXT TO THE BLACK ARROWS INDICATE THE PSA CONCENTRATIONS INJECTED. THE INSET SHOWS THE INITIALISATION OF THE OCP MEASUREMENT WITH AN INJECTION OF BUFFER (BLANK SOLUTION). 60
FIGURE 3-4 DOSE-RESPONSE CURVE OF THE APTASENSOR. THE POINTS REPRESENT THE AVERAGE FOR FOUR CHANNELS. THE LINE REPRESENTS A LINEAR FIT TO THE POINTS BETWEEN 1 AND 10 NG/ML (AS SHOWN IN THE INSET USING A LINEAR SCALE). ERROR BARS REPRESENTS THE MINIMUM AND MAXIMUM CHANGES OF OCP WHEN THE CORRESPONDING CONCENTRATION OF PSA IS INJECTED. 62
FIGURE 3-5 A COMPARISON OF RESPONSE WITH BLANK, HK2 (100 NG/ML), HSA (66,000 NG/ML) AND PSA (100 NG/ML) FABRICATED SENSORS. 63
FIGURE 4-1 STRUCTURE OF THE COBALT COMPLEX [CO(GA)2(AQPHEN)]CL WITH SYNTHETIC ROUTE. (I) ETOH, HEAT; (II) ETOH, 1 EQ. COCL2•6H2O, 2 EQ. GLYCOLIC ACID/NAOH(AQ). (ADAPTED FROM REGAN ET AL. (2014)) 72
FIGURE 4-2 TOP 3 DOCKED POSES FOR CO(GA)2(AQPHEN) INTERACTING WITH THE DNA SEQUENCE OPEN-D(ATCGAGACGTCTCGAT)$_2$. TOP 3 DOCKED POSES FOR CO(GA)2(AQPHEN) INTERACTING WITH THE DNA SEQUENCE OPEN-D(ATCGAGACGTCTCGAT)$_2$. (ADAPTED FROM REGAN ET AL. (2014)) 73
FIGURE 4-3 SCHEMATIC OF DNA – DNA SYSTEM WITH INTERCALATOR. (A) IMMOBILISED DNA PROBE. (B) HYBRIDISATION WITH COMPLEMENTARY STRAND DNA. (C) ATTACHMENT OF INTERCALATOR TO DNA/DNA DUPLEX. 74
FIGURE 4-4 R_{CT} OF SSDNA AND DSDNA (EIS). 79
FIGURE 4-5 HYBRIDISED DNA CHANGE IN R_{CT} WITH INTERCALATOR (EIS). 81
FIGURE 4-6 SMALL INTERACTION OF INTERCALATOR WITH BARE GOLD SURFACE (EIS). 82
FIGURE 4-7 THE EFFECT OF [CO(GA)$_2$(AQPHEN)]CL ON CHARGE TRANSFER RESISTANCE (R_{CT}). DATA ARE SHOWN FOR (1) MCH, (2) SSDNA + MCH AND (3) DSDNA + MCH. ERROR BARS REPRESENT STANDARD DEVIATIONS OF MEAN VALUES DETERMINED FROM THREE INDIVIDUAL EXPERIMENTS (N = 3). 83
FIGURE 4-8 DNA AND INTERCALATOR BINDING ACTIVITY (OCP). GREEN ARROW REPRESENTS THE INJECTION OF COMPLEMENTARY STRANDED DNA. BLUE ARROW REPRESENTS THE INJECTION OF CO-AQPHEN INTERCALATOR. ..86
FIGURE 5-1 SCHEMATIC OF A PEI-CAPPED AUNP. 94
FIGURE 5-2 SCHEMATIC OF PNA – DNA SYSTEM WITH 20 NM POSITIVELY CHARGED AUNPS. (A) IMMOBILISED PNA PROBE. (B) HYBRIDISATION WITH TARGET OLIGONUCLEOTIDES (PNA). (C) ELECTROSTATIC ATTACHMENT OF 20 NM POSITIVELY CHARGED AUNPS TO PNA/DNA DUPLEX. 95
FIGURE 5-3 PNA/DNA HYBRIDISATION WITH 20 NM AUNPS ATTACHMENT (OCP). 100

Figure 5-4 Dose response (OCP). Blue bars represent binding with target oligonucleotides, yellow bars represent AuNPs amplification, red bar represent blank upon AuNPs amplification. Error bars represents the minimum and maximum changes of OCP detected. 101
Figure 5-5 Nyquist plot represents the charge transfer resistance of the PNA – DNA system (EIS). Black curve shows PNA probes on the surface, red curve shows only a slight change when positively charged AuNPs are added to PNA probes, blue curve shows PNA/DNA duplex, pink curve shows the attachment of AuNPs to PNA/DNA duplex for signal enhancement. 104
Figure 5-6 Cole-Cole plot represents the capacitance of the PNA – DNA system (EIS). Black curve shows PNA probe on the surface, red curve shows a slight decrease after PNA/DNA hybridisation, blue curve shows attachment of AuNPs for enhancement. (Adapted from Jolly *et al.* (2015)) 105
Figure 6-1 Schematic of a phosphorylated protein. 114
Figure 6-2 Schematic of Fc. (Adapted from Sigma-Aldrich http://www.sigmaaldrich.com/). 115
Figure 6-3 Schematic of protein phosphorylation system with AuNP and Fc. (i) Protein immobilisation. (ii) Thio-phosphorylation. (iii) Attachment of AuNP to phosphorylated protein. And finally, (iv) attachment of Fc to AuNP. 117
Figure 6-4 Protein phosphorylation with attachment of AuNPs and Fc (OCP). Injection of (i) ATP-S, PKC-a, and PKC lipid activator with PKC-a kinase inhibitor in one sample, (ii) AuNP, (iii) Fc. 121
Figure 6-5 Responses from injection of each step (OCP). (i) Red bar represents thio-phosphorylation, (ii) green bar represents thio-phosphorylation with inhibitor, (iii) and (iv) blue bar and light blue bar represent attachment of AuNP to (i) and (ii) respectively, and finally, (v) and (vi) purple bar and yellow bar represent attachment of Fc to (iii) and (iv) respectively. Error bars represents the minimum and maximum changes of OCP detected. 123
Figure 6-6 Multimodal detection of protein phosphorylation. (A) OCP. (B) Cole-Cole plot by EIS. (C) DPV. (D) LSPR. (Adapted from Formisano et al. (2015)). 124
Figure 6-7 Diagram representation of the system elements and sensors of the multimodal sensing system. The flow of the multimodal biosensing approaches is included. 125

立志今擺上 傳揚耶穌

用我的恩賜 獻上最好

讓我謙卑作祢僕人

存著敬畏去事奉神

全是祢恩典覆蓋 每步亮明燈

在祢恩手裡 滿布雲彩

效法基督愛 眼界變改

願鴿子天際降下來

陶造我裡面能盛載

神豐足的厚愛

I can do all things through Christ which strengtheneth me. Philippians 4:13

List of Publications

- **Wong, L.C.C.,** Jolly, P. & Estrela, P. 2017. Development of a sensitive multiplexed open circuit potential system for the detection of prostate cancer biomarkers. *BioNanoScience,* 8(2), 701-706. https://researchportal.bath.ac.uk/en/publications/development-of-a-sensitive-multiplexed-open-circuit-potential-sys https://doi.org/10.1007/s12668-017-0408-0

- [1] Formisano, N., [1] Bhalla, N., [1] **Wong, L.C.C.,** Di Lorenzo, M., Pula, G. & Estrela, P. 2015. Multimodal electrochemical and nanoplasmonic biosensors using ferrocene-crowned nanoparticles for kinase drug discovery applications. *Electrochemistry Communications,* 57, 70-73. **([1] These authors contributed equally to the manuscript.)** https://researchportal.bath.ac.uk/en/publications/multimodal-electrochemical-and-nanoplasmonic-biosensors-using-fer https://dx.doi.org/10.1016/j.elecom.2015.05.014

- Jolly, P., **Wong, L.C.C.,** Miodek, A., Lindsay, M.A. & Estrela, P. 2015. A simple and highly sensitive electrochemical platform for detection of micrornas. *Proceedings of 2015 IEEE Sensors,* 803-806. https://researchportal.bath.ac.uk/en/publications/a-simple-and-highly-sensitive-electrochemical-platform-for-detect https://dx.doi.org/10.1109/ICSENS.2015.7370378

- Regan, E.M., Hallett, A.J., **Wong, L.C.C.,** Saeed, I.Q., Langdon-Jones, E.E., Buurma, N.J., Pope, S.J.A. & Estrela, P. 2014. A novel cobalt complex for enhancing amperometric and impedimetric DNA detection. *Electrochimica Acta,* 128, 10-15. https://researchportal.bath.ac.uk/en/publications/a-novel-cobalt-complex-for-enhancing-amperometric-and-impedimetri https://dx.doi.org/10.1016/j.electacta.2013.10.028

Abstract

The specificity of biosensors is achieved by the use of biological probes with affinity to the targets to be detected. The electrochemical transducer converts the biological recognition process into an electrical signal. The resulting electrical signal is the response of the recognition from the biolayer. Potentiometric, amperometric and voltammetric detection are the fundamental electrochemical measurement techniques. In this thesis, direct open circuit potentiometry (OCP) is studied with several types of electrochemical systems. The biological interaction between the probes and the targets are characterised by measuring the variations of the true open circuit potential (OCP) that occurs at the surface of the working electrode when the charge density and the distribution of the immobilised biolayer change upon interactions with the target biomolecules. OCP is a detection technique which measures the recognition electrical signal in real time.

With the true OCP measurement system developed in-house, a number of electrochemical systems were studied by looking at the interaction with different biomolecules, to show that a true OCP measurement system could be achieved for biosensor development. The electrochemical systems that have been investigated include DNA – DNA detection with a novel cobalt complex for signal enhancement, PNA – DNA detection with gold nanoparticles for signal enhancement, and protein phosphorylation (for drug discovery applications) with gold nanoparticles for signal enhancement. A comparison with promising biosensing techniques such as electrochemical impedance spectroscopy (EIS) and other techniques is performed to demonstrate the benefits of OCP as a biosensing technique. An easily expandable multichannel OCP biosensor array instrumentation system was developed. The whole instrumentation is built and assembled with a custom designed electronic system, a microfluidic system and its applicability demonstrated for a range of electrochemical systems. Through an investigation of the instrumentation amplifier circuit and the multiplexing technique, and the analysis of experimental data, an optimisation for the OCP measurement system is achieved.

This thesis tackles a gap in the literature in terms of studies of OCP as a biosensing technique, providing a number of case studies that can contribute towards the development of potential new low-cost biosensors.

List of abbreviations

ATP	Adenosine Triphosphate
ATP-S	Adenosine Thiotriphosphate
AuNPs	Gold nanoparticles
CC	Chronocoulometry
CPE	Constant phase element
CV	Cyclic voltammetry
DNA	Deoxyribonucleic acid
DPV	Differential pulse voltammetry
ds-	Double-stranded
EDC	Ethyl-dimethylaminopropyl carbodiimide
EDL	Electrochemical double layer
EDTA	Ethylenediaminetetraacetic acid
EIS	Electrochemical impedance spectroscopy
ELISA	Enzyme-linked immunosorbent assay
Fc	6-(ferrocenyl)hexanethiol
GA	Glycolic acid
HSA	Human serum albumin
IHP	Inner Helmholtz plane
LOD	Limit of detection
LOQ	Limit of quantitation
LSPR	Localised surface plasmon resonance
MCH	6-mercapto-1-hexanol
miRNA	MicroRNA
MOPS	3-(N-morpholino)propanesulfonic buffer
NHS	N-hydroxysuccinimide
OCP	Open circuit potentiometry / Open circuit potential
OHP	Outer Helmholtz plane
PB	Phosphate buffer
PBS	Phosphate buffer saline
PCa	Prostate cancer
PCB	Printed circuit board
PEG	Polyethylene-glycol
phen	1,10-phenanthroline
PNA	Peptide nucleic acid
PSA	Prostate specific antigen

RNA	Ribonucleic acid
SAM	Self assembled monolayer
SPI	Serial peripheral interface
ss-	Single-stranded
UART	Universal asynchronous receiver-transmitter
USB	Universal serial bus

CHAPTER 1.

Introduction

This chapter presents the theory behind the development of a multichannel open circuit potential (OCP) detection platform for biosensing applications. In order to design and develop such a platform, it is necessary to understand the fundamentals of the biosensing techniques and electrochemical systems mentioned in this thesis. This chapter is therefore, a presentation on the fundamentals of biosensors and the OCP detection technique. Biosensing detection system approaches including electrochemical principles and the detection techniques used (potentiometric, impedimetric, amperometric) are described as well as the electronics fundamentals of OCP biosensing detection, plasmonic biosensing system and other systems. The principles of different electrochemistry systems that are used under OCP detection are also introduced. In general, these include deoxyribonucleic acid based (DNA-based) / peptide nucleic acids based (PNA-based) systems, and protein-based systems.

1.1 Introduction to Biosensors

1.1.1 Sensors Principles

According to the Oxford English Dictionary, a sensor is *"a device which detects or measures physical properties or changes and provides a corresponding output or measurement in response."* (OED, 2017).

Sensors are used to detect or measure a parameter, to indicate or otherwise respond to it. The term "sensors" is used to describe a whole device, which contains a transducer

and a detection element. Sensors could be divided into three main types, namely physical sensors which measure distance and mass for example; chemical sensors which measure chemical substances by a chemical reaction/response; and biosensors which measure chemical substances by using a biological detection element. Sensors are linked with a transducer to provide a visibly observable response. Transducer converts one form of energy into another form, including electrical, electromagnetic, light, thermal, chemical, acoustic, etc.

A chemical sensor is defined as a device that **"***responds to a particular analyte in a selective way through a chemical reaction and can be used for the qualitative or quantitative determination of the analyte.***"** (Eggins, 2002)

Biosensors are a sub-set of chemical sensors. This type of sensor can detect and measure chemical or even inorganic substances, while their target analytes are mainly biological components. Such a sensor is concerned with detecting and measuring a specific chemical substance or set of chemicals. A chemical sensor is divided into two main parts as shown in Figure 1-1 below, namely the front part, which is a region for selective chemistry to take place; and the back part, which is the transducer.

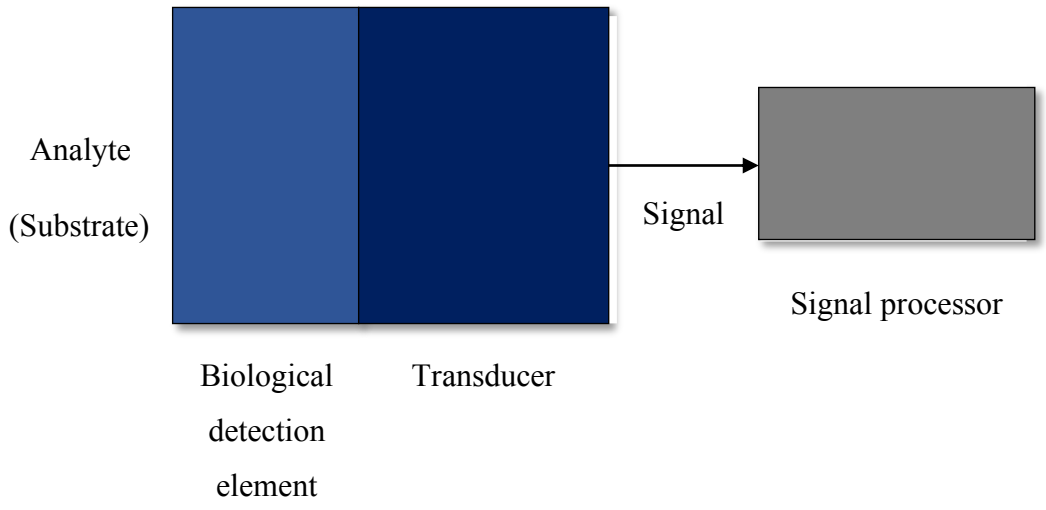

Figure 1-1 Schematic layout of a biosensor

- **Recognition Elements**

The recognition elements are the key component of all sensors. They impart the selectivity that enables the sensor to avoid interferences from other substrates and to respond selectively only to the particular analyte.

- **Transducers**

Transducers are devices that convert a physical or chemical change in the recognition element into a measurable signal. In chemical sensors, electronic signals are usually used to define the concentration measured of a particular chemical.

Transducers can be subdivided into different categories (Eggins, 2002), some of them includes:

- Electrochemical Transducers
- Optical Transducers
- Piezo-Electric Devices
- Thermal Sensors

This thesis will mainly focus on electrochemical biosensors which could be divided into three basic systems based on the electrochemical:

- Voltammetry (amperometry) - measurement of the cell current when an oxidizing or reducing potential of a redox species is applied between the cell electrodes.
- Conductometry - measurement by using an alternating current bridge method of the conductance (reciprocal of resistance) of the cell.
- Impedimetry – measurement of the resistive and capacitive properties based on the perturbation of the system at equilibrium by a small potential sinusoidal as an excitation signal.
- Potentiometry - continuous measurement of a cell OCP during a biological interaction occurring at the electrode surface.

1.2 Principles of Electrochemistry

1.2.1 Electrochemical Interface (Electric Double Layer)

Electrochemical reactions happen on the interfacial region between the working electrode surface and the electrolyte solution (bulk/buffer solution), and this interfacial region is called electric double layer (Hunter and White, 1987; Lyklema and Leeuwen, 1991). For instance, in case of metal working electrodes, as the sensing region is located on and near the working electrode metal surface, the sensitivity and the control of affinity elements can be improved whilst minimizing the amount of bulk solution and reagent volume. Electric connections from an electronic system are connected to the electrodes for detecting bio-recognition signals directly from the surface, which is the electrochemical interface. A typical electric double layer region is illustrated in Figure 1-2.

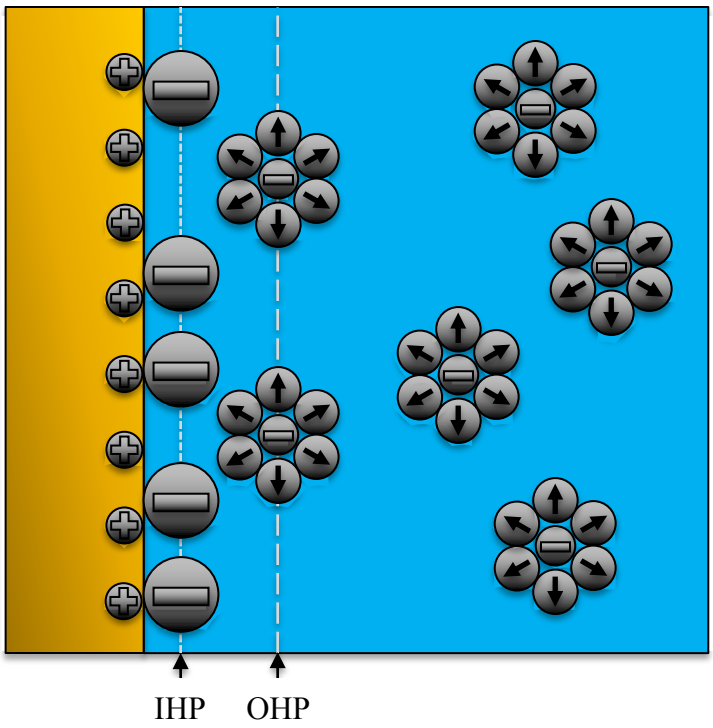

Figure 1-2 Illustration of the electric double layer. IHP is inner Helmholtz plane; OHP is outer Helmholtz plane.

In an electronic circuit that is used to measure the current flowing through the working electrode when immersed in an electrolyte solution, the electric double layer on the working electrode surface can be viewed as a capacitor connection illustrated in Figure 1-3. The electrochemical cell can then be represented as two parallel connected components in an electronic circuit, C_d corresponds to the differential capacity of the electric double layer, and R_f corresponds to the resistance to Faradaic current at the electrode surface.

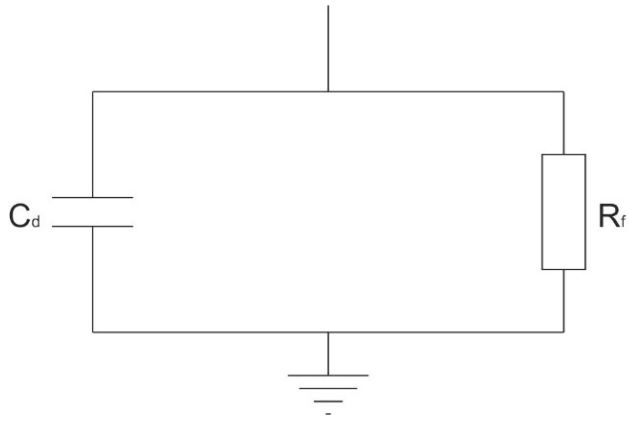

Figure 1-3. An electronic scheme equivalent to the electrochemical cell. C_d is differential capacity of the electric double layer; R_f is resistance to Faradaic current at the electrode surface.

Although the electrochemical cell is understandable in a simplified circuit; no general model, however, can fully express all the experimental situations. This is because the structure and the capacity of the electric double layer are dependent on more than one parameter, including the type of electrode material (metals, carbons, semiconductors, electrode porosity, the presence of layers of either oxides or polymeric films or other solid materials at the surface), type of solvent, type of supporting electrolyte, the extent of specific adsorption, and the temperature throughout the experiment (Scholz and Bond, 2002).

On the other hand, the composition of the electric double layer also influences the electron transfer rate. In general, either heterogeneous electrocatalysis (Vayenas and Bebelis, 1999; Wieckowski, 1999), some ions or molecules are specifically adsorbed on the electrode surface causing an enhancement of electrons transfer; or inhibitors, in which there is the adsorption of additional compounds, decreasing the electron transfer rate on the electrode, or even a total passivation of the electrode surface to the electrolyte by some surface-active compounds that are strongly adsorbed. In this thesis (Chapter 4-6), examples of both enhancement and passivation by using different compounds will be presented.

Applying a potential from an external source (such as a potentiostat) to the electrode, results in a generation of charge on the metal surface of the electrode, σ_M, and in the solution, σ_S. Since the charge at the electrode is related to the electric double layer capacitance or capacity, the differential capacitance can be described by Eq. (1):

$$C_d = \frac{\partial \sigma_M}{\partial E} \tag{1}$$

The integral capacitance can be described by Eq. (2):

$$C_i = \frac{\sigma_M}{E - E_{\sigma=0}} \tag{2}$$

where C_d is differential capacitance, C_i is integral capacitance, σ_M is charge on surface and E is electric surface potential.

1.2.1.1 Electric double layer models

Through the evolution of electrochemistry starting from the 19th century, theories and methods have been developed for the correlation between the electrical properties and

chemical effects at the electrochemical interface (Bard and Faulkner, 1980; Southampton Electrochemistry Group., 1985; Wang, 2006). To understand the electric double layer and determine the spatial charges distribution on the electrochemical interface, a few different theories could be used, including the model of Helmholtz, Gouy-Chapman, Gouy-Chapman-Stern (GCS), and Grahame. Schematics of the electric double layer structure for these models are shown below accordingly, illustrated in Figure 1-4, Figure 1-5, and Figure 1-6.

1.2.1.1.1 Helmholtz

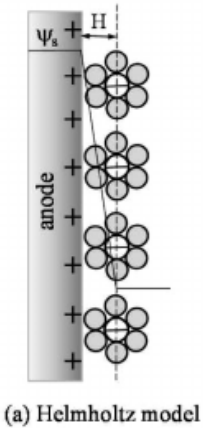

Figure 1-4 Schematics of the electric double layer structure showing charge distribution model. (a) Helmholtz model. (Adapted from Wang and Pilon (2011))

The concept of the existence of electric double layer can be traced back to 1879, when Helmholtz (Helmholtz, 1853) first theoretical model assumed the presence of a compact layer of counter-ions that are attracted to the electrode surface when the charged electrode is immersed in an electrolytic solution. Counterions of the charge, on the other hand are repelled, thus forming two layers of opposite polarity at the interfacial region between the electrode and electrolyte. He showed that the electric double layer is a molecular dielectric and stores charge electrostatically within, with the stored charge linearly dependent on the voltage that has been applied. In this early

model, a constant differential capacitance is predicted to be independent from the charge density and the thickness of the double-layer (Bagotsky, 2006; Bard and Faulkner, 2001; Butt and Kappl, 2010; Masliyah *et al.*, 2006; Signorelli *et al.*, 2009; Srinivasan, 2006), with the charge density is depending on the electrolyte dielectric constant.

This early model however does not consider some important factors, including the diffusion of ions in solution, the possibility of adsorption onto the electrode metal surface, and the interaction of opposite charges between the electrolyte solvent and the electrode.

1.2.1.1.2 Gouy-Chapman

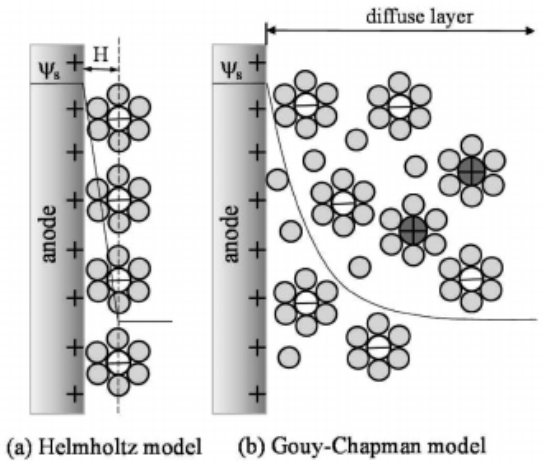

Figure 1-5 Schematics of the electric double layer structure showing comparison of different charge distribution models. (a) Helmholtz model, (b) Gouy-Chapman model. (Adapted from Wang and Pilon (2011))

Louis Georges Gouy (Gouy, 1910) and David Leonard Chapman (Chapman, 1913) suggested that the capacitance is dependent on the applied potential and ionic concentration of the electrolyte, rather than just a constant. This Gouy-Chapman model significantly improved on the Helmholtz model, by introducing the diffuse model of the electric double layer. The diffuse model described that the electric double

layer is not as compact as the previous rigid design, whereby the charge distribution of ions is determined by electrostatics and statistical mechanics (Bagotsky, 2006; Bard and Faulkner, 1980; Masliyah *et al.*, 2006). This is made on the assumption of understanding them as point charges, having high mobility ions, dielectric continuum solvent, and a perfect conductor. Under these criteria, it allows Maxwell–Boltzmann statistics to be applied to describe the charge distribution, thus showing that the electric potential decreases exponentially when away from the metal surface.

However, the model also has an unphysical behaviour suggested by the nonlinear Poisson-Boltzmann equation. The variation of the capacitance with electrode potential is predicted correctly when the electrode potential is at the minimum capacity, but an unlimited rise of capacity was predicted for large electrode potentials. This is because the ions were assumed wrongly to be point charges with infinite size that are able to approach the electrode surface arbitrarily close, which leads to the capacity to rises without limit. This, however, is not possible as ions are stopped from approaching the surface at a distance that corresponds to their radii.

1.2.1.1.3 Gouy-Chapman-Stern

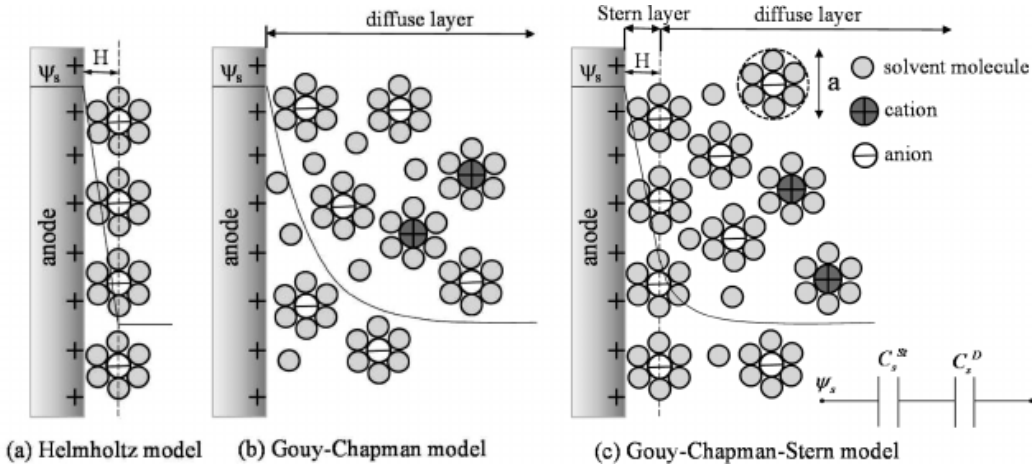

Figure 1-6 Schematics of the electric double layer structure showing comparison of different charge distribution models. (a) Helmholtz model, (b) Gouy-Chapman model, and (c) Gouy-Chapman-Stern model. (Adapted from Wang and Pilon (2011))

The Gouy-Chapman-Stern (GCS) model refined the Gouy-Chapman model, by accounting for finite size of ions and combining the Helmholtz and Gouy-Chapman models as two layers (Stern, 1924). A schematic of the GCS model is shown in Figure 1-6. The two layers, namely, the Stern layer, referring to the first compact layer of immobile ions that is strongly adsorbed onto the electrode surface, while assuming no free charge is within (Bagotsky, 2006; Bard and Faulkner, 1980; Hunter and White, 1987; Masliyah *et al.*, 2006), and the diffuse layer, referring to the mobile ions on the second layer and the Gouy-Chapman model applies (Bard and Faulkner, 1980, 2001; Butt and Kappl, 2010; Hunter and White, 1987; Lyklema and Leeuwen, 1991; Masliyah *et al.*, 2006; Ohshima, 2006). The total capacitance of the electric double layer is the series connected capacitances of the Stern layer and diffusion layer, which for symmetric electrolytes can be described as Eq. (3a) and (3a):

$$\nabla \cdot (\epsilon_0 \epsilon_r \nabla \psi) = \begin{cases} 0 & \text{in the Stern layer} \quad (3a) \\ 2\mathrm{zeN_A} c_\infty \sinh\left(\frac{ze\psi}{k_B T}\right) & \text{in the diffuse layer} \quad (3a) \end{cases}$$

where $\mathrm{N_A}$ is the Avogadro's number ($\mathrm{N_A} = 6.022 \times 10^{23}$ mol^{-1}), ϵ_0 is the free space permittivity of the electrolyte solutions, ϵ_r is the relative permittivity of the electrolyte solutions, ψ is the local electric potential in the diffuse layer determined by the Poisson-Boltzmann (PB) equation, T is the absolute temperature, k_B is the Boltzmann constant ($k_B = 1.381 \times 10^{-23}$ m^2 kg K^{-1} s^{-2}). For binary symmetric electrolytes, $z_1 = -z_2 = z$ when solution containing only a $z - z$ type of electrolyte and $c_{\infty 1} = c_{\infty 2} = c_\infty$.

A change in the charge density of a biolayer immobilised on an electrode induces a change in the electrode surface charge density, which thus alters the surface potential of the electrode. The surface potential φ_0, which is the OCP, can then be described and calculated by the so-called Grahame equation, Eq. (4):

$$\varphi_0 = \frac{\sigma_0 x_{\mathrm{H}}}{\varepsilon_{\mathrm{x}}\varepsilon_0} + \frac{2k_B T}{ze}\,\sinh^{-1}\frac{\sigma_0 + \sigma_1}{(8\varepsilon\varepsilon_0 k_B T n_0)^{1/2}} \qquad (4)$$

Where σ_0 is the electrode surface charge density, σ_1 is the charge density of a biolayer immobilised on an electrode, k_B is the Boltzmann constant, T the absolute temperature, e the elementary charge, ε the relative dielectric constant of water, ε_{x} the relative dielectric constant of the biolayer–compact layer system, ε_0 the permittivity of free space, n_0 the buffer ionic strength per unit volume, z the absolute value of the electrolyte ionic charge when solution containing only a $z - z$ type of electrolyte and x_{H} is the distance of the outer Helmholtz plane with respect to the electrode.

With the improvements in the GCS model, a better understanding of the electric double layer and predictions for experiment can be made, but the model is still limited by a number of simplifications. The model still contains the assumption of all ions having the same size, the use of symmetric electrolytes, the constant permittivity, the ion adsorption rate and the ion-surface interaction that is neglected. As the complexity increases significantly when taking away the assumption made above, future studies are completed by using Poisson-Boltzmann equation through the use of simulation software (Li, 2008).

1.3 Self-Assembled Monolayers

A surface-modified electrode is needed for the detection of biomolecular targets. Probes with required affinity are immobilised to fabricate the modified surface. To immobilise the sensor metal surface, which provides a surface for self-assembled monolayers to form on, can be achieved by two main types of methods, physical and chemical modification, resulting in different qualities and properties. A uniform, well-structured and reproducible self-assembled monolayer (SAM) is needed to achieve a systematic approach for electrochemical analysis (Bain *et al.*, 1989a; Bain *et al.*, 1989b; Bain and Whitesides, 1989; Finklea, 1996; Love *et al.*, 2005; Vericat *et al.*, 2014).

Gold (Au) is a material with some interesting properties; the chemical stability, surface chemistry, biocompatibility, unique optical properties and a convenient range of processing technologies. With its oxide-free, clean and relatively flat gold surfaces that can be easily used as a modified surface at ambient room temperature, this has led the use of thiolated SAMs on gold in a lot of biological systems. With gold as the electrode surface, this is one of the most highly reported techniques because it results in a highly controlled density of biological probe (Hong *et al.*, 1999). In some of the cases, such as oligonucleotide-based probes, the key aspect to take into account for the immobilisation process is to obtain an optimum density on the gold surface (Keighley *et al.*, 2008). The advantage of gold in multiple kinds of biological devices, such as electronics and optical systems, have been demonstrated, in addition, multi-modal biosensing approaches (Formisano *et al.*, 2015) can be benefited.

Reaction of sulphur in the proximity of gold is described in Eq. (5):

$$RSH + Au \leftrightarrow RS - Au + H^{+} + e^{-} \quad (5)$$

The process to form a SAM can be achieved in only a few seconds to minutes when immersed in mM concentration immobilisation solution. While a dense coverage with the adsorbates can be achieved in a quick timing, the reorganisation process can take up to hours before forming a maximal density and low defects SAM. An immediate reaction between sulphur-gold can achieve a 80-90% coverage within minutes, but to form a well organised layer, no less than 12-16 hours is needed (Schreiber, 2000).

The formation of a well organised SAM depends not only on immobilisation incubation time, surface roughness and surface purity, but also an important factor is the length of the alkane thiols (Darling *et al.*, 2002; Finklea, 1996) used. In a study Love *et al.* (2005) shows that the maximum density of alkane thiol on gold surface is 4.64×10^{14} molecules/cm^2 with a gap of 4.99 Å between two adjacent molecules.

To assemble a well organised SAM, the time dependent formation process is important, this includes a two-stage process where a spontaneous assembling process

occurs in the first few minutes. In the first stage, alkane thiols lie flat on the gold electrode surface through physisorption. A process in which the electronic structure of the molecules are barely perturbed upon adsorption, also known as the 'lying down' phase (Camillone *et al.*, 1994). Following with a process that a semi-crystalline structure is formed due to van der Waals forces, with lateral movements until a tilted angle of 30˚ is achieved between the hydrocarbon chains and electrode surface (Love *et al.*, 2005). Worth mentioning that the movements of the thiols on the electrode surface enables the ability of surface redistribution, resulting a formation of well-organised layer with defects healing ability (Ulman, 1996).

The provision of having various functional terminal group with SAM enables researchers to engineer novel biosensors designs. SAMs have been used to immobilise various molecules from DNA (Regan *et al.*, 2014), PNA (Jolly *et al.*, 2015), protein (Formisano *et al.*, 2015), DNA aptamers (Wong *et al.*, 2017), etc. The tailoring of SAM layers has led to the development of mixed SAMs, which in fact opened up an unlimited possibility for biosensor fabrication. In a study Keighley *et al.* (2008) discussed the effect on hybridisation efficiency of DNA probe density using co-immobilised binary SAM on gold electrodes surface. And carefully selection of the spacer molecules can control the surface properties, such as hydrophobicity or hydrophilicity, and chemical reactivity. This inclusion of spacer molecules could therefore minimise the unwanted non-specific binding that occurs on the surface, and hence, improve the overall detected electrochemical signals (Herne and Tarlov, 1997). Through different SAM configurations, an improvement of sensitivity of the biosensors is demonstrated.

1.4 Label-Free Detection Techniques

Label-free technologies provide enormous opportunities for probing biomolecular interactions without spatial-interference, steric hindrance, auto-fluorescent and quenching effects of labels. Freeing from a preparatory step for labelling (dyes, tags, or specialised reagents), increasing the throughput screening targets at a single time, and consequently, lowering the overall cost. Conventional label-based technologies,

Table 1-1 Examples based on label-free detection technologies.

Reference	Sensing Technique	Sensing Type	Target
Estrela et al., 2004	Capacitance-Voltage (*C-V*) by MOS diode / Current-Voltage by (*I-V*) MOSFET	Electrical	DNA
Grow et al., 2003	Surface-enhanced Raman scattering (SERS) microscopy	Optical	Toxin
Kukol et al., 2008	Electrochemical impedance spectroscopy (EIS)	Electrical	DNA
Nagel et al., 2002	Passive THz resonating technology (electromagnetic waves)	Electromagnetic	DNA
Sorgenfrei et al., 2011	Single-molecule fluorescence resonance energy transfer (smFRET)	Electrical	DNA
ollmer and Arnold, 2008	Whispering-gallery-mode biosensing	Optical	Single-molecule
Wang et al., 2005	Conductance by silicon nanowire (SiNW) FET	Electrical	Protein

however, are usually labour intensive, time consuming and cumbersome, resulting with a higher cost when comparing to label-free technologies. Hence, an increasing amount of studies (Table 1-1) based on label-free detection technologies have been made with different detection methods (Estrela *et al.*, 2004; Grow *et al.*, 2003; Kukol *et al.*, 2008; Nagel *et al.*, 2002; Sorgenfrei *et al.*, 2011; Vollmer and Arnold, 2008; Wang *et al.*, 2005). Label-free technologies have gained a high interest in the past decade for the development of biosensors that could achieve high throughput screening capabilities. The global label-free detection market is currently valued at USD 1.22 Billion in 2015, and expected to reach USD 2.13 Billion by 2020, at a

compound annual growth rate of 11.86% from 2015 to 2020 (marketsandmarkets.com, 2016).

Different techniques can be used for label-free detection, for instance open circuit potential (OCP), electrochemical impedance spectroscopy (EIS), differential pulse voltammetry (DPV), localised surface plasmon resonance (LSPR), etc. This section will further describe these label-free detection techniques.

1.4.1 Open Circuit Potential Measurement

Open circuit potential (OCP) measurement is the main electrochemical detection technique that is discussed in this thesis. OCP is a potentiometric detection technique that is the direct measurement of variation of charge on the biolayer by differential voltage measurements, and dielectric impurities can cause variation through affecting the capacitance of the biolayer. This change in charge and capacitance as a function of time is recorded as voltage. The variation of charge and capacitance during binding/attachment of molecules can be monitored by OCP in real time. Estrela *et al.* (2008) first demonstrated that electrical detection of protein interactions can be achieved by the direct measurement of true OCP variations through an instrumentation amplifier. A typical OCP measurement of this example is shown in Figure 1-7. Shifts in the OCP of -11, -8 and -21 mV were observed upon the interaction of lysates with different peptide aptamers, while -12 and -19 mV shifts were also observed upon interaction with different lysates. Other works have used OCP for the detection of different molecules or pH changes, however, the electronic designs for OCP measurement are different (Krysa *et al.*, 2015; Wang *et al.*, 2011).

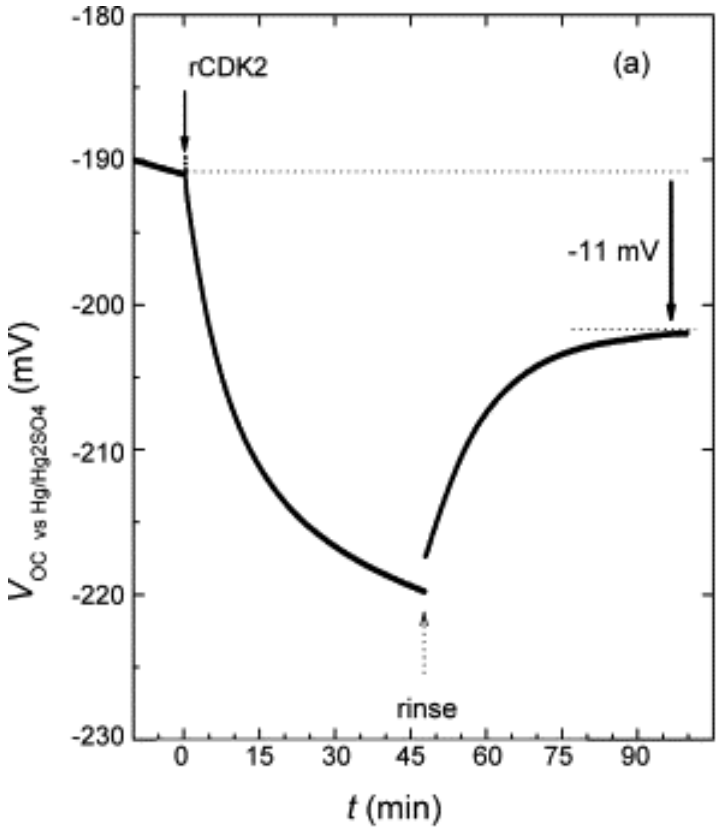

Figure 1-7 A typical OCP signal with binding and subsequent rinising. Interaction of STM^{Cys+}–pep2 with rCDK2 probed by OCP measurements. (Adapted from Estrela et al. (2008))

A true OCP presented in this thesis is the measure of potential difference by an ultra-low input bias current instrumentation amplifier, in order to detect the charge and capacitance variation on the biolayer. Through a standard potentiostat, a small current is applied during the measurement of OCP, and this may be the cause for a disruption to the biolayer. The main difference of this detection method compared to the approach that a normal potentiostat uses, is that the amplifier does not apply any current into the electrochemical system for OCP measurement, thus preventing any affection or disruption to the biolayer. As an example, unwanted current that is caused by potentiostats in a measurement can affect protein conformation, and hence binding affinity. Therefore, the OCP measured through standard potentiostats are not measuring the true OCP due to the electronic architecture of the system, but instead providing a good estimation of what the true OCP value would be. A deeper discussion

about the use of instrumentation amplifier and its circuit architecture is presented in Chapter 2. Although for most biological systems the measurements with standard potentiostats provide a good approximation, a true OCP measurement is more desirable.

A difference in the circuitry when comparing to traditional potentiostat is shown through the simplified schematic below in Figure 1-8. Although the biosensor system still comprises of a working electrode to carry out biological interactions, and a reference electrode to set the differential measurement reference potential, the counter electrode however is replaced with a platinum wire for grounding the cell, which is used to protect the system from current flowing through. A counter electrode is no longer needed for establishing a closed circuit for passing current as in a three-electrode cell that is used to perform electroanalytical chemistry, since the potential difference is measured directly through the two input channels of an instrumentation amplifier.

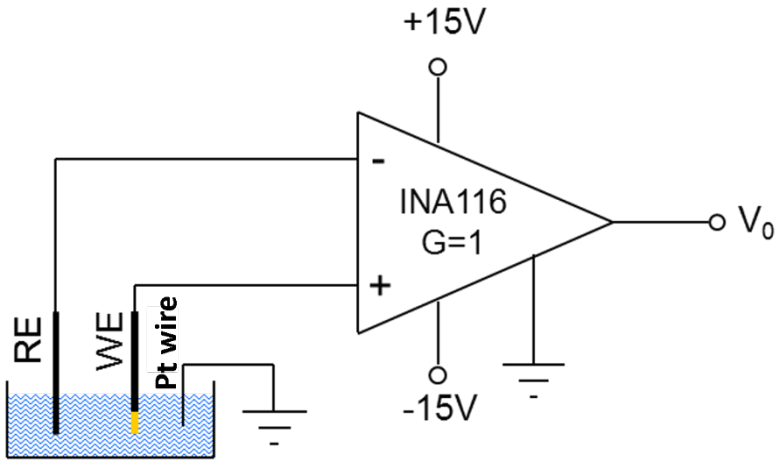

Figure 1-8 Schematic of the basic design of a single channel OCP measurement system. WE is working electrode; RE is reference electrode; Pt wire is platinum wire for grounding.

1.4.2 Electrochemical Impedance Spectroscopy

Electrochemical impedance spectroscopy (EIS) is an impedimetric detection technique that is based on the perturbation of a system at equilibrium by applying a small amplitude sinusoidal excitation over-potential as the signal, and measuring the current response with phase information, which can be used for the analysis of both the resistive and capacitive properties of the biolayer (Berggren *et al.*, 2001; Katz and Willner, 2003; Li, 2008). A variety of biomolecules have been used as detection elements for recognition events through EIS with different degrees of success. This includes enzymes, antibodies, nucleic acids, cells and microorganisms (Formisano *et al.*, 2015; Katz and Willner, 2003; Regan *et al.*, 2014; Rodriguez *et al.*, 2005; Yang *et al.*, 2015) that are immobilised on metal surfaces to develop new biosensors. As the technique is mature, it is used as a confirmation technique in the study.

When a reaction happens within the cell, mass transport of the redox species will take place due to the maintenance of equilibrium conditions, which diffusion, migration and convection can proceed in the solution phase. However, convection and migration both are neglected during practice. This is because the electrochemical measurement is measured under a still environment, which the biolayer is immersed in an excess of supporting electrolyte. Diffusion under Fick's second law that is derived from Fick's first law and the mass conservation in absence of any chemical reactions can be described as: diffusion electrochemical interface can be described in term of the electrochemical properties. To describe the biolayer in the most simplified way, a Randles equivalent circuit can be used, as in Figure 1-9.

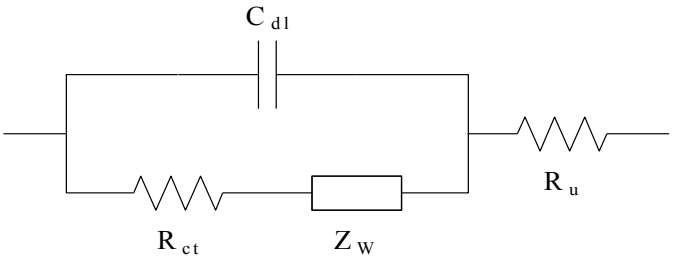

Figure 1-9 Randles equivalent circuit. C_{dl} is double layer capacitance, R_{ct} is charge transfer resistance, Z_W is Warburg eimpedance element, and R_u is solution uncompensated resistance.

1.4.3 Differential Pulse Voltammetry

Another commonly used electrochemical technique is differential pulse voltammetry (DPV), a hybrid form of linear sweep and pulsed voltammetry (Bard and Faulkner, 1980; Kawagoe *et al.*, 1993). Alterations in the concentration of a biomolecule can be detected by measuring the cell current as a function of time and as a function of the potential between the indicator and reference electrode. The potential is varied using pulses in increasing amplitude steps and the current is sampled both before and after each voltage step. This excitation and response waveform is illustrated in Figure 1-10.

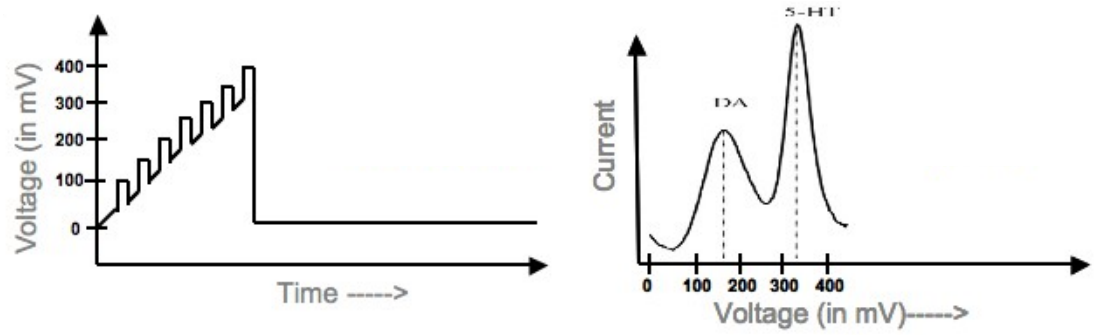

Figure 1-10 DPV excitation (left) and response waveform (right).

DPV is a hybrid type of voltammetry detection method of linear sweep and pulsed voltammetries. It has found excellent usage for selectivity; however, it is time consuming when compared to other voltammetry detection methods.

According to Faraday's law, the charge is directly proportional to the total amount of biomolecules that undergoes a loss, which is oxidation, or gain, which is reduction, of electrons, and can be described by Eq. (6):

$$Q = n\,F\,e \tag{6}$$

where Q is the total charge generated (coulombs), n is the number of moles of a specific biomolecule that undergoes oxidation or reduction, F is Faraday constant (96,485.332 89(59) C mol^{-1}) and e is the number of electrons per biomolecule lost or gained.

And the current is the change in charge as a function of time, and can be described by Eq. (7):

$$I = \frac{dQ}{dt} \tag{7}$$

Thus, showing information about changes in the concentration of the specific biomolecule of interest through the current response with respect to time.

1.4.4 Localised Surface Plasmon Resonance

Apart from all the electrochemical detection techniques mentioned above, localised surface plasmon resonance (LSPR), the only non-electrochemical detection system that is used in the thesis, a kind of plasmonic biosensors that is used during the study on a protein based biosensor that have been developed into a multimodal electrochemical and nanoplasmonic biosensor (Formisano *et al.*, 2015).

LSPR is the collective of the electron charge oscillations as light shinned on metallic nanoparticles with a specific dielectric constant. In order to show the presence of plasmons, the plasmonic material (Anker *et al.*, 2008) has to satisfy mainly two criteria: large negative real dielectric constant and small imaginary dielectric constant refractive index. The concept of plasmonic biosensor is based on the detection of the interaction of surface plasmon wave produced at the interface of the plasmonic material, and as an isotropic media, which the permittivity, ε, and permeability, μ, of the medium are uniform in all directions.

Bhalla *et al.* (2015) demonstrated the use of LSPR and electrolyte insulator semiconductor (EIS)-based proton detection to screen inhibitors of kinases. The work was then followed with the use of field effect transistors (FETs) devices as complementary biosensors to demonstrate the ability to confirm phosphorylation of proteins (Formisano *et al.*, 2015). Furthermore, in the same report, OCP was demonstrated as a complementary biosensing technique to LSPR. The use of OCP to monitor in real time and confirm phosphorylation of proteins, with a second confirmation by LSPR, was first demonstrated by the work reported in this thesis.

1.5 General Overview of the Thesis

This thesis is a presentation on the development of a simple yet sensitive electrochemical detection platform based on OCP measurements for biosensing applications. It is hypothesised that OCP detection technique can be used as a sensitive electrochemical detection technique in a simultaneous multichannel biosensing approach for varies biomolecule sensing applications. By exploiting the charge of biomolecules that are on the biolayer, the dielectric properties at the surface of the biolayer, and the biological interactions between the probes and targets can be characterised by OCP.

The thesis could be broadly divided into three major parts where the first part describes the design and implementation of the OCP system with the instrumentation amplifier for true OCP sensing, following with electronics and data acquisition interfacing, and finally a series of investigation of applications for molecular diagnostics. The thesis will transition from the development of a single channel setup to a multichannel setup, as in Figure 1-11, demonstrating simultaneous parallel sensing for diagnostics.

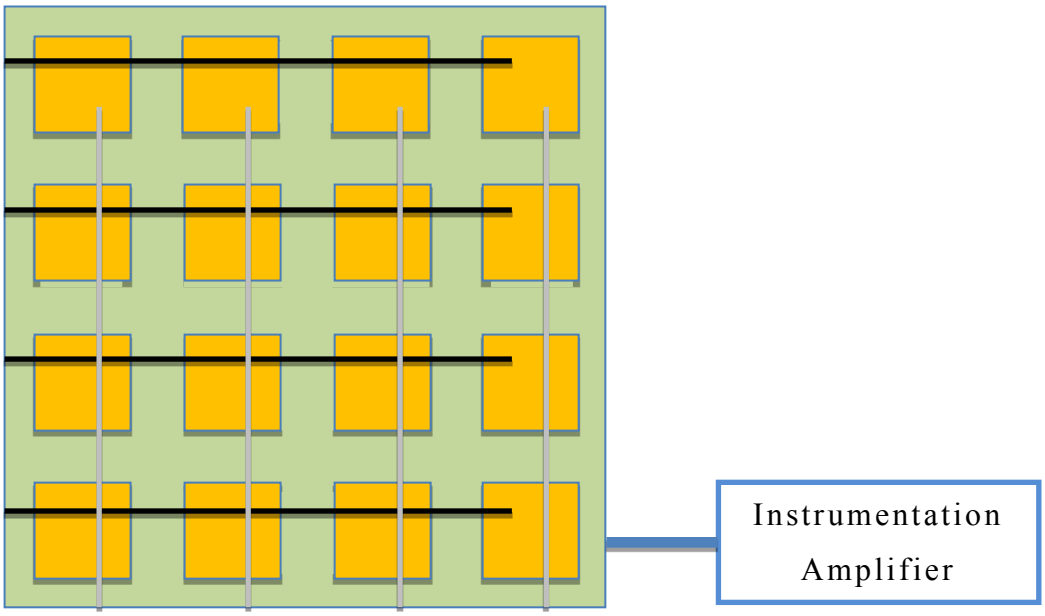

Figure 1-11 Multichannel chip to illustrate multichannel based OCP detection system.

Multiplexing, miniaturisation and integration of a full biosensing system is appealing due to larger numbers of biosensing channels, smaller reaction volumes, integration of various functionalities, and simplification of electronic circuits can be achieved.

The combination of multiple detection techniques into a multimodal biosensor with simultaneous detection from multi-channels is favourable to the current industrial and research field. The study will further deepen into integration of other detection techniques to prove a multimodal detection platform complementing each other for an enhanced accuracy in data output and validation.

This particular thesis will highlight the following points:

- The development of hardware, from OCP electronics to electrochemical detection platform setup, and the software for the microcontroller and the system control.
- Multichannel simultaneous parallel sensing of biomolecules interaction.
- Investigate the potential use cases on different electrochemical systems with OCP electrochemical detection technique, including DNA-based/PNA-based systems and protein-based systems.

- Different enhancement techniques for achieving a better performance on different biosensor applications.
- Integration with other techniques to provide a rigid and enhanced accuracy detection system.

1.5.1 Outline of the Thesis

In order to develop an OCP biosensing platform with multiplexed technique, it is essential to understand the electrochemistry theory and electronic circuit theory. Until now, Chapter 1 discussed the principle of electrochemistry by electrochemical interface, with a general introduction to biosensors. Closing by introducing different label-free detection techniques for biosensing that is used to validate or integrate as complimentary detection techniques to enhance the accuracy.

Chapter 2 details the system design approaches to develop a biosensing platform, specifically for a multiplexed OCP biosensing electronic hardware, and software. For a reliable and accurate measurement of the true OCP, the selected instrumentation amplifier and circuit design techniques play crucial roles through the development. Therefore, the chapter extends into the electronic designs that have been used in the reported work. And finally, the techniques and design concept for a whole integrated system, which also includes different detection techniques, to demonstrate a 'proof of concept' platform for future biosensing.

Since understanding, developing and demonstrating the ability of the multiplexed OCP biosensing platform is fundamentally important in this thesis, the OCP biosensing platform is used in the studies of different electrochemical systems. The studies include DNA, PNA, protein, etc. Investigation of different electrochemical systems with side by side comparison of other detection techniques are done in the following chapters. The project can, therefore, demonstrate the power of OCP biosensing platform, and further develop suitable enhancement techniques for each electrochemical system.

To characterise the OCP measurement system, the detection of prostate cancer biomarkers is used as a case study in Chapter 3. The study used the final version of the OCP measurement system, which has included a flow cell and implemented auto-sampling technique, in order to demonstrate the applicability and the robustness of the system. In addition, the system is presented as a 'proof of concept' platform for biosensing. A sensitive label-free detection integrated system with simultaneous multichannel measurement of OCP variations for the detection of prostate specific antigen (PSA) is presented. The sensor differentiation ability, which is demonstrated with the detection of a wide range of concentrations of PSA, and a challenge for clinical use case are discussed.

Chapter 4 presents a study of OCP detection of DNA – DNA interaction. The use of intrinsic charge carried by the phosphate backbone of DNA was studied with OCP. As the target DNA carried out the hybridisation process, a potential change was observed due to the charge it carried. However, as label-free techniques are less sensitive in hybridisation detection, a cobalt complex, which acts as an intercalating molecule, was used to enhance the signal. OCP results were compared to EIS measurements for validation.

Following the study on the detection of DNA, Chapter 5 presents a study of OCP detection of PNA – DNA interaction. Such a study was performed to make a comparison with DNA – DNA interaction, as PNA does not carry a negatively charged backbone. Finally, positively charged gold nanoparticles are used for electrostatic attachment known to only PNA/DNA duplex. Validation of OCP results were again compared to EIS measurements, with Nyquist plots that represent the charge transfer resistance, and Cole-Cole plots that represent the capacitance of the system.

In the last experimental chapter, Chapter 6 presents a study of OCP detection of drugs that inhibit kinase activity. The study was performed for the detection of protein phosphorylation driven by kinase, with the use of ferrocene-crowned nanoparticles for signal enhancement. This highlights the ability of OCP detection, which could be used on different molecule sizes.

In addition, to further proof that OCP could be seamlessly integrated with multiple detection techniques, a multimodal system, which includes LSPR, EIS and DPV, was demonstrated and have shown promising results. The OCP results were outperforming other detection techniques here as clear results could be seen before signal enhancing molecules were attached. Results were validated under the same electrochemical system, and OCP detection technique can be concluded with high levels of accuracy and reliability on a single multimodal platform.

References

Anker, J.N., Hall, W.P., Lyandres, O., Shah, N.C., Zhao, J. & Van Duyne, R.P. 2008. Biosensing with plasmonic nanosensors. *Nature Materials,* 7**,** 442-453.

Bagotsky, V.S. 2006. *Fundamentals of electrochemistry,* Hoboken, N.J.: Wiley-Interscience.

Bain, C.D., Biebuyck, H.A. & Whitesides, G.M. 1989a. Comparison of self-assembled monolayers on gold - coadsorption of thiols and disulfides. *Langmuir,* 5**,** 723-727.

Bain, C.D., Evall, J. & Whitesides, G.M. 1989b. Formation of monolayers by the coadsorption of thiols on gold - variation in the head group, tail group, and solvent. *Journal of the American Chemical Society,* 111**,** 7155-7164.

Bain, C.D. & Whitesides, G.M. 1989. Formation of monolayers by the coadsorption of thiols on gold - variation in the length of the alkyl chain. *Journal of the American Chemical Society,* 111**,** 7164-7175.

Bard, A.J. & Faulkner, L.R. 1980. *Electrochemical methods : Fundamentals and applications,* New York: Wiley.

Bard, A.J. & Faulkner, L.R. 2001. *Electrochemical methods : Fundamentals and applications,* New York: John Wiley.

Berggren, C., Bjarnason, B. & Johansson, G. 2001. Capacitive biosensors. *Electroanalysis,* 13**,** 173-180.

Bhalla, N., Di Lorenzo, M., Pula, G. & Estrela, P. 2015. Protein phosphorylation detection using dual-mode field-effect devices and nanoplasmonic sensors. *Scientific Reports,* 5.

Butt, H.-J. & Kappl, M. 2010. *Surface and interfacial forces,* Weinheim: Wiley-VCH.

Camillone, N., Eisenberger, P., Leung, T.Y.B., Schwartz, P., Scoles, G., Poirier, G.E. & Tarlov, M.J. 1994. New monolayer phases of n-alkane thiols self-assembled on au(111) - preparation, surface characterization, and imaging. *Journal of Chemical Physics,* 101**,** 11031-11036.

Chapman, D. 1913. A contribution to the theory of electrocapillarity. *Philos. Mag., Ser. 6,* 25**,** 475-481.

Darling, S.B., Rosenbaum, A.W., Wang, Y. & Sibener, S.J. 2002. Coexistence of the (23 x root 3) au(111) reconstruction and a striped phase self-assembled monolayer. *Langmuir,* 18**,** 7462-7468.

Eggins, B.R. 2002. *Chemical sensors and biosensors,* New York: John Wiley.

Estrela, P., Paul, D., Li, P., Keighley, S.D., Migliorato, P., Laurenson, S. & Ferrigno, P.K. 2008. Label-free detection of protein interactions with peptide aptamers by open circuit potential measurement. *Electrochimica Acta,* 53**,** 6489-6496.

Estrela, P., Stewart, A.G., Migliorato, P. & Maeda, H. 2004. Label-free detection of DNA hybridization with au/sio2/si diodes and poly-si tfts. *Ieee International Electron Devices Meeting 2004, Technical Digest***,** 1009-1012.

Finklea, H.O. 1996. Electrochemistry of organized monolayers of thiols and related molecules on electrodes. *Electroanalytical Chemistry: A Series of Advances, Vol 19,* 19**,** 109-335.

Formisano, N., Bhalla, N., Wong, L.C.C., Di Lorenzo, M., Pula, G. & Estrela, P. 2015. Multimodal electrochemical and nanoplasmonic biosensors using ferrocene-crowned nanoparticles for kinase drug discovery applications. *Electrochemistry Communications,* 57**,** 70-73.

Gouy, G. 1910. Constitution of the electric charge at the surace of an electrolyte. *J. Phys. Theor. Appl.,* 9**,** 457-468.

Grow, A.E., Wood, L.L., Claycomb, J.L. & Thompson, P.A. 2003. New biochip technology for label-free detection of pathogens and their toxins. *Journal of Microbiological Methods,* 53**,** 221-233.

Helmholtz, H. 1853. Ueber einige gesetze der vertheilung elektrischer ströme in körperlichen leitern mit anwendung auf die thierisch-elektrischen versuche. *Annalen der Physik und Chemie,* 165**,** 211–233.

Herne, T.M. & Tarlov, M.J. 1997. Characterization of DNA probes immobilized on gold surfaces. *Journal of the American Chemical Society,* 119**,** 8916-8920.

Hong, H.S., Kim, S.J. & Lee, K.S. 1999. Long-term oxidation characteristics of oxygen-added modified zircaloy-4 in 360 degrees c water. *Journal of Nuclear Materials,* 273**,** 177-181.

Hunter, R.J. & White, L.R. 1987. *Foundations of colloid science,* New York/Oxford Oxfordshire: Clarendon Press/Oxford University Press.

Jolly, P., Wong, L.C.C., Miodek, A., Lindsay, M.A. & Estrela, P. 2015. A simple and highly sensitive electrochemical platform for detection of micrornas. *2015 Ieee Sensors***,** 803-806.

Katz, E. & Willner, I. 2003. Probing biomolecular interactions at conductive and semiconductive surfaces by impedance spectroscopy: Routes to impedimetric immunosensors, DNA-sensors, and enzyme biosensors. *Electroanalysis,* 15**,** 913-947.

Kawagoe, K.T., Zimmerman, J.B. & Wightman, R.M. 1993. Principles of voltammetry and microelectrode surface-states. *Journal of Neuroscience Methods,* 48**,** 225-240.

Keighley, S.D., Li, P., Estrela, P. & Mighorato, P. 2008. Optimization of DNA immobilization on gold electrodes for label-free detection by electrochemical impedance spectroscopy. *Biosensors & Bioelectronics,* 23**,** 1291-1297.

Krysa, J., Zlamal, M., Kment, S., Brunclikova, M. & Hubicka, Z. 2015. Tio2 and fe2o3 films for photoelectrochemical water splitting. *Molecules,* 20**,** 1046-1058.

Kukol, A., Li, P., Estrela, P., Ko-Ferrigno, P. & Migliorato, P. 2008. Label-free electrical detection of DNA hybridization for the example of influenza virus gene sequences. *Analytical Biochemistry,* 374**,** 143-153.

Li, P. 2008. *A study of electrochemical transduction mechanisms in biosensor applications.* Doctor of Philosophy, University of Cambridge.

Love, J.C., Estroff, L.A., Kriebel, J.K., Nuzzo, R.G. & Whitesides, G.M. 2005. Self-assembled monolayers of thiolates on metals as a form of nanotechnology. *Chemical Reviews,* 105**,** 1103-1169.

Lyklema, J. & Leeuwen, H.P.v. 1991. *Fundamentals of interface and colloid science,* San Diego: Academic Press.

marketsandmarkets.com 2016. Label-free detection market by technology (surface plasmon resonance, bio-layer interferometry), products (consumables, microplates, biosensor chips), applications (binding kinetics, binding thermodynamics, lead generation) - global forecasts to 2020. USA, .

Masliyah, J.H., Bhattacharjee, S. & John Wiley & Sons. 2006. Electrokinetic and colloid transport phenomena. Hoboken, N.J.: Wiley-Interscience,.

Nagel, M., Bolivar, P.H., Brucherseifer, M., Kurz, H., Bosserhoff, A. & Buttner, R. 2002. Integrated thz technology for label-free genetic diagnostics. *Applied Physics Letters,* 80**,** 154-156.

OED. 2017. *Sensor, n.* [Online]. Oxford University Press. Available: http://www.oed.com/view/Entry/176005 [Accessed 15 June 2017].

Ohshima, H. 2006. *Theory of colloid and interfacial electric phenomena,* Amsterdam ; New York: Elsevier Academic Press.

Regan, E.M., Hallett, A.J., Wong, L.C.C., Saeed, I.Q., Langdon-Jones, E.E., Buurma, N.J., Pope, S.J.A. & Estrela, P. 2014. A novel cobalt complex for enhancing amperometric and impedimetric DNA detection. *Electrochimica Acta,* 128**,** 10-15.

Rodriguez, M.C., Kawde, A.N. & Wang, J. 2005. Aptamer biosensor for label-free impedance spectroscopy detection of proteins based on recognition-induced switching of the surface charge. *Chemical Communications***,** 4267-4269.

Scholz, F. & Bond, A.M. 2002. *Electroanalytical methods : Guide to experiments and applications,* Berlin ; New York: Springer.

Schreiber, F. 2000. Structure and growth of self-assembling monolayers. *Progress in Surface Science,* 65**,** 151-256.

Signorelli, R., Ku, D.C., Kassakian, J.G. & Schindall, J.E. 2009. Electrochemical double-layer capacitors using carbon nanotube electrode structures. *Proceedings of the Ieee,* 97**,** 1837-1847.

Sorgenfrei, S., Chiu, C.Y., Gonzalez, R.L., Yu, Y.J., Kim, P., Nuckolls, C. & Shepard, K.L. 2011. Label-free single-molecule detection of DNA-hybridization kinetics with a carbon nanotube field-effect transistor. *Nature Nanotechnology,* 6**,** 125-131.

Southampton Electrochemistry Group. 1985. *Instrumental methods in electrochemistry,* Chichester: Ellis Horwood.

Srinivasan, S. 2006. *Fuel cells : From fundamentals to applications,* New York: Springer.

Stern, O. 1924. The theory of the electrolytic double layer. *Z. Elektrochem. Angew. Phys. Chem.,* 30**,** 508-516.

The NIST Reference on Constants, Units, and Uncertainty. 2016. *Codata value: Faraday constant* [Online]. US: National Institute of Standards and Technology. Available: http://physics.nist.gov/cgi-bin/cuu/Value?f [Accessed March 16 2016].

Ulman, A. 1996. Formation and structure of self-assembled monolayers. *Chemical Reviews,* 96**,** 1533-1554.

Vayenas, C.G. & Bebelis, S. 1999. Electrochemical promotion of heterogeneons catalysis. *Catalysis Today,* 51**,** 581-594.

Vericat, C., Vela, M.E., Corthey, G., Pensa, E., Cortes, E., Fonticelli, M.H., Ibanez, F., Benitez, G.E., Carro, P. & Salvarezza, R.C. 2014. Self-assembled monolayers of thiolates on metals: A review article on sulfur-metal chemistry and surface structures. *Rsc Advances,* 4**,** 27730-27754.

Vollmer, F. & Arnold, S. 2008. Whispering-gallery-mode biosensing: Label-free detection down to single molecules. *Nature Methods,* 5**,** 591-596.

Wang, H.N. & Pilon, L. 2011. Accurate simulations of electric double layer capacitance of ultramicroelectrodes. *Journal of Physical Chemistry C,* 115**,** 16711-16719.

Wang, J. 2006. *Analytical electrochemistry,* Hoboken, N.J.: Wiley-VCH.

Wang, W.S., Huang, H.Y., Chen, S.C., Ho, K.C., Lin, C.Y., Chou, T.C., Hu, C.H., Wang, W.F., Wu, C.F. & Luo, C.H. 2011. Real-time telemetry system for amperometric and potentiometric electrochemical sensors. *Sensors,* 11**,** 8593-8610.

Wang, W.U., Chen, C., Lin, K.H., Fang, Y. & Lieber, C.M. 2005. Label-free detection of small-molecule-protein interactions by using nanowire nanosensors. *Proceedings of the National Academy of Sciences of the United States of America,* 102**,** 3208-3212.

Wieckowski, A. 1999. *Interfacial electrochemistry : Theory, experiment, and applications,* New York: Marcel Dekker.

Wong, L.C.C., Jolly, P. & Estrela, P. 2017. Development of a sensitive multiplexed open circuit potential system for the detection of prostate cancer biomarkers. *BioNanoScience,* 8(2), 701-706.

Yang, Z.G., Kasprzyk-Hordern, B., Goggins, S., Frost, C.G. & Estrela, P. 2015. A novel immobilization strategy for electrochemical detection of cancer biomarkers: DNA-directed immobilization of aptamer sensors for sensitive detection of prostate specific antigens. *Analyst,* 140**,** 2628-2633.

CHAPTER 2.

OCP Measurement System

This chapter introduces the open circuit potential (OCP) measurement system that is designed and assembled for the detection of true OCP of biosensing. The hardware circuit design is discussed, in order to develop a high-throughput low bias current measurement system through the use of off-the-shelf components, which could then be easily manufactured as a bench top instrumentation system. In order to achieve optimal standard of the circuitry, design techniques of the circuit and special care on the use of instrumentation amplifiers are investigated and discussed. This will be followed with the discussion on the software for the embedded system of the electronics and the modular LabVIEW control interface.

2.1 Introduction

In this study, to achieve real-time simultaneous multichannel detection measurements, a multiplexed measurement technique is needed to read out the OCP between different pairs of instrumentation amplifiers inputs. A further study in designing the method for multiplexing is needed to achieve an expandable measurement setup. With the readout circuit completed, optimisation on the readout accuracy and protection of the circuit is needed, such as preventing noise or spikes during measurement due to external noise or environment should be taken care of. As the OCP voltage change should be measured accurately in the range of millivolts (mV) or microvolts (μV), a small noise introduced in the system can highly affect the final readout result, especially when detecting small changes upon reaction in real time through this system.

2.1.1 Instrumentation Amplifier

In order to design a successful biosensing electronic system for the OCP detection technique, the instrumentation amplifier plays a key role in this study as it is the first electronic component that connects to the biosensing electrode. Instrumentation amplifiers have been used in measurement systems for decades; and it is one of the most crucial components here for OCP measurements. It is our first priority to understand the fundamentals of the amplifier before any designing steps. The specification of these amplifiers varies between power consumption, offset performance, noise and distortion performance, and packaging size. Hence, the need for an instrumentation amplifier that has both good sensitivity and stability during the electrochemical detection process is essential.

2.1.1.1 Fundamentals of an Instrumentation Amplifier

An instrumentation amplifier is a differential voltage-gain device that measures the difference between the voltages existing at its two input channels and amplifies the differential signal with a defined gain. The key characteristics of an instrumentation amplifier are high input impedance, high common-mode rejection, lower output offset, and low output impedance.

Basic design of the integrated circuit includes three operational amplifiers and several resistors, with an external resistor to set the voltage gain. A basic schematic of an instrumentation amplifier is shown in Figure 2-1.

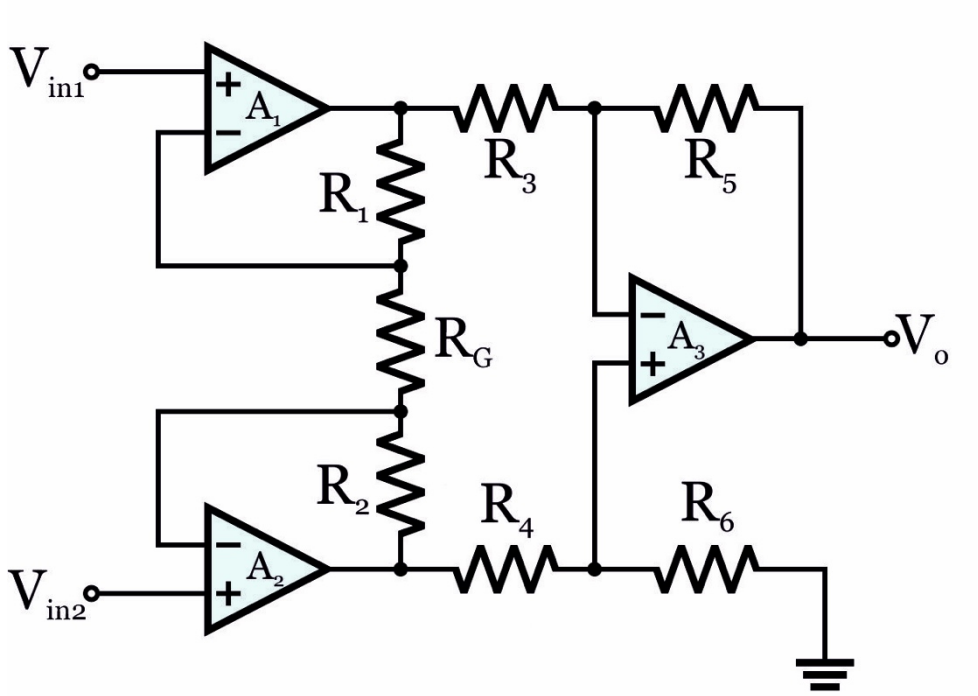

Figure 2-1 Basic schematic of an instrumentation amplifier.

Op-amps A_1 and A_2 of the instrumentation amplifier are in the non-inverting configuration, which acts as the voltage gain stage circuitry and provide high input impedance. Op-amp A_3 is in a unity gain differential configuration, with high precision resistors that have same resistance value (R_3-R_6).

An external resistor, which is the gain-setting resistor, R_G, can be used for setting the gain of the amplifier. Op-amp A_1 receives the input signal V_{in1} on its non-inverting (+) input and amplifies this signal with a voltage gain, A_{V1}, that can be defined as:

$$A_{V1} = 1 + \frac{R_1}{R_G} \tag{8}$$

Op-amp A_1 also has V_{in2} as an input signal to its inverting (-) input through op-amp A_2 and the signal path formed by R_2 and R_G. The input signal V_{in2} is amplified by op-amp A_1 with a voltage gain of

$$A_{V2} = \frac{R_2}{R_G} \tag{9}$$

Thus, the overall closed-loop gain, A_{cl}, of the instrumentation amplifier can be described as

$$A_{cl} = 1 + \frac{(R_1 + R_2)}{R_G} \tag{10}$$

In practice one uses $R_1 = R_2 = R$. Eq. (10) shows that the gain can be defined by the external resistor, R_G, when R_1 and R_2 have a known value that is equal and fixed. This external resistor, R_G, can be calculated by applying Eq. (10).

$$R_G = \frac{2R}{A_{cl} - 1} \tag{11}$$

2.1.1.2 Instrumentation Amplifier – Texas Instruments INA116

To measure the true OCP and such small changes in voltage at the input stage of the circuit, a careful selection process on the instrumentation amplifier is needed. A list (Table 2-1) of instrumentation amplifiers was being screened for the design of the OCP detection electronic circuit, and the Texas Instruments INA116 instrumentation amplifier (INA116) was selected for this specific biosensing application due to the properties highlighted below.

Table 2-1 A selection of instrumentation amplifiers.

Part Number	Number of Channels (#)	CMRR (Min) (dB)	Input Bias Current (+/-) (Max) (nA)	Gain (Min) (V/V)	Gain (Max) (V/V)	Gain Error (+/-) (Max) (%)	Approx. Price (US$)
INA116	1	86	0.000025	1	1000	0.7	8.70 | 1ku
INA322	1	60	0.01	5	1000	0.4	0.95 | 1ku
INA2332	2	60	0.01	5	1000	0.4	0.95 | 1ku
INA2331	2	90	0.01	5	1000	0.1	1.20 | 1ku
INA331	1	90	0.01	5	1000	0.1	0.80 | 1ku
INA332	1	60	0.01	5	1000	0.4	0.54 | 1ku
INA156	1	72	0.01	10	50	0.4	1.20 | 1ku
INA2321	2	90	0.01	5	1000	0.1	1.75 | 1ku
INA321	1	90	0.01	5	1000	0.1	1.10 | 1ku
INA111	1	106	0.02	1	1000	2	5.49 | 1ku
MAX4208	1	106	0.001	1	Adj.	0.25	1.65 | 1ku
MAX4209	1	106	0.001	10	1000	0.25	1.62 | 1ku
MAX4460	1	90	0.1	1	Adj.	0.35	1.33 | 1ku
MAX4461	1	90	0.1	1	100	0.3	1.24 | 1ku
MAX4194	1	60	20	1	10000	0.1	2.31 | 1ku
AD8224	2	100	0.01	1	1000	0.2	4.17 | 1ku
AMP02	1	115	0.01	1	10000	0.5	6.16 | 1ku
AD8220	1	100	0.025	1	1000	0.2	2.25 | 1ku
LT1168	1	126	0.25	1	10000	0.5	3.70 | 1ku

The INA116 is a complete monolithic FET-input amplifier, with an extremely low input bias current of 3fA at 25°C normal operating room temperature (Burr-Brown, 1995). To achieve this ultra-low input bias current, Difet® inputs at the IC pins are provided and special guarding techniques are implemented during assembly process.

A 3-op amp topology is implemented in the INA116 to form an instrumentation amplifier. The basic connections of this amplifier are shown in Figure 2-2.

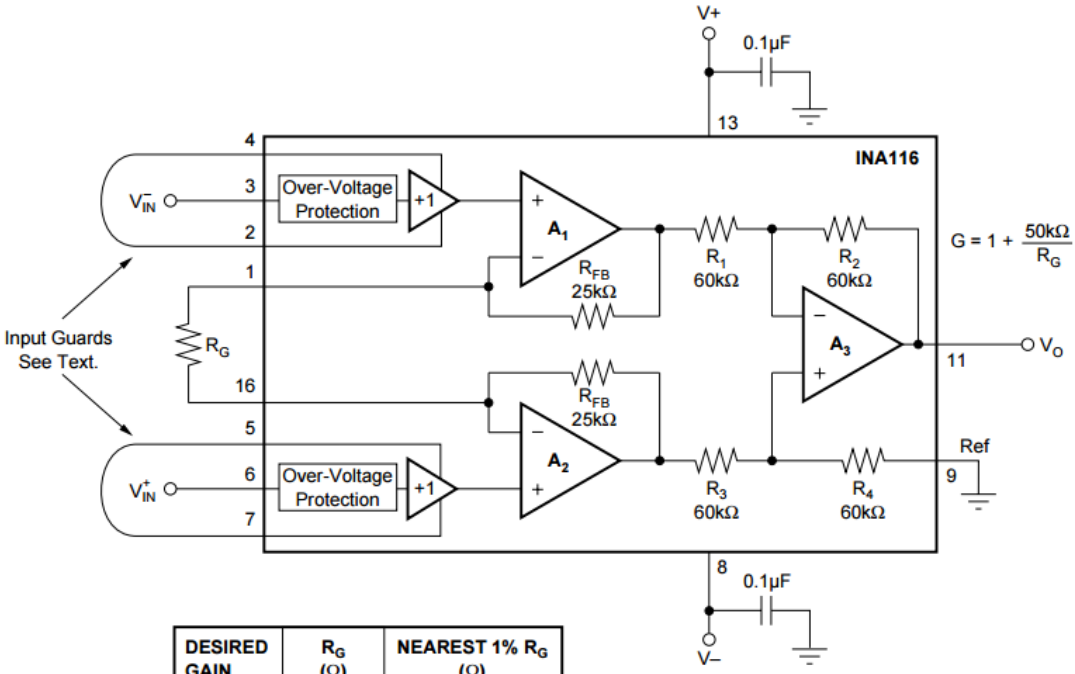

DESIRED GAIN	R_G (Ω)	NEAREST 1% R_G (Ω)
1	NC	NC
2	50.00k	49.9k
5	12.50k	12.4k
10	5.556k	5.62k
20	2.632k	2.61k
50	1.02k	1.02k
100	505.1	511
200	251.3	249
500	100.2	100
1000	50.05	49.9
2000	25.01	24.9
5000	10.00	10
10000	5.001	4.99

NC: No Connection.

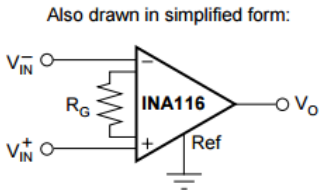

Figure 2-2 Basic Connections of the INA116 instrumentation amplifier. (Adapted from Burr-Brown (1995))

2.1.1.3 Bill of Materials of INA116 Electronic Circuit

A bill of materials (BOM) of the INA116 electronic circuit is listed with the required components and quantities in Table 2-2. A careful selection of components is used in the system; these include high performance medical/instrumentation grade capacitors.

Table 2-2 Bill of materials (BOM) of the INA116 electronic circuit board.

Designation	Quantity	Description
X1, X2, X3, X4, X5, X6, X7, X8	8	50 Ω Straight PCB Mount SMA Jack
IC1, IC2, IC3, IC4	4	INA116 Ultra Low Input Bias Current Instrumentation Amplifier
IC5	1	24-/16-Bit 4-Channel Simultaneous-Sampling Cascadable Sigma-Delta Analog-to-Digital Converters
Q1	1	24.576 MHz SMD Crystal
R1	1	Ferrite Bead
C1, C2, C3, C4, C5, C6, C7, C8, C17, C19, C21	11	1µF Decoupling Capacitors
C9, C10, C11, C12, C13, C14, C15, C16, C18, C20	10	0.1 µF Decoupling Capacitors

2.2 OCP Measurement System Design – Electronics

The OCP electronic system setup provides a differential voltage measurement with high input impedance and low input bias current. Since there is no current directly applied to the electrochemical system, a true and accurate measurement of the OCP variations can be performed. To accurately measure the variations, the Texas Instruments INA116 instrumentation amplifier is used to form the electronic detection circuit, measuring the variations between the working electrode and the reference electrode. A schematic in Figure 2-3 shows the core biosensing electronic circuit used for OCP detection.

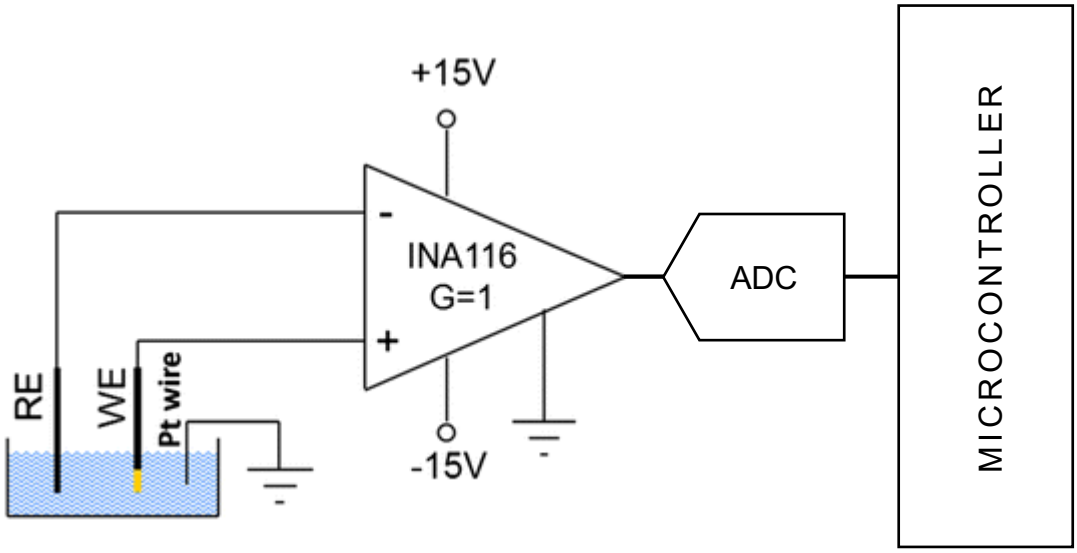

Figure 2-3 Schematic of the basic design of a single channel OCP measurement system. WE is the working electrode; RE is the reference electrode; the Pt wire is grounding the solution.

The core biosensing electronic circuit for OCP detection is described as the following: Inside the electrochemical cell, platinum (Pt) wire is used to ground the electrolyte. This is designed as a protective measure for preventing amplifier overflow. A stable and isolated ±15 V power circuit supplies the power specifically for the instrumentation amplifier to improve the working condition of the amplifier up to maximum performance. This power supply and connected power lines are separated from all other signal lines or power lines of other electronics. The differential

measurement output (V_0) from the amplifier is then passed into an analog-to-digital converter (ADC). To eliminate any further errors that can be caused by the mismatch of multichannel electronic components, the amplifiers of all channels are set to a unity gain differential configuration (G = 1).

2.2.1 A Simultaneous Multichannel Design for Parallel Biosensing

A simultaneous multichannel design for parallel biosensing with OCP detection technique is suggested, with beliefs that this can enable the extraction of extra information from a single experiment, and to tackle more advanced experiments. This can also reduce the time for sampling multiple samples, minimise the variations (temperature, interaction time, solutions and buffers) between experiments, and enable live comparisons of multiple samples.

To achieve multichannel detection with the system, an approach for the electronic circuitry is needed for the detection of such continuous & simultaneous parallel OCP analog signals from all the instrumentation amplifiers (Spieler, 2003a; Spieler, 2003b). Several approaches were studied in terms of performance, noise (Ott, 1988) and implementation. Assembly techniques of the OCP electronic system that improves the OCP signal are included in Appendix I.

First approach

The first approach includes a switch multiplexing multiple working electrodes as the input of an instrumentation amplifier. The working electrodes and reference electrodes are passed through the switch into an instrumentation amplifier, followed by an ADC for analog-to-digital conversion. Switching from one electrode to the next while the ADC converts the OCP analog signal into digital data allows for a low-cost design for the analog-to-digital conversion process for multiple biosensing inputs. However, through investigation, the switching noise from one channel to another is significant, which could affect the OCP results. The noise result from cross-talk occurs between the differential voltage outputs (high input impedance and low input bias current).

Second approach

The second approach separates all the channels with individual instrumentation amplifiers and ADCs. This is a parallel design that allows each of the instrumentation amplifiers to output individual OCP analog signals followed by an ADC for analog-to-digital conversion. Although this approach is feasible, a huge number of electronic components would be included in the design, which not only increases the overall cost, but also lowers the simplicity of the overall design.

Third approach

The third approach (Figure 2-4) introduces a hybrid method for multiplexing inputs with simple single command controls by using a multichannel, simultaneous-sampling, cascadable ADC within the design. With a small packaging ADC IC, multiplexing and analog-to-digital conversion can be achieved in one place. Each of the OCP signals from the instrumentation amplifier is multiplexed and converted through a single ADC and can be read from a simple interface by a microcontroller. This approach eliminates both cross-talks from differential voltage outputs mentioned in the first approach as well as the potential for mismatch between channels. In addition, the design of this electronic system has the ability to be a modular system should more devices need to be added.

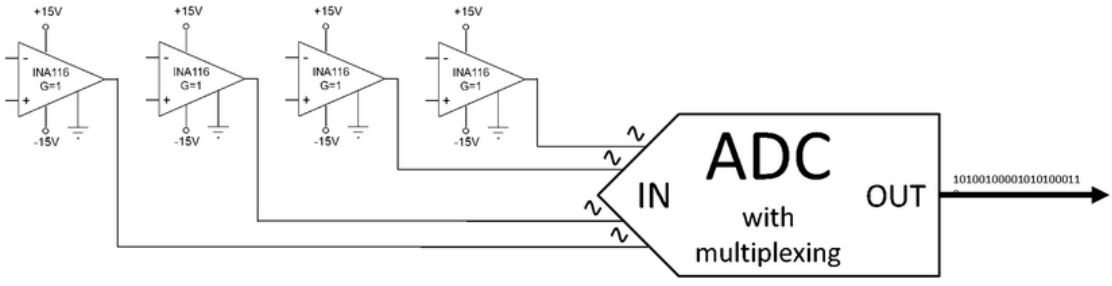

Figure 2-4 Schematic of the multiplexed OCP detection circuit constructed with four INA116 instrumentation amplifiers and one MAX11040K ADC.

The selected approach

The third approach, illustrated in Figure 2-4, is selected for the design of the OCP measurement system. A 24-bit, 4-channel, simultaneous-sampling, cascadable, sigma-delta analog-to-digital converter (ADC) MAX11040K (Maxim Integrated, USA) was selected for sampling the differential outputs of the instrumentation amplifiers, which are the OCP analog signals. A multiple-channel multiplexing design is illustrated in Figure 2-5.

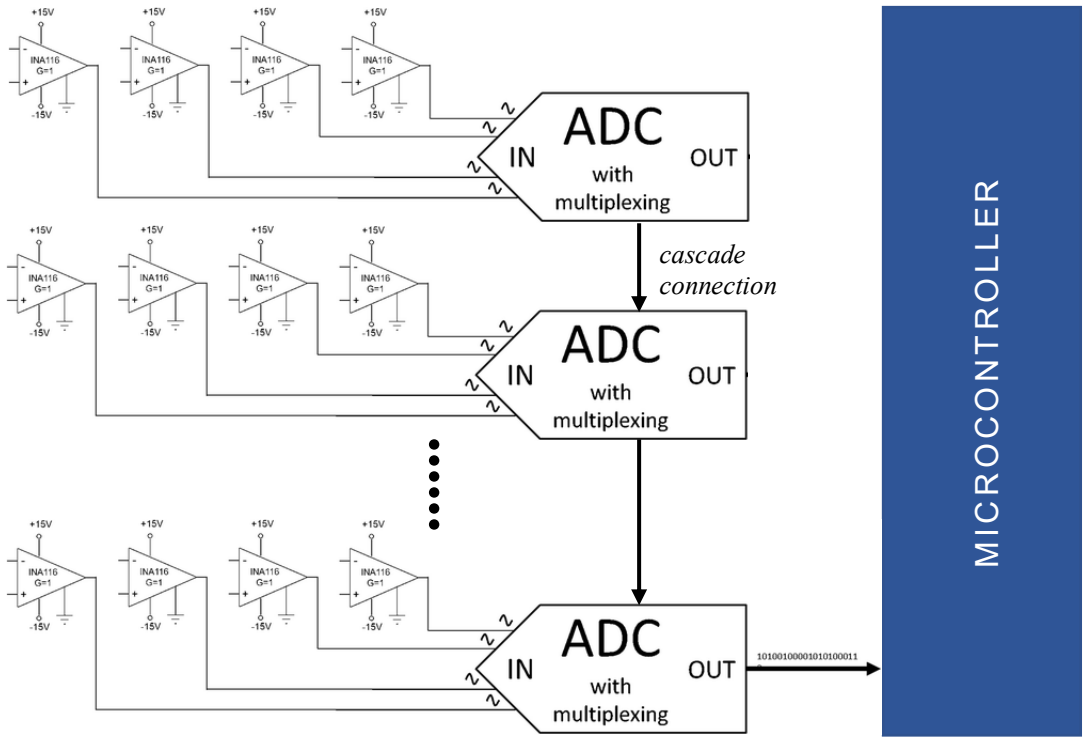

Figure 2-5 Simplified schematic of the multiplexed OCP detection circuit constructed with cascaded ADCs to provide 32 channels.

The differential analog input range is ±2.2 V when using the internal reference voltage (V_{REFIO}), which is well within the input OCP signal. Code transitions occur halfway between successive integer least significant bit (LSB) values with 1 LSB = (0.88 × V_{REFIO}) × 2 / 16,777,216 in 24-bit mode. This specific ADC allows high resolution and simultaneous sampling of four channels on its own and up to 32 channels by using

a built-in cascade feature to synchronise as many as eight devices on a single serial interface, illustrated in Figure 2-5. The simplicity of the device allows reading data from all the cascaded devices using a single command, with the eight devices effectively operating as one device. In this thesis, a single ADC is used for the production and biosensing applications, which gives a 4-channel simultaneous-sampling system.

2.2.2 Specification of the electronic circuit

A list of design specification of the OCP electronic circuit is listed in Table 2-3.

Table 2-3 Specification of the OCP electronic circuit

Power	5 V (USB), 9 V
Sensing Type	Real-time
Channel Per Instrumentation Amplifier	1
Simultaneous Sampling Channels	4
Maximum Channels (Expansion)	32
Bias Current	±3 fA
Input Range	±2.2 V
Input Over-voltage Protection	±40 V
Data Resolution	24 Bits
Least Significant Bit (LSB)	$(0.88 \times V_{REFIO}) \times 2 / 16{,}777{,}216$
Differential Nonlinearity	0.1 LSB
Integral Nonlinearity	0.001 % Full Scale
Data Output Rate	0.25 - 64 ksps

2.3 OCP Measurement System Design – Software

In order to bridge the biosensing electronic interface to a human control interface, a client-server model is used as a distributed application structure that can enable multiple devices to gather data, record and further analyse the captured data, with the ability to perform multiplexed measurement system expansion if needed. The software architecture also increases the possibility to perform measurements with additional channels.

2.3.1 Data Acquisition – Client End

A microcontroller is used as the bridge for the communication between the analog-to-digital converter (ADC) and personal computer (PC) in order to convert and record the OCP into digital format, as illustrated in Figure 2-6.

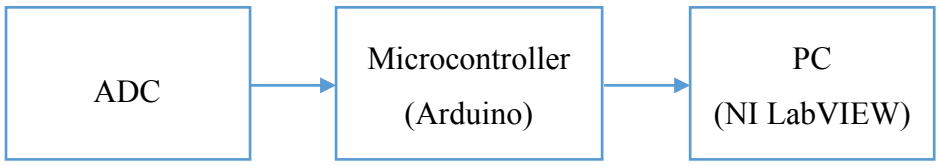

Figure 2-6 Arduino software design architecture for the transmission of OCP digital data.

In the first stage, starting with reading the OCP with the ADC, Serial Peripheral Interface (SPI) communication protocol is used for communicating with the ADC, which sets the ADC configurations and control the conversions. Following on, SPI also acts as a return path for the converted digital data, which passes the digital data back to the microcontroller. The last stage is to enable the microcontroller (client) to utilise Universal Serial Bus (USB) communication protocol to send off the continuous flow of captured data to the PC (server) in a simple solution for further processing.

2.3.1.1 Serial Peripheral Interface

SPI is a bus system that is commonly used for the transmission of digital data between microcontroller and small peripherals. The easy setup uses separate clock (SCLK), two data lines Master Out / Slave In (MOSI) and Master In / Slave Out (MISO) for the communications in both directions, along with a select line (SS) for the selection of the active device. Figure 2-7 shows these signals in a single-slave configuration with SPI master connected to a single slave device (point-to-point topology).

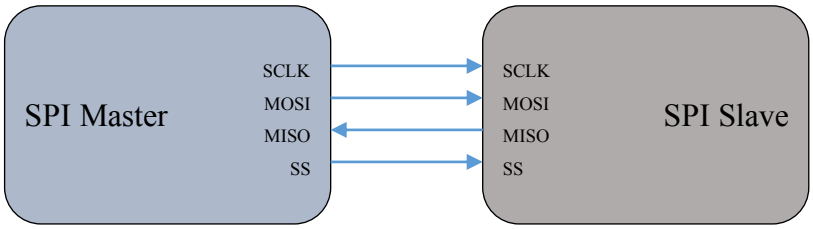

Figure 2-7 SPI busses topology with SPI master connected to a single slave (point-to-point topology).

SPI is a synchronous solution, a faster communication protocol when comparing to asynchronous serial. The receiving hardware can be as simple as a shift register device, which makes implementation much more convenient. Devices communicate using a Master / Slave relationship, in which the master initiates the data frame. The master generates the clock and selects a slave device; data is then transferred in both directions simultaneously. A total of four signal lines are needed for the communication, and more SS possibly included when multiple slave devices are implemented in the system. While other protocols can send random amounts of data at any time given, the communications with SPI must be well-defined in advance with both master and slave devices. Given such limitations, SPI is better suited for data streaming application between microprocessors or digital signal processors, and data transfer from ADCs.

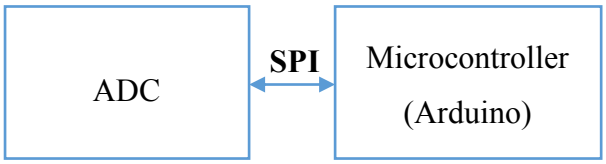

Figure 2-8 SPI protocol is used for the communication between ADC and microcontroller.

In the OCP electronic measurement system, the ADC is naturally thought of as a data stream source. The OCP analog signal is regularly sampled and converted into digital form through the ADC. Upon receiving requests from the microcontroller, the converted digital data are passed from the ADC to the microcontroller through SPI (Figure 2-8). To enable SPI connection with multiple slaves, extra SS lines are used. By triggering the selected SS line from the device to low, while keeping all others high, the specific device can be enabled. A simple SPI busses topology with SPI master connected to multiple slaves is illustrated in Figure 2-9.

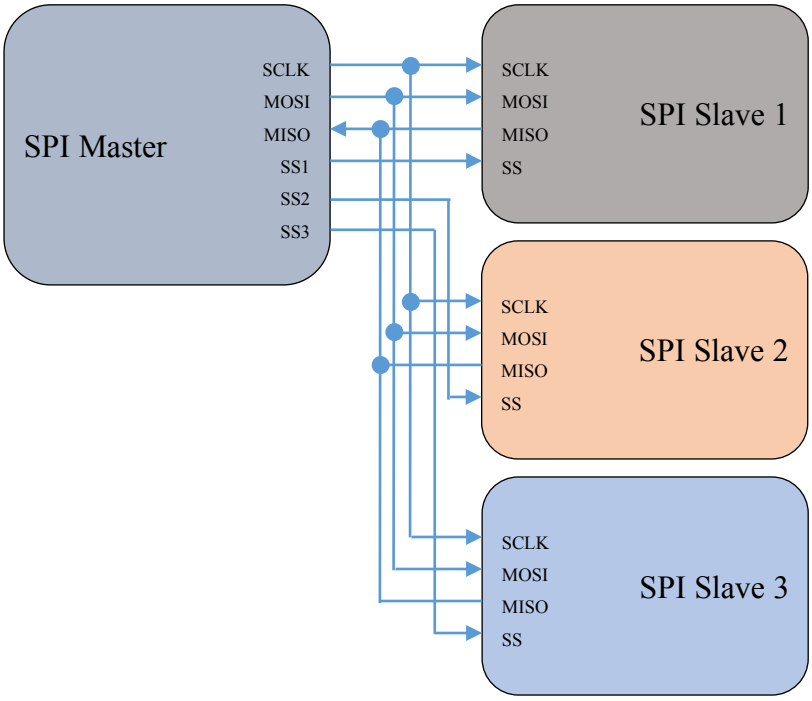

Figure 2-9 SPI busses topology with SPI master connected to multiple slaves.

The disadvantage is that when an increased amount of slave devices are implemented, the amount of SS lines required by this method will increase in like manner, and the master can only accommodate a limited amount of devices depending on the available I/O pins.

To overcome this issue, some of the SPI devices have implemented a communication protocol that is able to use only one single SS line in the system by daisy-chaining all the devices together, with the MISO (output) of one device connecting to the MOSI (input) of the next device. In this daisy-chaining topology, a single SS line connects all the slaves. Once all the data is transferred, the SS line is raised, which in turn causes all the devices to be activated simultaneously. The data is passed from the first device, adding into the data chain till the end device, and transferred as a whole back to the master once all the commands have been processed. The MAX11040K ADC from Maxim Integrated that has been selected and used in the OCP electronic circuit design is capable of such daisy-chaining topology, with the daisy-chaining circuit design illustrated in Figure 2-10. This cascadable advantage of the ADC enabled a simple expansion capability of sensing channels for the OCP measurement system without dominating the I/O pins on the microcontroller for extra ADCs.

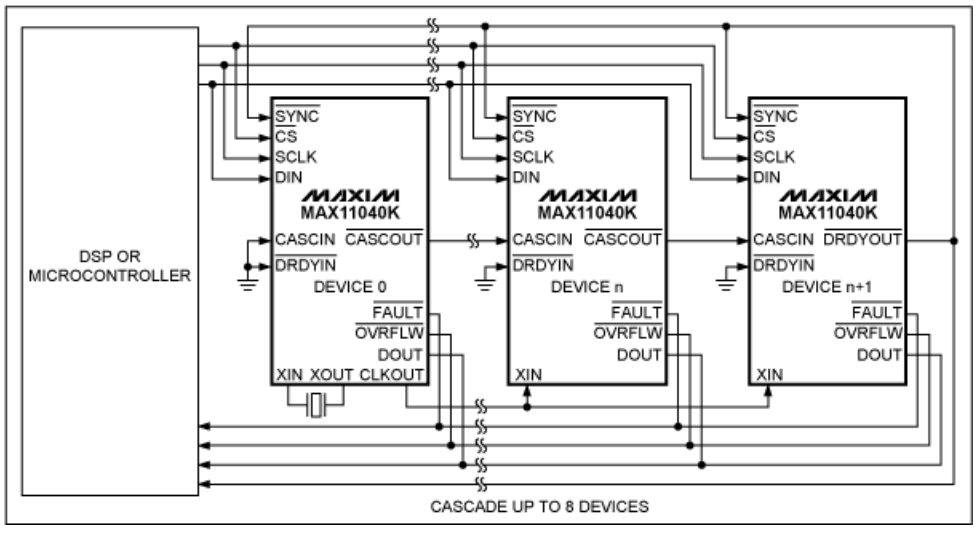

Figure 2-10 Daisy-Chaining Multiple MAX11040K (Adapted from Maxim Integrated Products (2015))

The microcontroller initialise the ADC follow with SPI.transfer() function for data transfer. By following the datasheet guideline, with the correct data request command sent, data are then streamed back to the microcontroller in an 8-bit format. The data processed by shifting register to reform the correct integers of the data, before sending to the PC.

2.3.1.2 Universal Serial Bus

A simple solution is needed for the transmission of OCP data from the microcontroller to PC, and USB serial communication protocol was selected and implemented in the OCP measurement system (Figure 2-11) for this purpose.

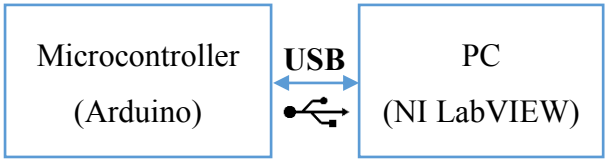

Figure 2-11 USB protocol is used for the communication between microcontroller and PC.

USB is an industry standardised communication protocol since 1996. It is designed for the connection of peripherals to PC, both to transmit data and to supply power (Axelson, 2007, 2015; Hyde, 2001). Universal asynchronous receiver-transmitter (UART) is a hardware device for asynchronous serial communication, for which the data format and transmission speeds are configurable. It takes bytes of data and sequentially transmits the individual bits to the destination. Arduino supports serial output and can directly assign the on-chip USB UART serial interface to output the OCP data. The print data function directly sends data to the serial port as human-readable ASCII text.

To send the OCP data that are captured and converted into digital format by the ADC, a simple Serial.print() function is used. Data is then sent out through USB to the PC. For a more efficient way on transferring and storing the OCP data, the data are built

into a table format during transmission, which can be easily stored into a table structured format upon receiving at the server end for further data processing and data analysis.

2.3.2 Data Acquisition – Server End

The server end software is built with LabVIEW, a simplified hardware integration solution to integrate hardware systems. LabVIEW is designed for data acquisition, instrument control, and industrial automation with all kinds of hardware. The dataflow programming language executes commands by following the structure of a graphical block diagram, with different function-nodes available by just connecting them with wires to form a program. Functions are executed once the data is available at the nodes and the functions could be run in parallel, which enables multi-processing and multi-threading software designs (Blume, 2007; Travis and Kring, 2007). The extensive support for interfacing to devices and instruments, a large library of functions for data acquisition, signal generation, signal conditioning, mathematics, statistics, analysis, etc., and as a concurrent language for parallel programming, all these being advantages making LabVIEW to be one of the most suitable for the server end data acquisition programming.

The server end data acquisition software has two main functions: enabling the OCP data transfer through USB from the microcontroller, followed with the functions to store and display the OCP data. A simplified flowchart for the software is illustrated in Figure 2-12.

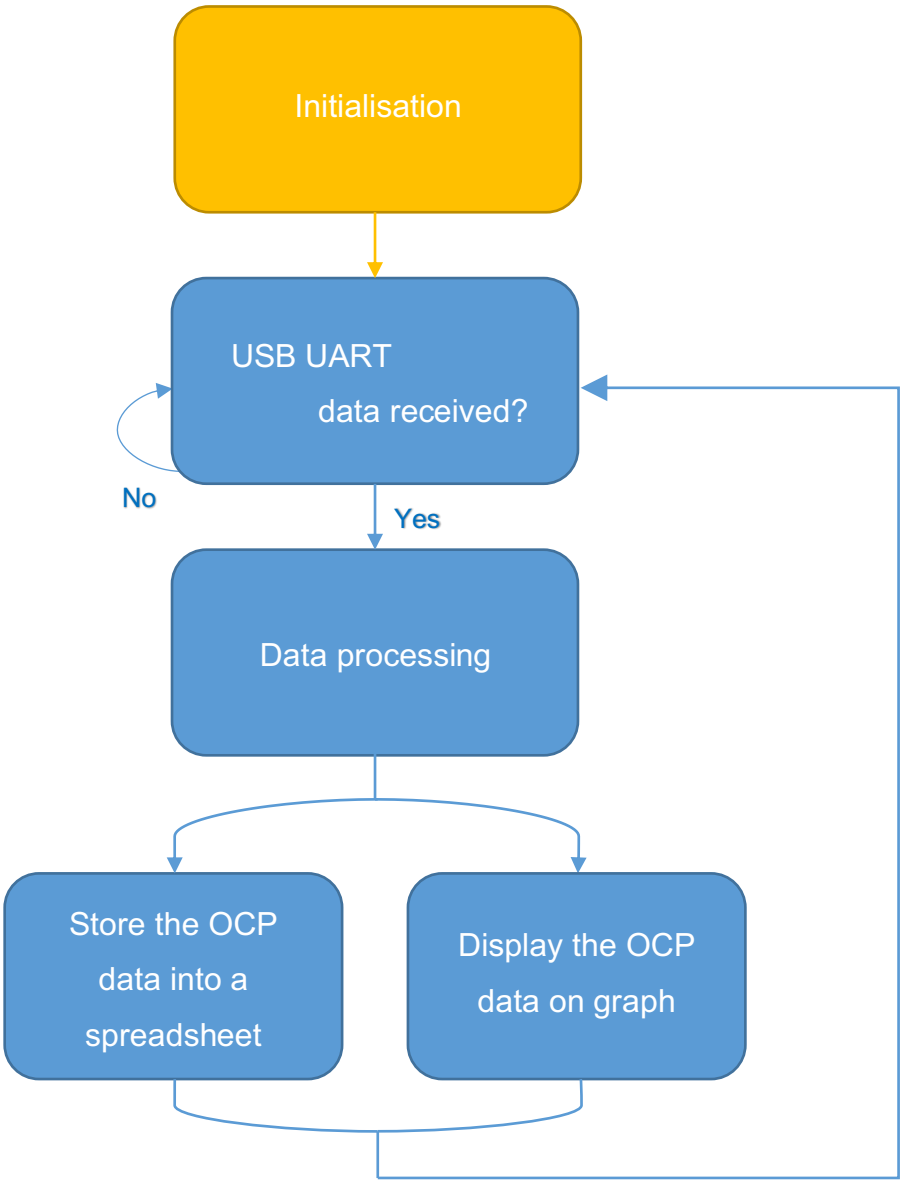

Figure 2-12 Flow diagram of the OCP measurement system server end software.

First, the software initialises and prepares the software environment for receiving USB UART serial data transfer. Upon receiving data, the software unpacks the stream of data and allocates the data into variables of different OCP channels. Each step of the OCP data is then stored into a spreadsheet formatted file with the corresponding timestamp, and simultaneously visualised on a live updated graph through the software display panel. With the help of a live display, monitoring the condition of the experiment could be done as the OCP measurement occurs. The human interface of

the LabVIEW software is also programmed to control pumps and valves, making it a controlled and seamless experience during the experiment.

2.4 Summary

This chapter introduced the selected amplifier and the main electronic components used in OCP detection. Following the discussion of the design and assembly method of the whole system for the detection of true OCP of biosensing; this chapter discussed the method for multiplexing in order to achieve a robust and expandable measurement setup. A discussion with the protocol for data transmission was also presented. Assembly techniques of the OCP electronic system are included in Appendix I.

In its present configuration, with one instrumentation amplifier per channel and one ADC per four channels, the circuitry costs around $50 per four channels using off-the-shelf components, making the system an attractive cost-effective alternative to other electrochemical systems.

In the next chapter, a real electrochemical system (the detection of prostate cancer biomarkers) is used as a case study to demonstrate the ability of the true OCP measurement system that has been introduced in this chapter.

References

Axelson, J. 2007. *Serial port complete : Com ports, usb virtual com ports, and ports for embedded systems,* Madison, WI: Lakeview Research.

Axelson, J. 2015. *Usb complete : The developer's guide,* Madison, WI: Lakeview Research.

Blume, P.A. 2007. *The labview style book,* Upper Saddle River, NJ: Prentice Hall.

Burr-Brown 1995. Ultra low input bias current instrumentation amplifier. *INA116 datasheet.* Burr-Brown.

Hyde, J. 2001. *Usb design by example : A practical guide to building i/o devices,* Hillsboro, Or.: Intel Press.

Maxim Integrated Products 2015. Max11040k/max11060 24-/16-bit, 4-channel, simultaneous-sampling, cascadable, sigma-delta adcs. *MAX11040K/MAX11060 datasheet.* Maxim Integrated Products, Inc.

Ott, H.W. 1988. *Noise reduction techniques in electronic systems,* New York: Wiley.

Spieler, H. 2003a. Analog and digital electronics for detectors. *In:* ICFA Instrumentation School, 8-19 Dec 2003, Itacuruca, Rio de Janeiro, Brazil. 1-43.

Spieler, H. 2003b. Front-end electronics and signal processing. *Instrumentation in Elementary Particle Physics,* 674**,** 76-100.

Travis, J. & Kring, J. 2007. *Labview for everyone : Graphical programming made easy and fun,* Upper Saddle River, NJ: Prentice Hall.

CHAPTER 3.

Characterisation of the OCP Measurement System with the Detection of Prostate Cancer Biomarkers as a Case Study

Following from the previous chapter, a discussion of the whole integrated system for true OCP measurement achieved by using a flow cell and auto-sampling technique is presented, in order to demonstrate a 'proof of concept' platform for biosensing. To demonstrate the ability and limits, here we present the full OCP measurement system with the detection of prostate cancer biomarkers as a case study. This is also the first time a sensitive label-free detection integrated system with simultaneous multichannel measurement of OCP variations for the detection of prostate specific antigen (PSA) is presented (Wong *et al.*, 2017). The investigation of the system stability with simultaneous multichannel measurement was performed. Following this, the investigation of the sensor differentiation ability was also demonstrated with the detection of a wide range of concentrations of PSA (0.1 to 100 ng/mL). Furthermore, a challenge for clinical use case with 4% human serum albumin and human kallikrein2 as control proteins are demonstrated and discussed, which fully demonstrated the applicability of the system and the robustness of the true OCP multichannel approach.

The work presented in this chapter has been partly published in Wong *et al.* (2017). The author contributed to this research on the background research, the electronic hardware design and software programming of the OCP integrated system, the design and production of the flow cell system, the thermal evaporation process and preparation of gold working electrodes, the fabrication of PSA aptasensors, the electrochemical characterisation measurements with OCP detection technique, and finally, the analytical and selectivity performance study of the PSA aptasensors with the additional clinical level performance study.

3.1 Background

For many biosensing applications, there has been increasing interest in the use of aptamers. Although antibodies have dominated commercial adoption, aptamers provide a wide range of advantageous properties such as long-term stability, affordability and ease of development compared to antibodies (Bruno, 2015; Lee *et al.*, 2015). They can also be regenerated without loss of integrity or selectivity (Mairal *et al.*, 2008). There are plenty of reports covering the development of aptasensors based on different detection techniques from optical to electrochemical routes. However, in the niche of potentiometric sensors, OCP has still not been investigated.

PSA is a 30 kDa protein found in blood and is the sole biomarker currently used for prostate cancer (PCa). PCa is the most commonly diagnosed cancer amongst men in Europe and the USA, and is the second-highest cause of cancer-related morbidity worldwide (Jeong *et al.*, 2010). Changes in PSA levels in the blood can be used for PCa screening with levels higher than the cut-off level of 4 ng/mL prompting biopsy procedures to be considered (Catalona *et al.*, 1991; Healy *et al.*, 2007; Jeong *et al.*, 2010; Savory *et al.*, 2010).

A range of assays for PSA such as electrochemical assays (Okuno *et al.*, 2007), cantilever assay (Wee *et al.*, 2005), enzyme-linked immunosorbent assay (Acevedo *et al.*, 2002), and chemiluminescent immunoassay (Albrecht *et al.*, 1994; Seto *et al.*, 2001) have been developed, which are mostly based on antibodies as the recognition

elements. In recent studies (Jolly *et al.*, 2015; Liu *et al.*, 2012; Savory *et al.*, 2010), instead of using antibodies as the recognition elements, an anti-PSA DNA aptamer was utilised to detect PSA. The development of an anti-PSA DNA aptamer was first demonstrated by Savory *et al.* (2010), since then, only one group reported the detection of PSA using anti-PSA DNA aptamers (Liu *et al.*, 2012). Until recently, Jolly *et al.* (2015) reported a simple and sensitive aptasensor via Electrochemical impedance spectroscopy (EIS) measurement by employing a new type of thiol terminated sulfobetaine molecules.

With the motivation to explore and develop a simple and cost-effective OCP measurement system for research, and an interest in cancer research, a study of the detection of prostate cancer biomarkers is reported in this chapter by employing the true OCP measurement system as an electrochemical characterisation tool.

3.2 Experimental Preparation and Characterisation Method

3.2.1 Electrochemical Characterisation

OCP measurements were carried out using the latest edition custom design electronic measurement system based on the INA116 ultra-low input bias current instrumentation amplifiers design. The simultaneous measurement setup, illustrated in Figure 3-1, consisted of a linear array of four working electrodes with a radius of 2.0 mm, an Ag/AgCl (3 M NaCl) reference electrode (BASi, USA), and a platinum wire (ALS Co., Japan) for grounding the solution in the electrochemical cell.

The working electrode linear array was prepared in-house by thermal evaporation (BOC Edwards, USA) with 20 nm thickness of chromium and 100 nm thickness of gold on a glass slide. The OCP was measured in a solution of 10 mM phosphate buffer (PB) (pH 7). The reference electrode was connected via a salt bridge filled with the same 10 mM PB (pH 7) solution. The OCP was recorded in real time; solutions of PSA from the lowest to the highest concentrations were injected into the flow cell. A multiplexed design of four working electrodes was measured at the same time through

four different channels for the potential changes, by using a common reference electrode.

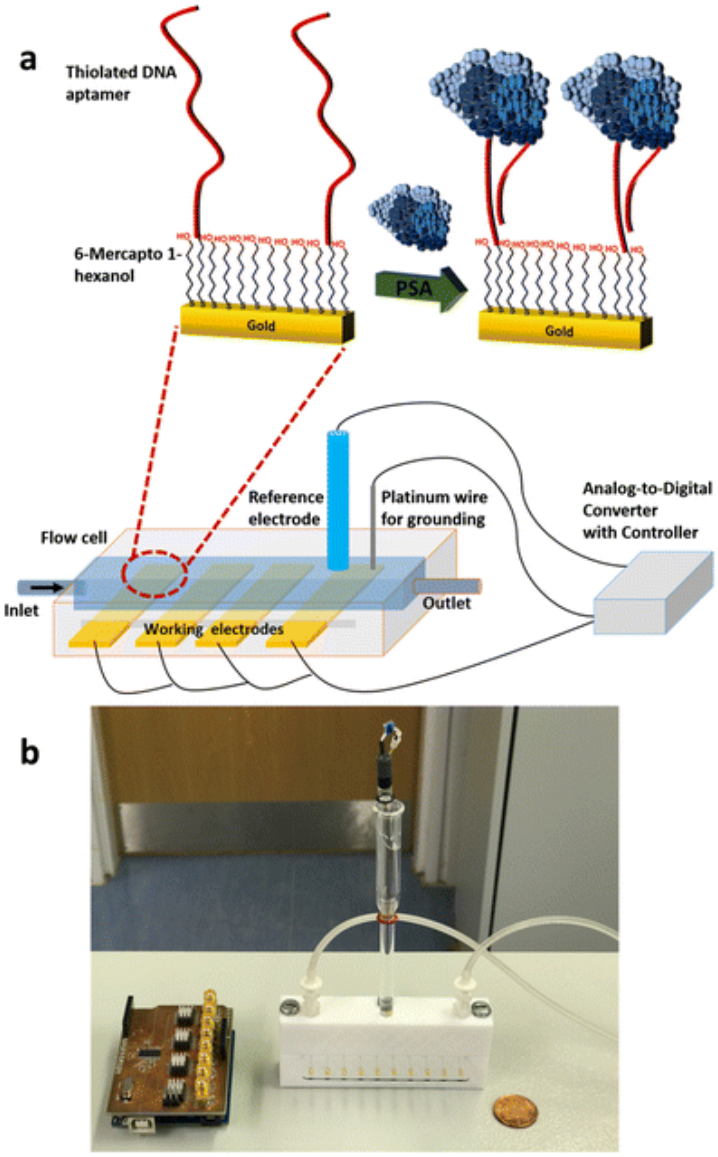

Figure 3-1 (a) An illustration of the whole OCP system setup, including the fabricated PSA aptasensor loaded in a flow cell. (b) A photo of the flow cell and circuit board.

Binding studies were carried out under a flow rate of 100 µl/min using a peristaltic pump (323-Du, Watson Marlow, UK) and an in-house built polytetrafluoroethylene

(PTFE) flow cell with an inner chamber of approximate dimensions 25 mm^3 × 8 mm^3 × 5 mm^3 (length × width × height) and an internal volume of 1 ml.

3.2.2 Fabrication of PSA Aptasensor

Experiments with PSA aptamer were performed using the gold evaporated electrodes following a previously reported protocol (Formisano *et al.*, 2015; Jolly *et al.*, 2015). Briefly, the clean gold electrodes were exposed to 5 µl of immobilisation solution containing thiolated DNA aptamer and 6-mercapto-1-hexanol (MCH, Sigma, UK) for 16 h in a humidity chamber. An optimised 0.5% DNA aptamer mole fraction to total thiol was used to fabricate the biosensor (Formisano *et al.*, 2015). A high concentration of MCH (10 mM) was prepared in pure ethanol which was then diluted in 10 mM PB (pH 7) to the required working concentrations. Prior to addition of MCH, DNA aptamers were heated to 95 °C for 10 min followed by gradual cooling over 30 min to room temperature (Savory *et al.*, 2010). After immobilisation, the electrodes were rinsed with excess Milli-Q water to remove unattached thiols. In order to ensure complete thiol coverage of the gold surface, the electrodes were thereafter backfilled with 1 mM MCH for 1 h. The electrodes were then rinsed with Milli-Q water and placed in 10 mM PB (pH 7) for stabilisation.

3.2.3 Binding Studies

The fabricated DNA aptamer modified electrodes were hosted in a cell with an automated flow system. Injections of analyte were performed in 15 min intervals under a flow rate of 100 µl/min. Different concentrations of PSA from 0.1 ng/mL to 100 ng/mL were prepared in 10 mM PB (pH 7) from stock solutions. Control proteins such as 100 ng/ml hK2 and 66 mg/ml HSA were also prepared in 10 mM PB (pH 7).

3.3 Results and Discussion

3.3.1 Real-Time OCP Measurements

The OCP data was monitored in real time for live display and recording. All the points of the measurement are plotted through a voltage (OCP) *vs.* time graph. Thus, even the smallest changes can be viewed in real time during the experiment. The data is recorded into a table with timestamp and OCP value and saved in a spreadsheet format. Variations of the OCP values show the binding activity of the biomolecules, and further analysis such as dose response can be obtained through calculation and comparison analysis.

3.3.1.1 Stability of the System

Before any investigation on a biosensor for the detection of binding activities, it is vital to start with a high stability measurement system to undertake this kind of continuous sampling biological detection experiments. It is important that the system has high stability, with low noise and accurate measurement output, in order to obtain the true OCP signal data. With the continuous monitoring ability from the true OCP platform, this could be a simple and convenient electrochemical characterisation tool to obtain reliable data via OCP measurement. While other electrochemical characterisation techniques have been widely used; these are not the best way to perform stability test or extended duration experiments, since most of these other techniques may alter the biosensor surface when a current is applied, changing the configuration of the biosensor surface, or simply that they are not capable of continuous monitoring approach. To achieve a continuous low noise and stable OCP signal, the final system has implemented the techniques we have discussed in Chapter 2 and Appendix I. Without the optimisation of the OCP electronics, noise up to 1 mV and unstable shifting signals could occur, which is unsuitable to start the OCP measurement. A comparison of an optimised initialisation and an unoptimised initialisation of the OCP signal is illustrated in Figure 3-2.

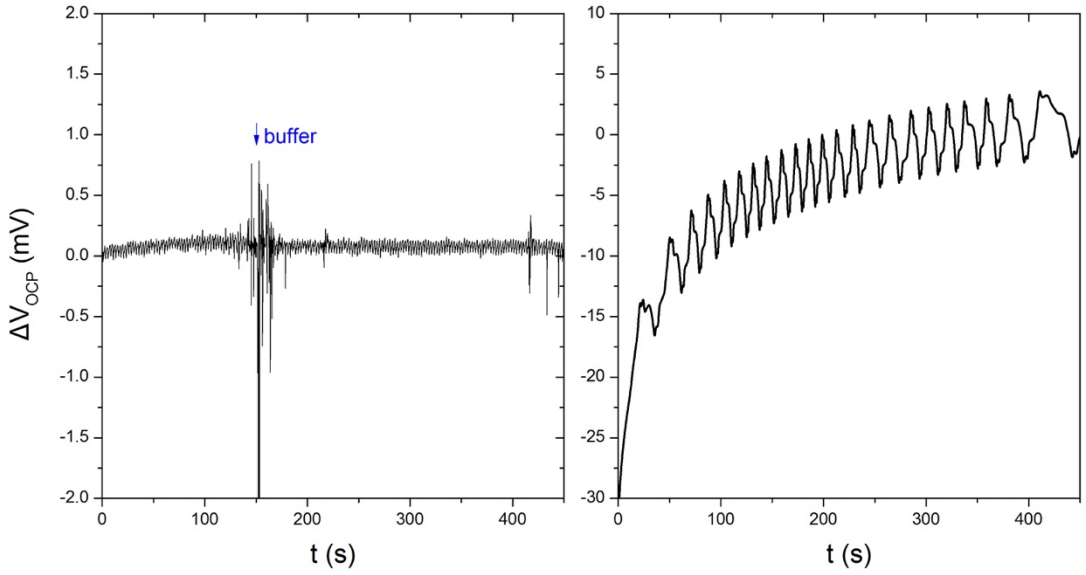

Figure 3-2 (Left) An optimised initialisation OCP signal of the change in OCP *vs* time, with an injection of buffer (blank solution). Showing the optimised stability and noise. (Right) An unoptimised initialisation OCP signal. Showing an unsuitable initialisation signal to start OCP detection.

Temperature is also a key factor that can affect the stability of the OCP measurement. In order to control the continuous measurement under a stable environment, a stable temperature is provided and monitored throughout the measurement. The experiment is setup in a clean room that have regulated room temperature. The room is regulated continuously at 25 °C for all experiments. An electronic controlled water bath is used in the setup to control the temperature of the cell, which hosts the electrodes and detections take place. All solutions are kept under room temperature until being used.

3.3.1.2 Multichannel Approach

Multichannel measurements can reduce time consumption from the whole experiment and minimise the errors from separating experiments one to another. Figure 3-3 shows a typical real-time OCP data plot for the fabricated aptasensor upon injection of different concentrations of PSA in four separate channels of the linear array of electrodes.

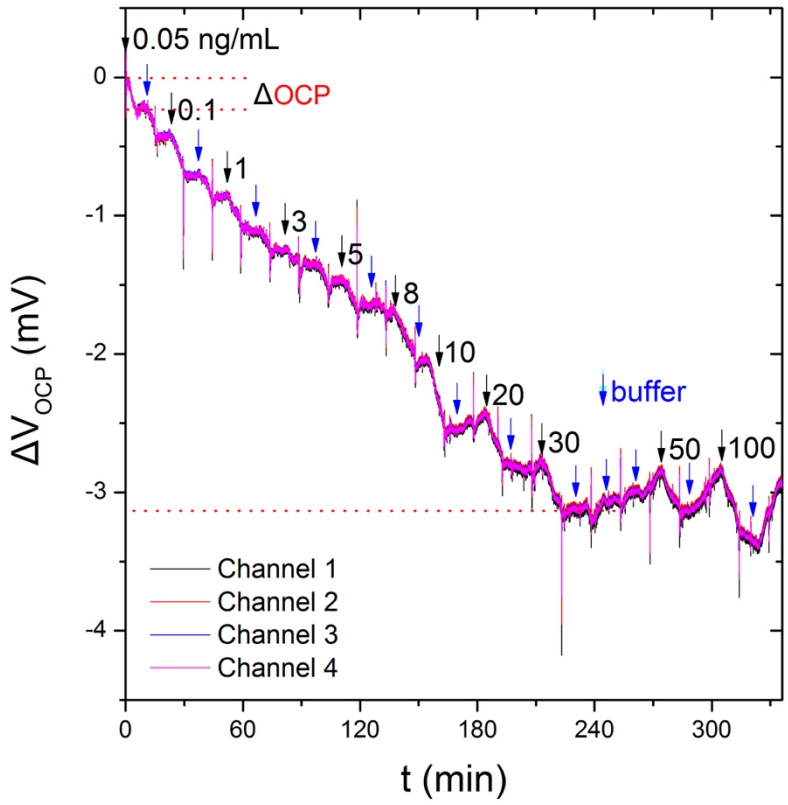

Figure 3-3 A typical OCP behaviour of the aptasensor with the response of consecutive injections of different concentrations of PSA (black arrows) and rinsing buffer (blue arrows) on four separate electrodes of the array. The numbers next to the black arrows indicate the PSA concentrations injected. The inset shows the initialisation of the OCP measurement with an injection of buffer (blank solution).

The OCP value decreases for increasing concentrations of PSA (starting from 0.01 ng/ml), until it reaches saturation at around 20 ng/ml ($\Delta V_{OCP} \sim -3$ mV). As a control, samples containing the same volume of buffer without any PSA were also injected into the cell; no significant further variations in OCP were observed, indicating the variations measured are due to binding of PSA. It is worth mentioning that spikes in the measurements are observed when buffer or PSA sample enters the chamber, but the values stabilise after 15 min. As shown in the Figure 3-2, upon injection of buffer, the OCP returns to its original value. All four channels give identical responses to both PSA and buffer injections.

Without a proper method for multiplexing of the electronic circuit, cross-talks and noise occurs during switching of channels. To eliminate the errors, the method shown in 2.2.1 was selected to for the detection electronic circuitry.

3.3.2 Analytical and Selectivity Performance

3.3.2.1 Dose-Response and Linear Dose-Response

Quantitative assessment relies on constructing dose-response curves (Snyder, 1984), this is normally used in order to quantify the effect of drug added to a cell population over a range of concentrations (Fallahi-Sichani *et al.*, 2013). In this case study, a dose-response curve was obtained using all the four channels and is presented in Figure 3-4. An OCP signal change of -0.880 ± 0.005 mV is observed for 0.1 ng/ml of PSA, decreasing down to -2.850 ± 0.020 mV for 20 ng/ml.

Such a decrease in the OCP signal could be attributed by many factors. In Wang *et al.* (1981) and Zhang *et al.* (1995) studies, an isoelectric point, which is the pH of a particular molecule that carries no net charge (neutral), of PSA between 6.8 and 8 was reported, depending on the amount of glycosylation. As the OCP measurement was performed in 10 mM PB (pH 7), the decrease in OCP signal could be due to the combined effect of folding of DNA aptamer and the charge of PSA at pH 7. Upon binding of PSA to the immobilised DNA aptamer, the DNA aptamer undergoes a change in conformation causing more negative charges closer to the electrode surface. It is likely that the PSA is either neutral or negatively charged depending upon the amount of glycosylation sites. Further injections of PSA do not change this saturation signal. Although the data shows a higher error bar for the injection of 0.05 ng/ml, the error could be due to the very low concentration of PSA that has been captured on the relatively large sensor surface and the dilution process during preparation.

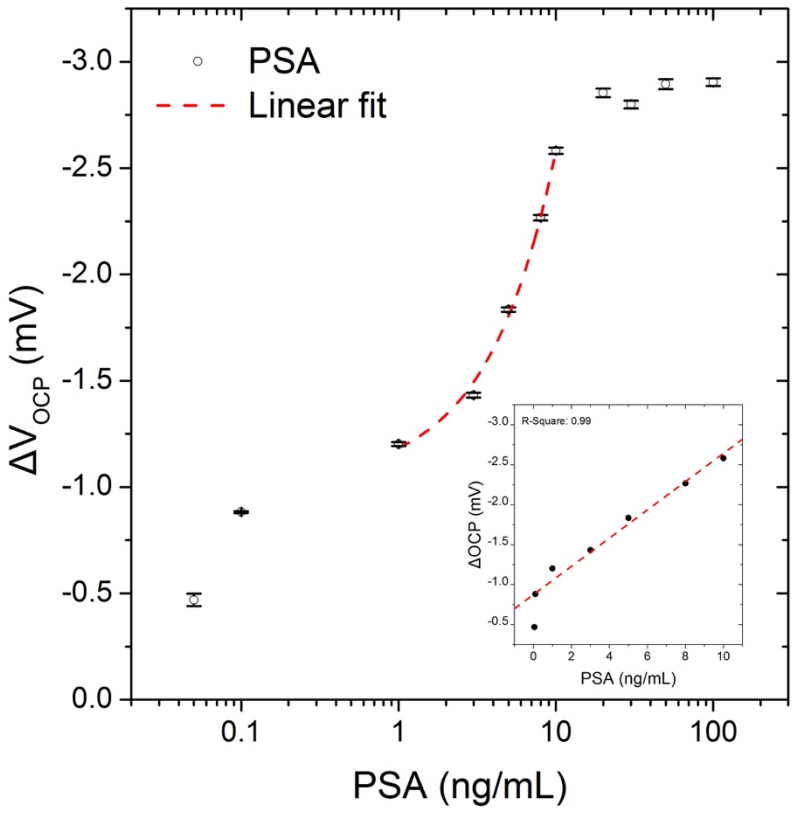

Figure 3-4 Dose-response curve of the aptasensor. The points represent the average for four channels. The line represents a linear fit to the points between 1 and 10 ng/ml (as shown in the inset using a linear scale). Error bars represents the minimum and maximum changes of OCP when the corresponding concentration of PSA is injected.

A consistent decrease in biological response upon binding of PSA was observed. A linear response is obtained from 0.1 to 10 ng/ml with an R^2 value of 0.99. The sensor can differentiate 0.1 ng/ml from blank measurements, which is well below the required clinical range (>1 ng/ml). Such an observation indicates that the sensitivity of the OCP measurement system is capable of differentiating small molecules (PSA is a single-chain polypeptide with a molecular mass of ≈30 kDa), binding activities and concentrations, furthermore, providing a new platform for drug discovery and analysis. With the results from the OCP measurement system, a 600-fold increase in sensitivity was achieved (Wong *et al.*, 2017) with the aptasensor via OCP response *vs.* impedance response by comparing with Jolly *et al.* (2015), for a simple aptamer/mercaptohexanol self-assembled monolayer approach.

3.3.2.2 Clinical level performance

After successful detection of PSA, the aptasensor was studied for non-specific binding. Moving from research to a clinical environment test, the fabricated sensor was further challenged with two control proteins: human serum albumin (HSA, 4%) and human kallikrein2 (hK2, 100 ng/mL). hK2 is another serine protease from the same kallikrein family as PSA and was chosen as a stringent control protein since is it shares 80% homology with PSA. Although the levels of hK2 in clinical samples are 100-fold lower than that of PSA, a much higher concentration of 100 ng/ml of protein was used to stringently evaluate the aptamer-based detection of PSA (Hong, 2014). A negligible change with hK2 (−0.174 ± 0.025 mV) was observed as compared to the signal change from PSA with same concentration (−2.900 ± 0.018 mV), plotted in Figure 3-5. This clearly indicates the specificity of the aptamer towards PSA.

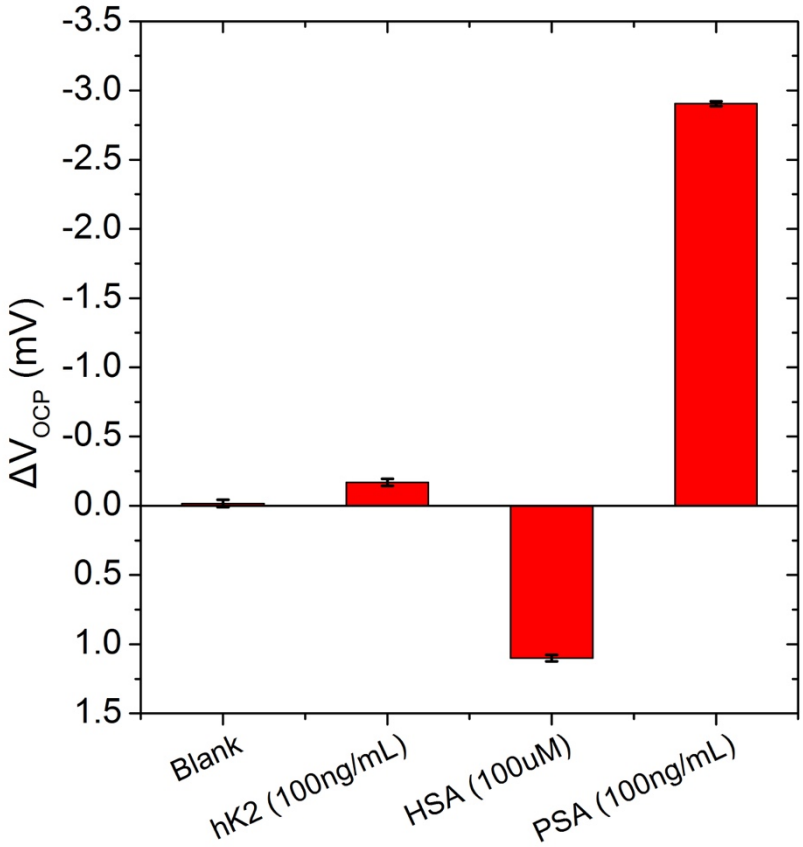

Figure 3-5 A comparison of response with blank, hK2 (100 ng/ml), HSA (66,000 ng/ml) and PSA (100 ng/ml) fabricated sensors.

As a further control, 4% HSA (*circa* 66 μg/ml) was used as a control protein since it is a major constituent of blood. The 4% HSA that have been used contains a much higher concentration when compared to the concentration of both hK2 and PSA. This is a key point of consideration that has been made in order to examine the antifouling efficiency of the fabricated aptasensor for its application when dealing with real blood samples. For comparison, a change of +1.100 ± 0.024 mV was observed with HSA in the opposite direction as of PSA. Such a signal change with HSA could be attributed to non-specific interaction of HSA with the SAM, due to the sticky nature of HSA as a protein. A total coverage with HSA over the SAM was made by adding the high concentration of HSA to the sensor. As HSA is known to be a bulky protein, even an attachment of the smallest amount can cause a change in the dielectric layer of the sensor surface, causing an opposite change of OCP. These effects that were observed with HSA can also be due to multiple reasons, such as blocking effect, charge effect, etc. A similar opposite response has been previously reported for impedance PSA aptasensors (Formisano *et al.*, 2015; Jolly *et al.*, 2015). These results, through a series of OCP measurement, indicate that the sensor can not only differentiate non-specific interactions in clinical level environment, but the aptamer clearly shows outstanding selectivity towards PSA. Future work can be done in order to understand the binding activities during the addition of HSA.

3.4 Summary

This chapter has presented the development of multichannel OCP measurement system with the detection of prostate cancer biomarkers as a case study for the characterisation of the OCP measurement system. This chapter presented and discussed the investigation of the system stability with simultaneous multichannel measurement in real time. Although optimisation of the measured OCP was a challenge, the multiple assembly techniques used for the electronic circuitry were able to minimise the noise in the signals and perform accurate measurement with stability. A full OCP measurement system is presented and discussed in the case study and the investigation of the sensor differentiation ability was performed.

PSA has been widely used for PCa screening and has been an important biomarker for PCa detection up to date. A lot of studies had been published with PSA, however there is only a limited amount of publications on PSA detection with the use of DNA aptamers, and none of them are studied with OCP. The experimental work in this chapter was published and presented a sensitive label-free, cost-effective OCP system that can be used to develop sensitive aptasensors. The investigation of the sensor differentiation ability with the analytical and selectivity performance was performed under OCP, showing the OCP measurement system has a good ability to study different kinds of electrochemical systems. A dose-response curve was obtained through the detection of a wide range of concentrations of PSA (0.1 to 100 ng/mL). The aptasensor developed for PSA using this OCP detection technique demonstrated a 600-fold increased sensitivity with similar aptasensor using EIS. The sensor displayed good selectivity when challenged with stringent control proteins. The aptasensor challenged with HSA (4%) and hK2 (100 ng/mL) for non-specific binding fully demonstrated the ability of the OCP measurement system to be used in a clinical environment. Furthermore, this study also shows the importance to obtain a stable and optimised signal before starting the OCP measurement, in order to perform the performance studies and differentiate the results on experiment with such low OCP changes. This strategy can be easily adapted for the detection of a wide range of biomarkers in a multiplexed platform using not only aptamers but also other receptor molecules such as peptides, antibodies and lectins.

References

Acevedo, B., Perera, Y., Ruiz, M., Rojas, G., Benitez, J., Ayala, M. & Gavilondo, J. 2002. Development and validation of a quantitative elisa for the measurement of psa concentration. *Clinica Chimica Acta,* 317**,** 55-63.

Albrecht, S., Brandl, H., Steinke, M. & Freidt, T. 1994. Chemiluminescent enzyme-immunoassay of prostate-specific antigen based on indoxyl phosphate substrate. *Clinical Chemistry,* 40**,** 1970-1971.

Bruno, J.G. 2015. Predicting the uncertain future of aptamer-based diagnostics and therapeutics. *Molecules,* 20**,** 6866-6887.

Catalona, W.J., Smith, D.S., Ratliff, T.L., Dodds, K.M., Coplen, D.E., Yuan, J.J.J., Petros, J.A. & Andriole, G.L. 1991. Measurement of prostate-specific antigen in serum as a screening-test for prostate-cancer. *New England Journal of Medicine,* 324**,** 1156-1161.

Fallahi-Sichani, M., Honarnejad, S., Heiser, L.M., Gray, J.W. & Sorger, P.K. 2013. Metrics other than potency reveal systematic variation in responses to cancer drugs. *Nature Chemical Biology,* 9**,** 708-+.

Formisano, N., Jolly, P., Bhalla, N., Cromhout, M., Flanagan, S.P., Fogel, R., Limson, J.L. & Estrela, P. 2015. Optimisation of an electrochemical impedance spectroscopy aptasensor by exploiting quartz crystal microbalance with dissipation signals. *Sensors and Actuators B-Chemical,* 220**,** 369-375.

Healy, D.A., Hayes, C.J., Leonard, P., McKenna, L. & O'Kennedy, R. 2007. Biosensor developments: Application to prostate-specific antigen detection. *Trends in Biotechnology,* 25**,** 125-131.

Hong, S.K. 2014. Kallikreins as biomarkers for prostate cancer. *Biomed Research International*.

Jeong, S., Han, S.R., Lee, Y.J. & Lee, S.W. 2010. Selection of rna aptamers specific to active prostate-specific antigen. *Biotechnology Letters,* 32**,** 379-385.

Jolly, P., Formisano, N., Tkac, J., Kasak, P., Frost, C.G. & Estrela, P. 2015. Label-free impedimetric aptasensor with antifouling surface chemistry: A prostate specific antigen case study. *Sensors and Actuators B-Chemical,* 209**,** 306-312.

Lee, J.W., Kim, H.J. & Heo, K. 2015. Therapeutic aptamers: Developmental potential as anticancer drugs. *Bmb Reports,* 48**,** 234-237.

Liu, B., Lu, L.S., Hua, E.H., Jiang, S.T. & Xie, G.M. 2012. Detection of the human prostate-specific antigen using an aptasensor with gold nanoparticles encapsulated by graphitized mesoporous carbon. *Microchimica Acta,* 178**,** 163-170.

Mairal, T., Ozalp, V.C., Sanchez, P.L., Mir, M., Katakis, I. & O'Sullivan, C.K. 2008. Aptamers: Molecular tools for analytical applications. *Analytical and Bioanalytical Chemistry,* 390**,** 989-1007.

Okuno, J., Maehashi, K., Kerman, K., Takamura, Y., Matsumoto, K. & Tamiya, E. 2007. Label-free immunosensor for prostate-specific antigen based on single-walled carbon nanotube array-modified microelectrodes. *Biosensors & Bioelectronics,* 22**,** 2377-2381.

Savory, N., Abe, K., Sode, K. & Ikebukuro, K. 2010. Selection of DNA aptamer against prostate specific antigen using a genetic algorithm and application to sensing. *Biosensors & Bioelectronics,* 26**,** 1386-1391.

Seto, Y., Iba, T. & Abe, K. 2001. Development of ultra-high sensitivity bioluminescent enzyme immunoassay for prostate-specific antigen (psa) using firefly luciferase. *Luminescence,* 16**,** 285-290.

Snyder, R. 1984. Basic concepts of the dose-response relationship. *Acs Symposium Series,* 239**,** 37-55.

Wang, M.C., Papsidore, L.D., Kuriyama, M., Valenzuela, L.A., Murphy, G.P. & Chu, T.M. 1981. Prostate antigen - a new potential marker for prostatic-cancer. *Prostate,* 2**,** 89-96.

Wee, K.W., Kang, G.Y., Park, J., Kang, J.Y., Yoon, D.S., Park, J.H. & Kim, T.S. 2005. Novel electrical detection of label-free disease marker proteins using piezoresistive self-sensing micro-cantilevers. *Biosensors & Bioelectronics,* 20**,** 1932-1938.

Wong, L.C.C., Jolly, P. & Estrela, P. 2017. Development of a sensitive multiplexed open circuit potential system for the detection of prostate cancer biomarkers. *BioNanoScience,* 8(2), 701-706.

Zhang, W.M., Leinonen, J., Kalkkinen, N., Dowell, B. & Stenman, U.H. 1995. Purification and characterization of different molecular-forms of prostate-specific antigen in human seminal fluid. *Clinical Chemistry,* 41**,** 1567-1573.

CHAPTER 4.

OCP Detection of DNA – DNA Interaction with Intercalator

This chapter investigates the detection of DNA – DNA interaction on gold electrode through open circuit potentiometry (OCP), with the use of a novel cobalt complex $[Co(GA)_2(aqphen)]Cl$ for enhancing the signal upon its attachment to dsDNA. The effect on DNA hybridisation and attachment of the compound are discussed. The use of electrochemical impedance spectroscopy (EIS) to validate the open circuit potential (OCP) changes is also presented.

The work presented in this chapter has been partly published in Regan *et al.* (2014). The author contributed to this research on the background research, the electronic hardware design and software programming of the OCP system, the preparation of gold working electrodes, the fabrication of DNA sensors, the electrochemical characterisation measurements with both EIS and OCP detection techniques, and the EIS and OCP analytical study of the DNA – DNA interaction with intercalator.

4.1 Introduction

The use of the intrinsic charge carried by the phosphate backbone of DNA for hybridisation detection has gained a high interest from the research field. The charge distribution and the charge density at the electrode-solution interface upon target DNA

hybridisation produces a change on the overall potential, which can be detected as a measurable potential change through OCP. Upon hybridisation, changes of the interfacial electrochemical impedance also enable the use of electrochemical impedance spectroscopy (EIS), cyclic voltammetry (CV) and differential pulse voltammetry (DPV) to detect the binding events that occur.

Label-free detection can be achieved since the potential change is generated by the intrinsic charge carried by the target DNA. Direct detection of hybridisation by label-free techniques is often more desirable in comparison to labelled techniques as they have less sample processing steps. Other advantages include the simplicity of direct detection through electrical readout and the compatibility of multiplexing array integration. Charge based detection methods have been considered as promising electrochemical detection techniques for DNA sensing.

An indirect labelling method by intercalating molecules has been used as signal enhancer while offering the same simplicity and compatibility described above, without requiring direct labelling of the target nucleic acid sequence. When the novel cobalt complex $[Co(GA)_2(aqphen)]Cl$ intercalates with dsDNA, the compound enhances the signal specifically to dsDNA upon attachment. The compound distorts the dsDNA helical structure, changing the overall charge distribution on the surface and affecting the electrostatic barrier to charge redox markers in solution, which could be detected with OCP and EIS/CV/DPV. The compound demonstrated the first sample of a signal compound that can enhance amperometric, impedimetric, and potentiometric signals for DNA detection. These findings enable the development of label-free techniques and multi-modal approaches for DNA detection.

In this chapter, charge changes, which alter the charge distribution upon DNA hybridisation, and intercalator attachment to dsDNA are both studied using OCP. The results are compared to EIS measurements. Through the understanding of these measurements of charge charges, the development of the OCP circuitry design was initiated.

4.1.1 Intercalator - the Cobalt Complex [Co(GA)$_2$(aqphen)]Cl

Intercalating molecules have been used to provide a further signal change to detect DNA hybridisation in various papers; these include cationic metal complexes, anti-cancer drugs (epirubicin, mitoxantrone), antibiotics (daunomycin) and redox-active molecules (methylene blue). (Erdem *et al.*, 2000; Erdem and Ozsoz, 2001a, b; Hashimoto *et al.*, 1994; Ozkan *et al.*, 2002; Yang *et al.*, 2007) Co(III), Ru(II), Fe(II) and Os(II/IV) suitable with commercially available ligands like 1,10-phenanthroline (phen) and 2,2'-bipyridine are used by cationic metal complexes which have been experimented in papers. (Del Pozo *et al.*, 2005; Erdem *et al.*, 1999b; Kara *et al.*, 2002; Millan and Mikkelsen, 1993; Pang and Abruna, 1998) These substances with reversible redox probes interact with ssDNA and dsDNA in different ways, which can provide a difference in signal upon attachment, thus allowing it changes upon attachment to dsDNA be measured and differentiated from attachment to ssDNA or non-specific binding. Studies have applied cationic metal complexes on the detection of DNA and antioxidants (Liu *et al.*, 2006), the detection of DNA related to hepatitis B virus (Erdem *et al.*, 1999a, 2000), calf thymus DNA and polynucleotides (Del Pozo *et al.*, 2005; Erdem *et al.*, 1999b; Millan and Mikkelsen, 1993). These studies have shown that in various types of detection, mostly through DPV and CV, different types of intercalators have been used to enhance the detection of the measured signal. For further signal enhancement, properties such as binding affinity, solubility and chemical stability within the intercalator could be modified. In this study, a cobalt complex is modified to show further enhancement of binding affinity of the complex to dsDNA and demonstrating as the first example of multimodal applications using metal complexes.

As an enhancer, which only attaches to dsDNA, the cobalt complex was designed to enhance the signal for DNA hybridisation and could act as a sensitive redox probe. Based on a study by Lin *et al.* (2011), a substance from the group was modified to form the cobalt complex [Co(GA)$_2$(aqphen)]Cl. The original cobalt complex used by Lin *et al.* (2011), containing a mixed ligand coordination sphere of 1,10-phenanthroline (phen) and glycolic acid (GA), demonstrated the ability to bind to dsDNA in the intercalative mode.

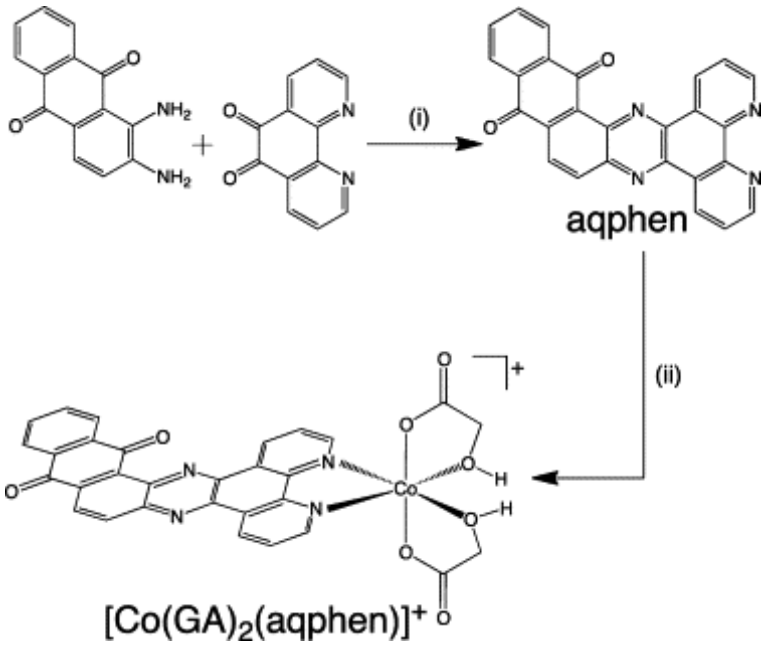

Figure 4-1 Structure of the cobalt complex [Co(GA)2(aqphen)]Cl with synthetic route. (i) EtOH, heat; (ii) EtOH, 1 eq. CoCl2•6H2O, 2 eq. glycolic acid/NaOH(aq). (Adapted from Regan et al. (2014))

In this study, the cobalt complex (Figure 4-1) was modified by collaborators at Cardiff University group (Regan *et al.*, 2014) to make the complex contain an extended planar ligand (aqphen = naphtho[2,3-a]dipyrido[3,2-h:2',3'-f]phenazine-5,18-dione) (Lopez *et al.*, 1996) with a conjugated anthraquinone unit. Improving the binding affinity to dsDNA of the cobalt complex showed an overall improvement for detection. The cobalt complex compound is designed to only bind to dsDNA, and thus, this modified cobalt complex is the first metal complex that is designed for multi-modal application. This can be used to enhance amperometric, impedimetric DNA detection, and now, potentiometric DNA detection through OCP, without the need for further multi-step amplification techniques. This could simplify and shorten the whole experimental work.

According to the molecular docking studies carried out in Cardiff University with AutoDock Vina (Trott and Olson, 2010), the cobalt complex $[Co(GA)_2(aqphen)]Cl$ with a $Co(GA)_2(aqphen)$ structure, is expected to intercalate with DNA between the base pairs as shown in Figure 4-2.

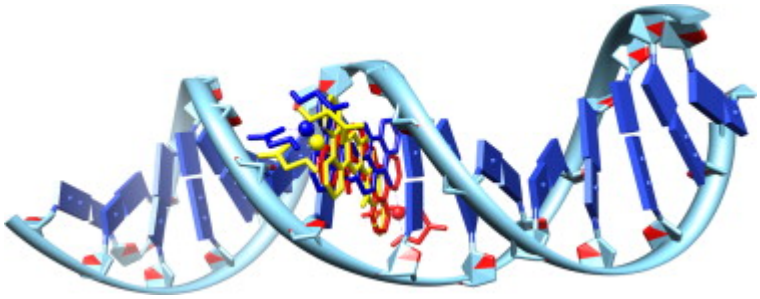

Figure 4-2 Top 3 docked poses for Co(GA)2(aqphen) interacting with the DNA sequence open-d(ATCGAGACGTCTCGAT)$_2$. Top 3 docked poses for Co(GA)2(aqphen) interacting with the DNA sequence open-d(ATCGAGACGTCTCGAT)$_2$. (Adapted from Regan et al. (2014))

A developed DNA structure (Jones *et al.*, 2011) including a pre-formed intercalation gap, open-d(ATCGAGA**CG**TCTCGAT)$_2$, was used as the biomacromolecular target in this study. Base on the structure, the cobalt complex is expected to interact with the DNA between its basepairs, which then differs the structure and has the ligand pairing electron delocalisation.

By attachment of the cobalt complex to this specific dsDNA sequence, the complex is designed so that it causes conformational changes to the DNA, which will reform the surface charge distribution. Thus, causing an overall potential change in OCP.

4.1.1.1 Synthesis and General Analysis of [Co(GA)$_2$(aqphen)]Cl

The cobalt complex was modified by collaborators at Cardiff University group (Regan *et al.*, 2014) with the following protocol.

Under a nitrogen atmosphere, $CoCl_2 \cdot 6H_2O$ (0.137 g, 0.576 mmol) was dissolved in ethanol (10 mL) and mixed with naphtho[2,3-*a*]dipyrido[3,2-*h*:2′,3′-*f*]phenazine-5,18-dione (aqphen) (0.237 g, 0.576 mmol) for 30 min. Then, an ethanol/water (95:5) solution (10 mL) of glycolic acid (0.090 g, 1.183 mmol) neutralised by KOH (0.066 g, 1.176 mmol) was added and the mixture stirred for 1 h. The resulting orange precipitate was filtered and dried *in vacuum*. Elemental analysis: Calcd. (%) for $C_{30}H_{20}N_4CoO_9Cl$: C, 53.39, H, 2.99, N, 8.30; Found: C, 53.67, H, 2.36, N, 7.86. ES

MS found *m/z* 546.0, calculated *m/z* 546.0 for $[M\text{-}C_2H_3O_3]^+$. HR MS found *m/z* 546.0366, calculated *m/z* 546.0369 for $[C_{28}H_{15}CoN_4O_5]^+$. UV–vis (DMSO): λ_{max} (ε/dm^3 mol^{-1} cm^{-1}) 282 (14650), 405 (3850) nm.

Aqueous stock solutions containing 1 mM $[Co(GA)_2(aqphen)]Cl$ were prepared by dissolving the required amount of the complex in water by heating or by heating to 70 °C in a sonicator bath for one hour.

4.2 DNA – DNA system with intercalator

Here we present the detection of DNA – DNA interaction with intercalator, a schematic of the system is illustrated in Figure 4-3. The potentiometric responses of DNA/DNA hybridisation and the attachment of intercalator are presented with a discussion compared with impedimetric responses.

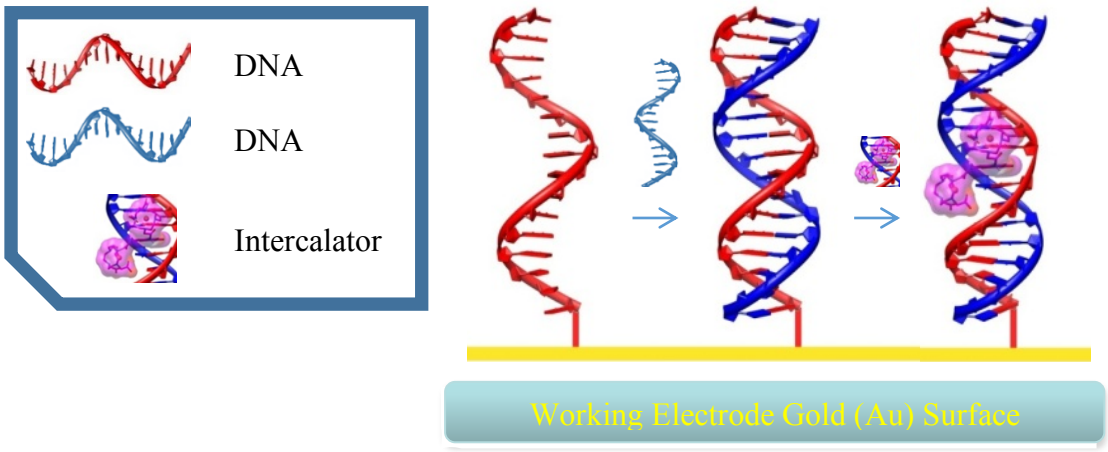

Figure 4-3 Schematic of DNA – DNA system with intercalator. (a) Immobilised DNA probe. (b) Hybridisation with complementary strand DNA. (c) Attachment of intercalator to DNA/DNA duplex.

4.2.1 Experimental Preparation and Characterisation Methods

4.2.1.1 Materials

Thiol-modified and non-modified DNA oligonucleotides were purchased from Sigma–Aldrich (HPLC purified). 6-Mercapto-1-hexanol (MCH, 97%), potassium phosphate monobasic solution (1 M), potassium phosphate dibasic solution (1 M), potassium sulphate, potassium hexacyanoferrate (III), potassium hexacyanoferrate (II) trihydrate, ethylenediaminetetraacetic acid (EDTA, 0.5 M) and magnesium chloride were all purchased from Sigma–Aldrich. $CoCl_2 \cdot 6H_2O$, 1,10-phenanthroline monohydrate and 1,2-diaminoanthraquinone were all used as purchased from Alfa Aesar. All synthesis reactions were performed with the use of vacuum line and Schlenk techniques. All aqueous solutions were prepared using Milli-Q 18.2 MΩ·cm at 25 °C ultra-pure water (Millipore, Billerica, MA, USA), with a Pyrogard filter (Millipore) to produce pyrogen-free & nuclease-free ultrapure water.

4.2.1.1.1 Oligonucleotides

The HPLC purified DNA oligonucleotides and DNA probe sequence used in this work are shown in Table 4-1.

Table 4-1 DNA sequence and DNA probe used in this DNA – DNA system.

Full complementary sequence for DNA probe	5'-TCT TCT TCT TCT TCT TCT TCT-3'
DNA probe: HS-$(CH_2)_6$-	AGA AGA AGA AGA AGA AGA AGA

4.2.1.2 Electrochemical Measurements

4.2.1.2.1 Open Circuit Potentiometry

OCP measurement on DNA hybridisation and attachment of cobalt complex were carried out using the custom made OCP detection electronic circuit described in Chapter 2. A three-electrode configuration was used consisting of a 1.6 mm diameter

gold disc working electrode (ALS Co., Ltd, Japan), a Hg/Hg_2SO_4 (K_2SO_4 sat.) reference electrode (ALS Co., Ltd, Japan) placed into a salt bridge, and a platinum wire (ALS Co., Ltd, Japan) for grounding the solution in the electrochemical cell. OCP was measured in a solution of 10 mM phosphate buffer (PB) pH 7.0. The reference electrode was connected via a salt bridge filled with 10 mM phosphate buffer (PB) pH 7.0. Hybridisation was carried out, followed with attachment of $[Co(GA)_2(aqphen)]Cl$, while OCP measurement was recorded in real time continuously until each step achieved a stable potential.

4.2.1.2.2 Electrochemical Impedance Spectroscopy

The $[Co(GA)_2(aqphen)]Cl$ solutions were prepared by collaborators at Cardiff University group (Regan *et al.*, 2014) at a concentration of 1.0×10^{-3} mol dm^{-3} in dimethylformamide (10 ml) and contained 0.1 mol dm^{-3} $[NBu^n_4][PF_6]$ as the supporting electrolyte. Under these conditions, E^0, for the one-electron oxidation of $[Fe(\eta\text{-}C_5H_5)_2]$ added to the test solutions as an internal calibrant, is +0.45 V vs reference electrode in dimethylformamide.

EIS was performed using a μAutoLab Type III FRA2 potentiostat (Metrohm, UK). A conventional three-electrode configuration was used consisting of a 1.6 mm diameter gold disc working electrode (ALS Co., Ltd, Japan), a Hg/Hg_2SO_4 (K_2SO_4 sat.) reference electrode (ALS Co., Ltd, Japan), and a platinum wire (ALS Co., Ltd, Japan) counter electrode. The electrochemical impedance spectrum was measured in a solution of 2 mM $K_4[Fe(CN)_6]$ + 2 mM $K_3[Fe(CN)_6]$ in 50 mM phosphate buffer (PB) + 100 mM K_2SO_4 pH 7.0, ionic strength 447 mM. The reference electrode was connected via a salt bridge filled with 50 mM PB + 100 mM K_2SO_4pH 7.0. The spectrum was measured over the frequency range of 100 kHz to 0.1 Hz, with a 10 mV a.c. voltage superimposed on a d.c. bias of −0.195 V, which corresponds to the formal potential of the redox couple. The charge transfer resistance (R_{ct}) and double-layer capacitance (C_{dl}) were measured before hybridisation, after hybridisation and after incubation with $[Co(GA)_2(aqphen)]Cl$ for 30 minutes.

4.2.1.3 Preparation of the DNA Self-Assembled Monolayer

The gold disc working electrodes were polished with 1 μm polishing diamond (ALS Co., Ltd, Japan) on a diamond polishing pad (ALS Co., Ltd, Japan), sonication in ultra-pure water, polished with 0.05 μm polishing aluminia (ALS Co., Ltd, Japan) on a aluminia polishing pad (ALS Co., Ltd, Japan), followed by sonication in ultra-pure water to remove polishing particles. In addition, polishing on a blank polishing pad, and sonication in ultra-pure water for a final time to fully remove any remaining particles. Electrodes were subsequently electrochemically cleaned in 0.5 M H_2SO_4 by scanning the potential between the oxidation and reduction of gold, between −0.05 V and +1.1 V versus a Hg/Hg_2SO_4 reference electrode for 60 cycles until there was no further change in the cyclic voltammogram. Electrodes were rinsed with ultra-pure water, dried in a stream of nitrogen, and exposed to 100 μL of mixed DNA/MCH immobilisation solution for 16 h in a humidity chamber.

Probe ssDNA had the 21-base sequence AGA AGA AGA AGA AGA AGA AGA and was modified on the 5′ end to give HS-$(CH_2)_6$-ssDNA. The DNA immobilisation buffer consisted of 0.8 M phosphate buffer (PB) + 1.0 M NaCl + 5 mM $MgCl_2$ + 1 mM EDTA pH 7.0. After immobilisation, electrodes were rinsed in 50 mM PB + 100 mM K_2SO_4 + 10 mM EDTA (pH 7.0) to remove any remaining Mg^{2+}. To ensure complete thiol coverage of the gold surface on the electrodes, the electrodes were backfilled with mercaptohexanol (MCH) by immersion in 100 μL of 1 mM MCH in ultra-pure water for 1 h. Electrodes were then rinsed with ultra-pure water and placed in to 10 mM PB pH 7.0 measurement buffer for 1 h.

4.2.1.4 DNA Hybridisation and $[Co(GA)_2(aqphen)]Cl$ Incubation

4.2.1.4.1 Open Circuit Potentiometry

Electrodes with immobilised DNA/MCH were immersed in the cell with 10 mM PB pH 7.0 measurement buffer. DNA that had a complementary binding sequence to the probe DNA (5′-TCT TCT TCT TCT TCT TCT TCT-3′) was injected into the cell when the OCP achieved a stable potential value. Electrodes were incubated with

complementary DNA (1 μM) diluted in 3ml of 10 mM PB pH 7.0 measurement buffer for 60 min under continuous measurement.

After DNA hybridisation, the cobalt complex $[Co(GA)_2(aqphen)]Cl$ was injected into the bulk solution in the cell. The electrodes were incubated in a mixture containing $[Co(GA)_2(aqphen)]Cl$ for 60 min under continuous measurement (the $[Co(GA)_2(aqphen)]Cl$ in H_2O stock solution was diluted into 3ml of 10 mM pH 7.0 measurement buffer).

The whole process is completed under room temperature at 25 °C to minimise unnecessary effect of the binding activity that is cause by varying temperature. All solutions are prepared and used in the temperature regulated clean room for the same apporach.

4.2.1.4.2 Electrochemical Impedance Spectroscopy

Electrodes with immobilised DNA/MCH were treated with DNA that had a complementary binding sequence to the probe DNA (5'-TCT TCT TCT TCT TCT TCT TCT-3'). Electrodes were incubated with complementary DNA (1 μM) diluted in 3ml of 10 mM PB pH 7.0 measurement buffer for 60 min under continuous measurement. After DNA hybridisation, the electrodes were incubated in a mixture containing $[Co(GA)_2(aqphen)]Cl$ for 60 min under continuous measurement (the $[Co(GA)_2(aqphen)]Cl$ in H_2O stock solution was diluted into 3ml of 10 mM pH 7.0 measurement buffer).

4.2.2 Discussion on DNA Hybridisation with Cobalt Complex

DNA hybridisation and attachment of cobalt complex $[Co(GA)_2(aqphen)]Cl$ for enhancing the OCP signal was investigated with comparison to EIS to show that its ability to enhance was not only in amperometric and impedimetric DNA detection, but also in potentiometric DNA detection.

4.2.2.1 Impedimetric Responses of the System with Electrochemical Impedance Spectroscopy

4.2.2.1.1 Impedimetric Response of DNA Hybridisation

On EIS measurements, the negatively charged redox couple $[Fe(CN)_6]^{3-/4-}$ is used in solution. The negative charge carried by the DNA backbone provides an electrostatic barrier to the redox markers, hindering its charge transfer to the gold electrode. Upon hybridisation, the increase in negative charge on the biolayer enhances this electrostatic barrier, thus further reducing the charge transfer. The measured variation in the values of R_{ct} can hence be used as a signal of DNA binding.

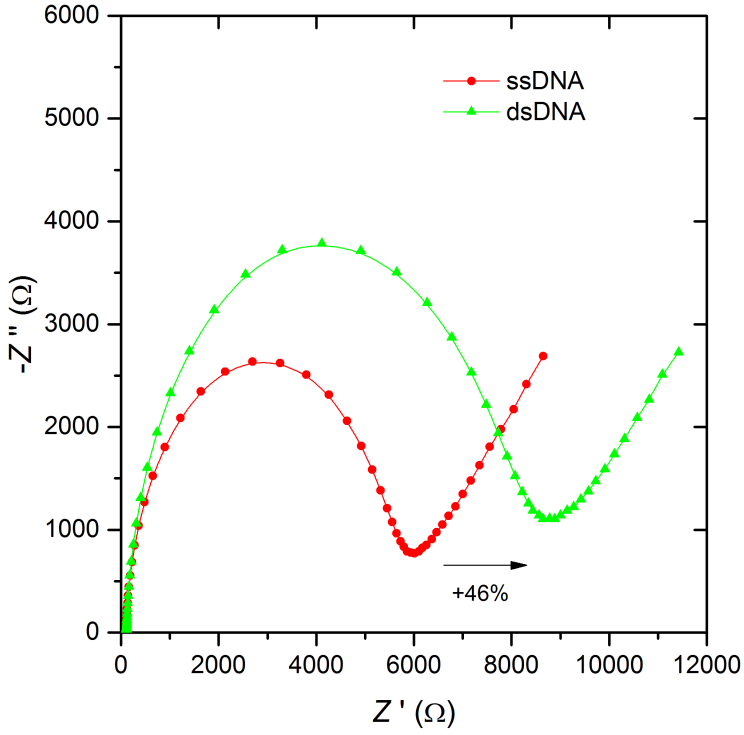

Figure 4-4 R_{ct} of ssDNA and dsDNA (EIS).

Upon hybridisation, the charge transfer resistance corresponds to the point in the Nyquist plot where the semi-circle crosses the Zreal axis, which increases from 5.9 kΩ to 8.6 kΩ. This is increased by 46% upon hybridisation as shown in Figure 4-4. A

set of 3 electrodes are used to validate the results in the experiment, the other two electrodes have an increase to 8.9 kΩ and to 9.2 kΩ. An average change in R_{ct} value upon hybridisation is 51% (SD: ±5.1%), with the experimental set. This result is similar to an increase of 45% previously reported by Keighley *et al.* (2008) using similar immobilisation methods and conditions but with a different length of oligonucleotides.

This large change is mostly due to the negative charge in the biolayer with the combination of the complementary strand DNA, and further blocking of the surface, which obstructs the redox process. No changes in R_{ct} value were observed when injecting non-complementary strand DNA to the sensors. This proved that only successful binding processes can increase the negative charge barrier across the surface of the electrode, thus increasing the value. This correlates to the result given a decrease in OCP upon successful DNA hybridisation.

Sample-to-sample variations in the values of R_{ct} and C_{calc} can be observed during the experiments. To ensure an optimal result, cleanliness of the surface of the gold prior to immobilisation with the biolayer and temperature of the immobilisation process are important to ensure DNA works to its best performance during measurements.

4.2.2.1.2 Impedimetric Response of Cobalt Complex Attachment

The intercalator showed high affinity for random sequences of dsDNA in the micromolar range. Furthermore, it has low oxidation and reduction potentials, which is promising for EIS measurements. Upon attachment of the intercalator to dsDNA, R_{ct} further increases to 9.8 kΩ, which is an additional 10% increase, illustrated in Figure 4-5.

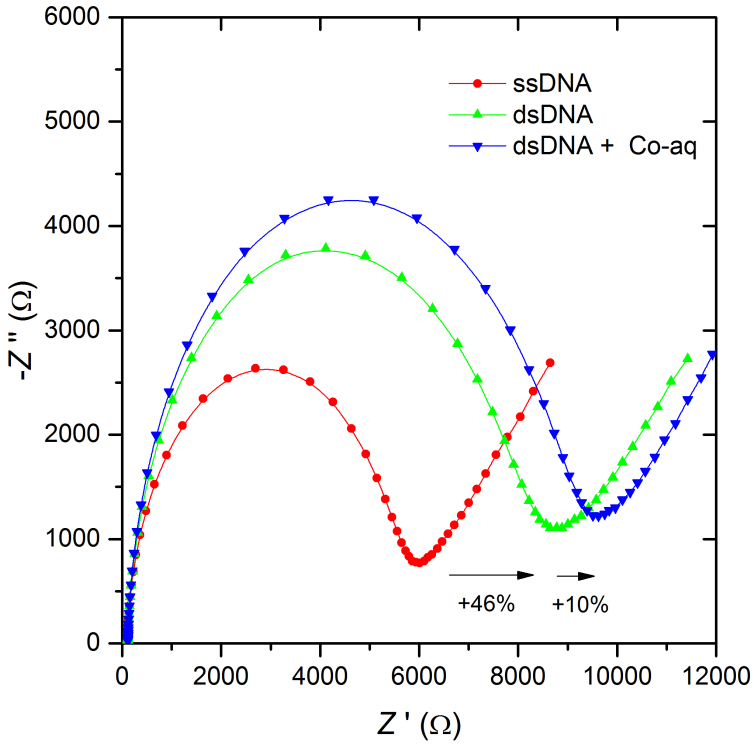

Figure 4-5 Hybridised DNA change in R_{ct} with intercalator (EIS).

The intercalator caused an additional 15.8% (SD: ±6.3%) after attachment with dsDNA. This is a significant enhancement of the signal, showing that this compound has very high potential for applications on DNA sensors.

4.2.2.1.3 Impedimetric Response of Intercalator on Bare Gold Surface

EIS measurements on samples containing only a self-assembled monolayer (SAM) similar to the one used for the DNA immobilisation have shown that the cobalt complex has no interaction with the SAM itself, illustrated in Figure 4-6.

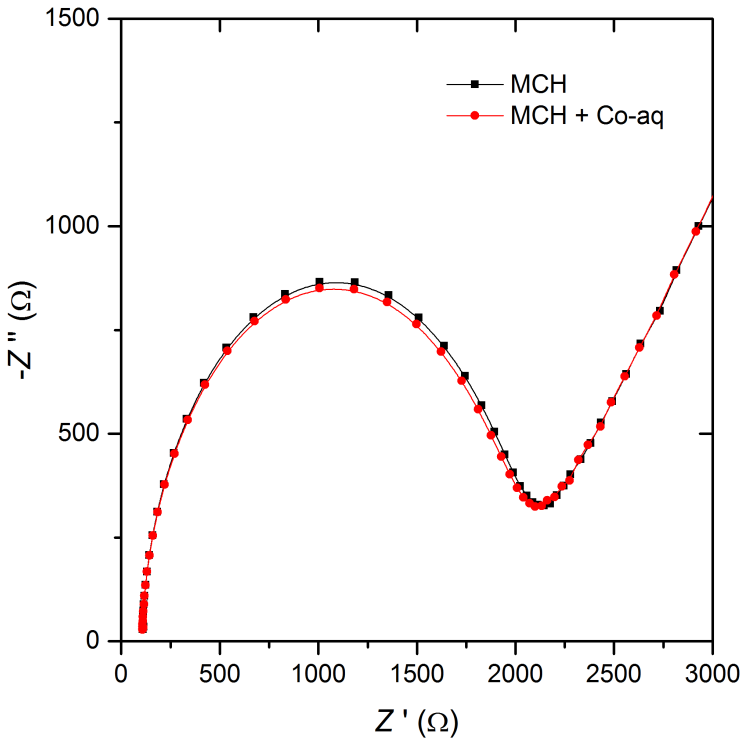

Figure 4-6 Small interaction of intercalator with bare gold surface (EIS).

On the other hand, using bare gold electrodes, very small variations in R_{ct} occur upon addition of the intercalator (~200 Ω), indicating a small interaction of the intercalator with Au.

The results confirm that the signal enhancement is due to intercalation with the DNA – DNA duplex. With the effect of the cobalt complex $[Co(GA)_2(aqphen)]Cl$ on R_{ct} comparing the total change upon MCH, ssDNA + MCH, and dsDNA + MCH shown in Figure 4-7 below, a validation could be made to prove that the change in OCP is due to the attachment of cobalt complex to dsDNA.

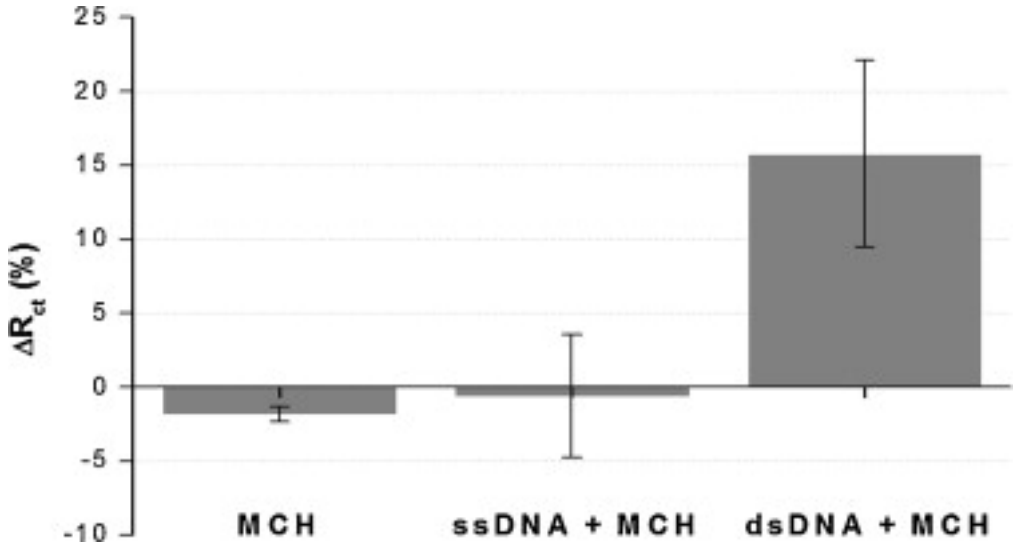

Figure 4-7 The effect of $[Co(GA)_2(aqphen)]Cl$ on charge transfer resistance (R_{ct}). Data are shown for (1) MCH, (2) ssDNA + MCH and (3) dsDNA + MCH. Error bars represent standard deviations of mean values determined from three individual experiments (n = 3).

We believe that the cobalt compound is functioning as a DNA intercalator, thus binding would cause structural changes to the dsDNA biolayer that affect the electrostatic barrier in EIS and an expansion with the dsDNA as it intercalates that affects the charges on the biolayer for OCP.

4.2.2.1.4 Fit and Simulation

Fit and simulation of the EIS results have been done to show the EIS results are correlated to the equivalent circuit model that has been proposed, illustrated in Table 4-2. Hence, the equivalent circuit model can be used as a simplified model to understand the relationship between the different components in the electrochemical system. The three steps include ssDNA, complementary stranded DNA attachment, and finally, intercalator attachment. The simulated results that used the equivalent circuit model demonstrated a good fitting with R_{ct} error ~1.5-1.6% and C_{dl} error ~1.5-1.7% in all steps.

Table 4-2 Fit and simulation. (a) ssDNA. (b) dsDNA. (c) dsDNA + Co-aq.

(a)

Element	Parameter	Value	Error (%)
Rct	R	4052.6	1.476
Cdl	C	9.74E-08	1.669
ZW	Y0	0.0001808	3.627
Ru	R	128.85	2.127
	χ^2	0.22456	

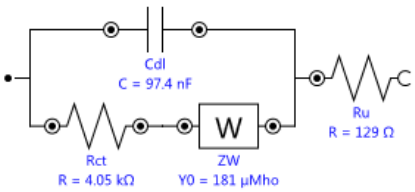

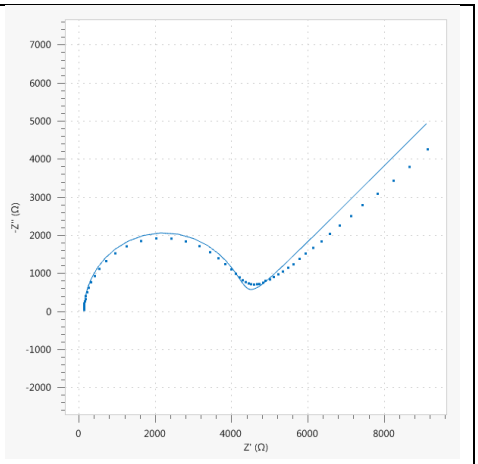

(b)

Element	Parameter	Value	Error (%)
Rct	R	5726	1.362
Cdl	C	9.91E-08	1.483
ZW	Y0	0.00018298	4.212
Ru	R	128.8	1.983
	χ^2	0.19778	

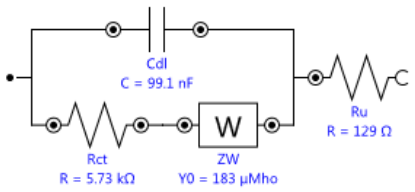

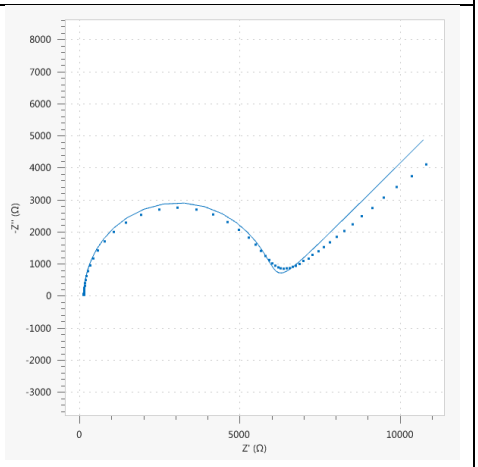

(c)

Element	Parameter	Value	Error (%)
Rct	R	6166.8	1.484
Cdl	C	9.66E-08	1.596
ZW	Y0	0.00018222	4.814
Ru	R	122.47	2.219
	χ^2	0.23774	

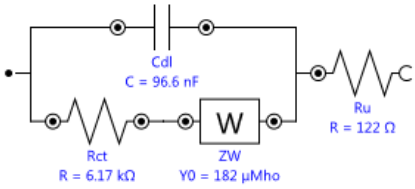

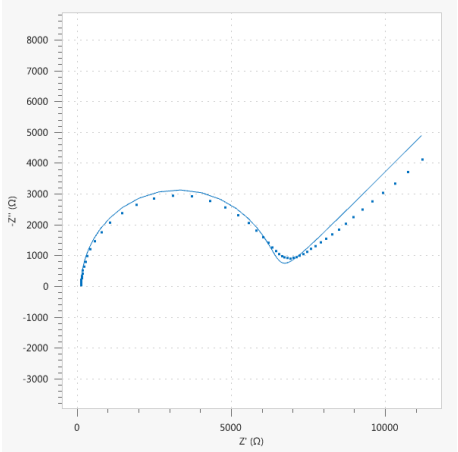

4.2.2.2 Potentiometric Responses of the System with Open Circuit Potentiometry

4.2.2.2.1 Potentiometric Response of DNA Hybridisation

DNA immobilisation onto gold electrodes has been performed at a range of conditions, in particular changing the DNA density at the substrate. These were then tested for variations in the OCP and EIS signals upon hybridisation. The potential of the electrochemical interface depends on the total charge that is modified on the surface of the electrode. This could be affected by the probe density, orientation and ionic strength, due to the intrinsic charge that is carried by the phosphate backbone of the probe that is attached to the surface.

The detection of DNA is based on the detection of charge carried by the complimentary stranded DNA target that binds and accumulates on the interfacial electrochemical layer, which is then modulated into a measurable potential. In OCP detection of target DNA, the potential after DNA hybridisation shows a negative shift. A negative shift comparing to the initial potential before hybridisation on the overall OCP is detected, because the intrinsic charge carried by the phosphate backbone of the complimentary stranded DNA is negatively charged. When the complimentary stranded DNA target binds to the ssDNA probe, the negative charge will be attached to the electrochemical interface, thus making the overall potential to become more negative.

Low potential changes were observed through the various experiments. As complementary stranded DNA was injected in a cell without flow, excessive DNA will be floating around inside the cell. The charge carried by the excessive DNA may cause a hindering effect throughout the measurement, thus reducing the actual potential that the OCP system should have measured.

Efforts have been made to obtain a stable and distinguishable potential changes upon binding of complementary stranded DNA on different electrodes. However, the binding activity was not significant with a change of OCP lower than 1 mV, and the signal was covered by a 10 $mV_{peak\text{-}to\text{-}peak}$ high potential of noise, illustrated in Figure 4-8.

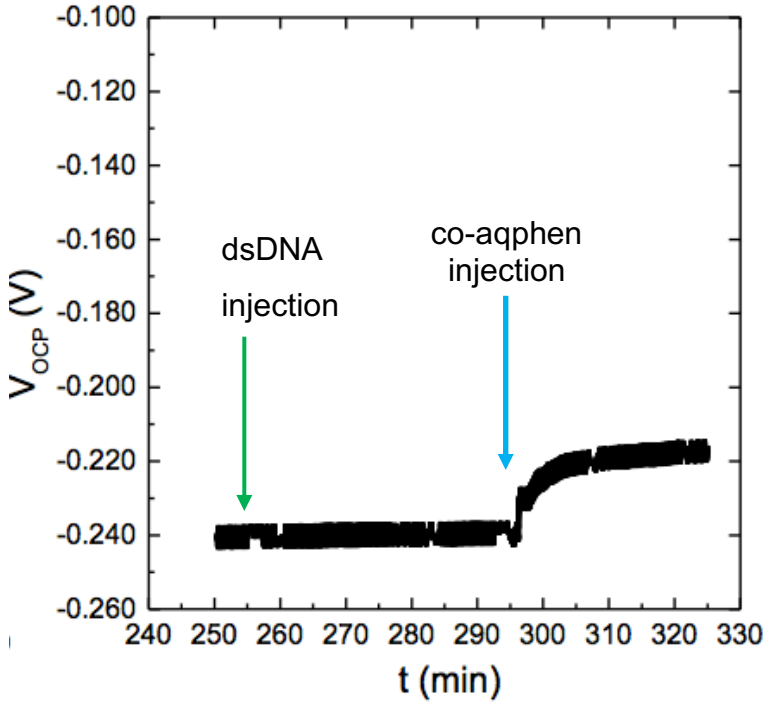

Figure 4-8 DNA and intercalator binding activity (OCP). Green arrow represents the injection of complementary stranded DNA. Blue arrow represents the injection of co-aqphen intercalator.

As the experiment was done with the initial designed of electronic system, which has not implement the appropriate protection techniques mentioned in Chapter 2; and also due to a non-optimised immobilisation, which causes the surface of the electrodes different from one to another, or non-optimised; thus, the OCP measurement is not reflecting the optimal changes. The enhancements made to the OCP electronic system for increasing the sensitivity have been addressed in Chapter 2.

4.2.2.2.2 Potentiometric Response of Cobalt Complex Attachment

Upon injection of the intercalator to dsDNA, a 20 mV potential change was observed, which is a large increase compared to the small changes observed upon DNA hybridisation, illustrated in .

The cobalt complex intercalates in the middle of the DNA sequence, which causes the structural change of the dsDNA. The structural change of the DNA causes a

redistribution of the charge of the biolayer, which redistributes the charges on the surface. As the intercalation of the cobalt complex expands the dsDNA on the surface, thus losing negative charge and causes an increase in overall potential.

4.3 Summary

This chapter has presented the detection of DNA – DNA interaction on gold electrode through EIS and OCP, with the use of a novel cobalt complex $[Co(GA)_2(aqphen)]Cl$ as a signal enhancer upon its attachment to dsDNA. With the success of demonstrating a promising OCP measurement system in the last chapter, an addition of three electrochemical systems are studied with OCP and validated with other electrochemical detection techniques, in order to demonstrate the OCP detection performance with different kinds of biomolecules.

Here a study of OCP detection of DNA – DNA interaction is presented. In this study, the use of intrinsic charge carried by the phosphate backbone of DNA was demonstrated. As the target DNA carried out the hybridisation process, a potential change should have occurred. However, as the experiment was performed under a non-optimised system (without a flow cell and optimisation methods described in Chapter 2), a high amount of noise was present in the OCP signal. Despite of the issues with the OCP measurement system, the intercalator performed an outstanding enhancement that enabled the measurement results to be distinguishable on top of the noise. The study through OCP and EIS showed the cobalt compound is functioning as a DNA intercalator, which would cause structural changes to the dsDNA biolayer that can affect the electrostatic barrier and hence, affect the charges on the biolayer.

References

Del Pozo, M.V., Alonso, C., Pariente, F. & Lorenzo, E. 2005. Electrochemical DNA sensing using osmium complexes as hybridization indicators. *Biosensors & Bioelectronics,* 20**,** 1549-1558.

Erdem, A., Kerman, K., Meric, B., Akarca, U.S. & Ozsoz, M. 1999a. DNA electrochemical biosensor for the detection of short DNA sequences related to the hepatitis b virus. *Electroanalysis,* 11**,** 586-588.

Erdem, A., Kerman, K., Meric, B., Akarca, U.S. & Ozsoz, M. 2000. Novel hybridization indicator methylene blue for the electrochemical detection of short DNA sequences related to the hepatitis b virus. *Analytica Chimica Acta,* 422**,** 139-149.

Erdem, A., Meric, B., Kerman, K., Dalbasti, T. & Ozsoz, M. 1999b. Detection of interaction between metal complex indicator and DNA by using electrochemical biosensor. *Electroanalysis,* 11**,** 1372-1376.

Erdem, A. & Ozsoz, M. 2001a. Interaction of the anticancer drug epirubicin with DNA. *Analytica Chimica Acta,* 437**,** 107-114.

Erdem, A. & Ozsoz, M. 2001b. Voltammetry of the anticancer drug mitoxantrone and DNA. *Turkish Journal of Chemistry,* 25**,** 469-475.

Hashimoto, K., Ito, K. & Ishimori, Y. 1994. Novel DNA sensor for electrochemical gene detection. *Analytica Chimica Acta,* 286**,** 219-224.

Jones, J.E., Amoroso, A.J., Dorin, I.M., Parigi, G., Ward, B.D., Buurma, N.J. & Pope, S.J.A. 2011. Bimodal, dimetallic lanthanide complexes that bind to DNA: The nature of binding and its influence on water relaxivity. *Chemical Communications,* 47**,** 3374-3376.

Kara, P., Ozkan, D., Kerman, K., Meric, B., Erdem, A. & Ozsoz, M. 2002. DNA sensing on glassy carbon electrodes by using hemin as the electrochemical hybridization label. *Analytical and Bioanalytical Chemistry,* 373**,** 710-716.

Keighley, S.D., Li, P., Estrela, P. & Mighorato, P. 2008. Optimization of DNA immobilization on gold electrodes for label-free detection by electrochemical impedance spectroscopy. *Biosensors & Bioelectronics,* 23**,** 1291-1297.

Lin, H.B., Wang, Q.X., Zhang, C.M. & Li, W.Q. 2011. Crystal structure and DNA binding studies of a cobalt(ii) complex containing mixed-ligands of 1, 10-phenathroline and glycollic acid. *Chinese Chemical Letters,* 22**,** 969-972.

Liu, J.F., Su, B., Lagger, G., Tacchini, P. & Girault, H.H. 2006. Antioxidant redox sensors based on DNA modified carbon screen-printed electrodes. *Analytical Chemistry,* 78**,** 6879-6884.

Lopez, R., Loeb, B., Boussie, T. & Meyer, T.J. 1996. Synthesis of a new phenanthroline derived ligand with acceptor properties. *Tetrahedron Letters,* 37**,** 5437-5440.

Millan, K.M. & Mikkelsen, S.R. 1993. Sequence-selective biosensor for DNA-based on electroactive hybridization indicators. *Analytical Chemistry,* 65**,** 2317-2323.

Ozkan, D., Kara, P., Kerman, K., Meric, B., Erdem, A., Jelen, F., Nielsen, P.E. & Ozsoz, M. 2002. DNA and pna sensing on mercury and carbon electrodes by using methylene blue as an electrochemical label. *Bioelectrochemistry,* 58**,** 119-126.

Pang, D.W. & Abruna, H.D. 1998. Micromethod for the investigation of the interactions between DNA and redox active molecules. *Analytical Chemistry,* 70**,** 3162-3169.

Regan, E.M., Hallett, A.J., Wong, L.C.C., Saeed, I.Q., Langdon-Jones, E.E., Buurma, N.J., Pope, S.J.A. & Estrela, P. 2014. A novel cobalt complex for enhancing amperometric and impedimetric DNA detection. *Electrochimica Acta,* 128**,** 10-15.

Trott, O. & Olson, A.J. 2010. Software news and update autodock vina: Improving the speed and accuracy of docking with a new scoring function, efficient optimization, and multithreading. *Journal of Computational Chemistry,* 31**,** 455-461.

Yang, J., Yang, T., Feng, Y.Y. & Jiao, K. 2007. A DNA electrochemical sensor based on nanogold-modified poly-2,6-pyridinedicarboxylic acid film and detection of pat gene fragment. *Analytical Biochemistry,* 365**,** 24-30.

CHAPTER 5.

OCP Detection of PNA – DNA Interaction with Gold Nanoparticles

Following the study on the detection of DNA – DNA interaction, this chapter investigates the detection of PNA – DNA interaction on gold electrode through open circuit potentiometry (OCP), with the use of gold nanoparticles (AuNPs) that are positively charged for enhancing the signal upon its attachment to PNA/DNA duplex. The effects on PNA/DNA hybridisation and the attachment of positively charged gold nanoparticles are discussed. As PNA is different from DNA by not carrying a negatively charged backbone, DNA – DNA and PNA – DNA system based on the charges they carried are investigated and compared.

The work presented in this chapter has been partly published in Jolly *et al.* (2015). The author contributed to this research on the background research, the electronic hardware design and software programming of the OCP integrated system, the design and production of the flow cell system, the thermal evaporation process and preparation of gold working electrodes, the preparation of 20 nm AuNPs, the fabrication of PNA sensors, the electrochemical characterisation measurements with both OCP and EIS (Nyquist plot) detection technique, and finally, the OCP and EIS analytical study of the PNA – DNA interaction with AuNPs.

5.1 Introduction

MicroRNAs (miRNAs) are small non-coding RNA that are found in living organisms and even some viruses, and have a length of around 22 nucleotides. They function in post-transcriptional RNA silencing and regulation of gene expression (Bartel, 2007). As they are involved in the regulation of gene expression, they are the fingerprints to a lot of diseases including cancer (Lu *et al.*, 2005), making them potential biomarkers. To use miRNAs as the fingerprints to understand the state of cancer and the progression, the detection of expression levels are used to obtain more information (Mitchell *et al.*, 2008).

Current detection techniques such as northern blotting (Varallyay *et al.*, 2008) and *in situ* hybridisation (Catuogno *et al.*, 2011) remain as the laboratory-grade standard. With the complexity and the lower sensitivity that these techniques carried, further development such as microarray technology and quantitative polymerase chain reaction (qPCR) (Chen *et al.*, 2005) have been introduced in the past years. However, although these systems are powerful, the complexity led these techniques to be confined in only central laboratory areas, leaving researchers hard to work on. Hence, the technology in the detection and quantification of the levels of miRNAs with higher simplicity and sensitivity has gain significant interest.

Electrochemical detection techniques are gaining higher interest because of the simplicity, sensitivity and robustness of the instrumentation setup. With current detection systems, various electrochemical detection enhancement techniques have been reported, which are possible for improving the state of the art in electrochemical miRNA detection. These techniques include using nanoparticles and enzymes for enhancing the levels of the detection of miRNAs.

As miRNA is made up of nucleotides and have a lot of similarities with DNA, for the ease of handling of DNA and to act as a stepping stone for future work, the detection of miRNA is replaced with DNA for its stability and simplicity for the first stage of the study. In this chapter, the development of OCP for the detection of DNA with PNA probe is presented. By exploiting the inherent charge of the target oligonucleotide, and a simple one-step amplification method with the positive charge of AuNP, OCP can

be presented as a sensitive DNA detection system with signal enhancement compatibility by AuNP. The charge distribution and the charge density at the electrode-solution interface upon target DNA hybridisation to the PNA probe produces a change on the overall potential that is similar to the DNA – DNA system, which can also be mediated as a measurable potential change through OCP. Upon hybridisation, changes of the interfacial electrochemical impedance also enable the use of electrochemical impedance spectroscopy (EIS) without the use of redox markers to detect the binding events that occur by measuring the capacitance change on the surface.

Different from the last chapter, PNA are immobilised on the surface as probes for detection. When comparing to DNA, the major differences of PNA is its uncharged and higher stability. Taking these two major differences as advantages, higher open circuit potential (OCP) signal amplitude upon hybridisation and stability is expected. In addition, literatures have reported PNA/DNA duplex with mismatches has lower stability than DNA/DNA duplex, which makes PNA more attractive to act as the probe for detection in order to achieve better confirmation results.

A different enhancement technique has been used while still offering a simple amplification strategy on the signal. By using positively charged AuNPs to electrostatically attach to only PNA/DNA duplexes (Demidov *et al.*, 1994; Ray and Norden, 2000), this attachment process disrupts the biolayer and produces a change in charge.

Charge changes on the biolayer upon PNA/DNA hybridisation, and AuNPs attachment to PNA/DNA duplexes are both studied using OCP. The results are compared to EIS measurements. A simple real-time measurement system for detection of DNA is developed. Through the understanding of the measurements of these charge changes, an enhancement method using positively charged AuNPs for OCP is reported. In addition, DNA – DNA system and PNA – DNA system is compared.

5.1.1 Gold Nanoparticles

Nanoparticles have been used in different kinds of detection techniques for the past decade, and the utilisation of nanoparticles, in particular gold and silver, has enabled more novel techniques showing promising results. AuNPs have received considerable attention among other nanostructured materials because of its unique optical properties, its utilisation in microelectronics, DNA detection, sequencing, and enhancement of detection signal. As reported in literature, Mirkin's group had developed a technique by utilizing the optical properties of AuNPs, as an alternative to fluorescent labelling, for the detection of DNA hybridisation of a specific DNA sequence with an array of sensors (Elghanian *et al.*, 1997; Taton *et al.*, 2000). Wang's group had used AuNPs in electrochemical stripping potentiometric measurements to detect hybridisation by analysing the trace of metals produced from AuNPs (Wang *et al.*, 2001). Zhang had used AuNPs to enhance the signal detected with Chronocoulometry (CC) by labelling AuNPs with oligonucleotides to the hybridisation sites, thus increasing the total amount of charges on the biolayer and the amount of redox marker for the signal (Zhang *et al.*, 2006). These groups showed promising use cases of the AuNPs, and finally, Kim's group have made the AuNPs more efficient for surface-enhanced Raman scattering, by coating the AuNPs with self-assembled poly-(ethylenimine) (PEI) (Kim *et al.*, 2008), illustrated in Figure 5-1.

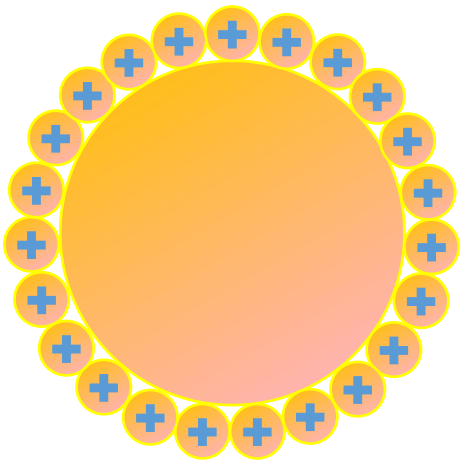

Figure 5-1 Schematic of a PEI-capped AuNP.

Although many successful case studies of signal enhancement by AuNPs have been shown in detection of DNA, the use of AuNPs in connection with OCP has not been addressed and thus, it would be interesting to see how the PEI-capped AuNPs, which are positively charged by the self-assembly of poly-(ethylenimine), could benefit DNA detection by OCP as enhancement molecules.

5.2 PNA – DNA System with Gold Nanoparticles

Here we present the detection of PNA – DNA interaction with positively charged AuNPs, a schematic of the system is illustrated in Figure 5-2. The potentiometric responses of PNA/DNA hybridisation and the attachment of positively charged AuNPs are presented with a discussion compared with impedimetric responses.

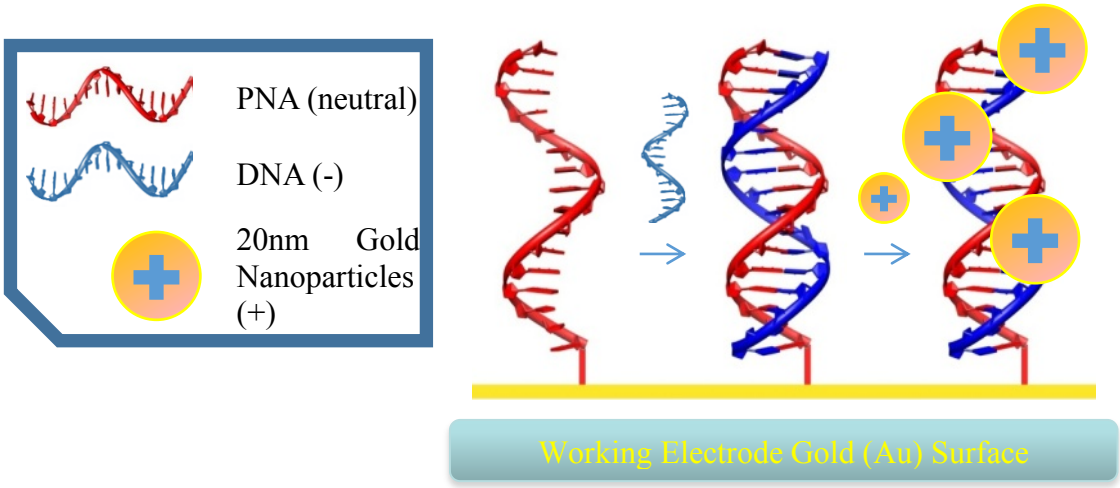

Figure 5-2 Schematic of PNA – DNA system with 20 nm positively charged AuNPs. (a) Immobilised PNA probe. (b) Hybridisation with target oligonucleotides (PNA). (c) Electrostatic attachment of 20 nm positively charged AuNPs to PNA/DNA duplex.

5.2.1 Experimental Preparation and Characterisation Methods

5.2.1.1 Materials

PNA and DNA oligonucleotides were purchased from Cambridge Research Biochemical, UK. Hydrogen tetrachloroaurate ($HAuCl_4$, 99.99%), branched poly-(ethylenimine) (PEI, MW ~25 kDa), 6-Mercapto-1-hexanol (MCH, 97%), potassium phosphate monobasic solution (1 M), potassium phosphate dibasic solution (1 M), dimethyl sulfoxide (DMSO) were all purchased from Sigma–Aldrich, UK. All aqueous solutions were prepared using 18.2 MΩ cm ultra-pure water (Millipore, USA) with a Pyrogard filter (Millipore, USA) to remove nucleases.

5.2.1.1.1 Oligonucleotides

The HPLC purified synthetic oligonucleotides and PNA probe sequence are shown in Table 5-1. A polyethylene-glycol (PEG) linker (AEEA, $C_{21}H_{23}NO_6$) is added to the PNA probe, which increases the length of the probe by nine atoms (8-amino-3,6-dioxaoctanoic acid).

Table 5-1 DNA sequence and PNA probe used in this PNA – DNA system. AEEA is a glycol linker (8-amino-3,6-dioxaoctanoic acid).

Full complementary sequence for PNA probe	3'-TCT TCT TCT TCT TCT TCT TCT TCT-5'
PNA probe: SH-C6-AEEA-	AGA AGA AGA AGA AGA G

5.2.1.2 Preparation of 20 nm Positively Charged Gold Nanoparticles

Preparation of 20 nm positively charged AuNPs procedure was adopted from Kim *et al.* (2008). An optimised ratio of aqueous $HAuCl_4$ solution was mixed with PEI and stirred vigorously at room temperature at 25 °C for 16 h to produce AuNPs. The sise of AuNPs were controlled by the amount of PEI added to the reaction mixture. The reacted mixture was then washed three times by ultra-centrifuged and filtered with

ultra-pure water. The 20 nm positively charged AuNPs, which are the PEI-capped AuNPs from the reacted mixture, were obtained, re-dispersed in water and gently sonicated before experiments.

5.2.1.3 Electrochemical Measurements

The 20 nm positively charged gold nanoparticles solution was made and contained 10mM phosphate buffer (PB) as the supporting electrolyte.

OCP measurement on the PNA/DNA hybridisation and attachment of positively charged gold nanoparticles were carried out using a custom made electronic measurement system based on INA116 ultra low input bias current instrumentation amplifier with a cell. The setup was used consisting of three 1.6 mm diameter gold disc working electrodes (ALS Co., Ltd, Japan), a Hg/Hg_2SO_4 (K_2SO_4 sat.) reference electrode (ALS Co., Ltd, Japan) placed into a salt bridge, and a platinum wire (ALS Co., Ltd, Japan) for grounding the solution in the electrochemical cell. The OCP was measured in a solution of 10 mM phosphate buffer (PB) pH 7.4. The reference electrode was connected via a salt bridge filled with 10 mM phosphate buffer (PB) pH 7.4. OCP measurement was recorded in real time and continuously until experiment finished. A maximum of three working electrodes were measured at the same time through three different channels simultaneously for the potential changes, by using a common reference electrode.

EIS was performed using a μAutoLab Type III FRA2 potentiostat (Metrohm, UK). A conventional three-electrode configuration was used consisting of a 1.6 mm diameter gold disc working electrode (ALS Co., Ltd, Japan), a Hg/Hg_2SO_4 (K_2SO_4 sat.) reference electrode (ALS Co., Ltd, Japan) placed into a salt bridge, and a platinum wire (ALS Co., Ltd, Japan) counter electrode, against which all potentials are quoted. The electrochemical impedance spectrum was measured in a solution of 2 mM $K_4[Fe(CN)_6]$ + 2 mM $K_3[Fe(CN)_6]$ in 50 mM phosphate buffer (PB) + 100 mM K_2SO_4 pH 7.0, ionic strength 447 mM. The reference electrode was connected via a salt bridge filled with 50 mM PB + 100 mM K_2SO_4 pH 7.0. The impedance spectrum was measured over the frequency range of 100 kHz to 0.1 Hz,

with a 10 mV a.c. voltage superimposed on a d.c. bias of −0.195 V, which corresponds to the formal potential of the redox couple.

5.2.1.4 Preparation of the PNA Self-Assembled Monolayer

Gold disc working electrodes with a radius of 1.6 mm (ALS Co., Ltd, Japan) were polished with 1 μm polishing diamond (ALS Co., Ltd, Japan) on a diamond polishing pad (ALS Co., Ltd, Japan), sonication in ultra-pure water, polished with 0.05 μm polishing alumina (ALS Co., Ltd, Japan) on a alumina polishing pad (ALS Co., Ltd, Japan), followed by sonication in ultra-pure water, polishing on a blank polishing pad, and sonication in ultra-pure water to remove any remaining particles. Electrodes were subsequently electrochemically cleaned in 0.5 M H_2SO_4 by scanning the potential between the oxidation and reduction of gold, between−0.05 V and +1.1 V versus a Hg/Hg_2SO_4 reference electrode for 60 cycles until there was no further change in the cyclic voltammogram. Electrodes were rinsed with ultra-pure water, dried in a stream of nitrogen, and co-immobilised with mixed PNA/MCH immobilisation solution for 16 h in a humidity chamber.

Probe thiolated ssPNA had sequence HS–$(CH_2)_6$– $C_{21}H_{23}NO_6$–AGA AGA AGA AGA AGA G. The PNA immobilisation solution consisted of ssPNA and mercaptohexanol (MCH) in 50% dimethyl sulfoxide (DMSO), 50% ultra-pure water (v/v). An optimised ratio of 1:5 for PNA probes immobilisation was adopted from the literature (Keighley *et al.*, 2008a). After immobilisation, electrodes were rinsed in ultra-pure water to remove any unattached thiols. To ensure complete thiol coverage of the gold surface, the electrodes were backfilled with mercaptohexanol (MCH) by immersion in 1 mM MCH in ultra-pure water for 1 h. Electrodes were then rinsed with ultra-pure water and placed into 10 mM PB pH 7.4 measurement buffer for 1 h.

5.2.1.5 DNA Hybridisation and Gold Nanoparticles Incubation

5.2.1.5.1 Open Circuit Potentiometry

Electrodes with immobilised ssPNA/MCH were immersed in the cell with 10 mM PB pH 7.4 measurement buffer. DNA that had a complementary binding sequence to the probe ssPNA was injected into the cell when the OCP achieved a stable potential value. Electrodes were incubated with complementary stranded DNA diluted in 3ml of 10 mM PB pH 7.4 measurement buffer for 60 min under continuous measurement.

After DNA hybridisation, 20nm positively charged AuNPs in 10 mM PB pH 7.4 were injected into the bulk solution in the cell. The electrodes were incubated for another 4 hours under continuous measurement until reaching a stable potential.

5.2.1.5.2 Electrochemical Impedance Spectroscopy

Electrodes with immobilised ssPNA/MCH were treated with DNA that had a complementary binding sequence to the PNA probe. Electrodes were incubated with complementary stranded DNA diluted in 10 mM PB pH 7.4 measurement buffer for 60 min before measurement. Following DNA hybridisation, another measurement was made after the electrodes were incubated in 20nm positively charged AuNPs.

5.2.2 Discussion on PNA/DNA Hybridisation with Positively Charged Gold Nanoparticles

5.2.2.1 Potentiometric responses of the system with Open Circuit Potentiometry

5.2.2.1.1 Potentiometric Response of PNA/DNA Hybridisation

In the OCP real-time measurement shown in Figure 5-3, the potential of PNA/DNA hybridisation was monitored from the start after reaching a stable signal with ssPNA probe surface to the injection of complementary stranded DNA surface when it reaches a stable signal. Upon injection, a decrease can be seen on the potential change. A change of potential has been measured for 30 minutes with a -3.13 mV overall decrease, with the concentration of 100 nM complimentary stranded DNA injection.

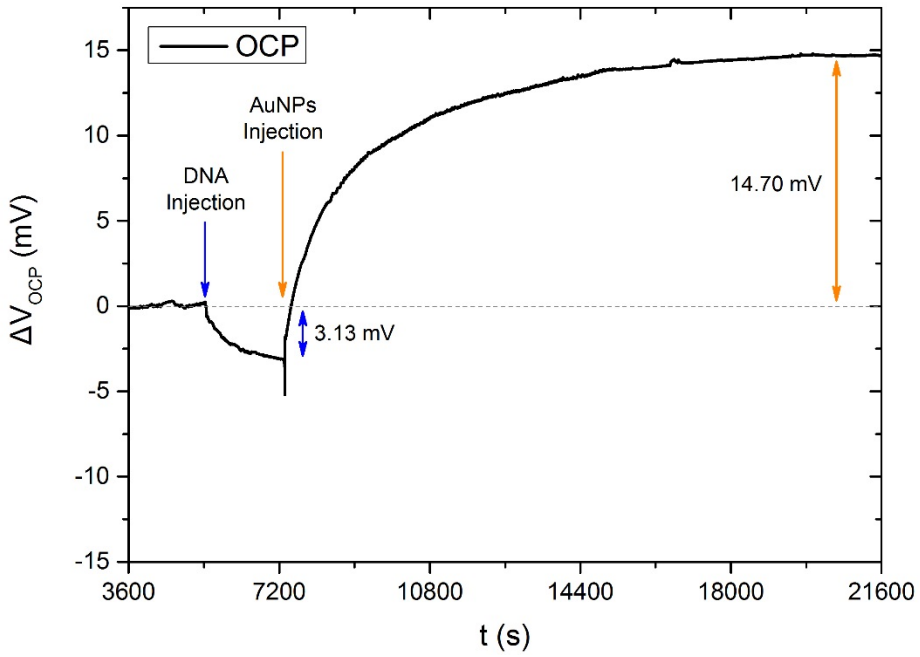

Figure 5-3 PNA/DNA hybridisation with 20 nm AuNPs attachment (OCP).

When complimentary stranded DNA attaches to PNA probes, as PNA has no charge, which forms an uncharged biolayer, and the complimentary stranded DNA has a negative charge due to the charge carried by the ionised phosphate backbone, a change from an uncharged biolayer to a negatively charged biolayer gives a negative shift upon binding on the overall open circuit potential.

Different concentrations have been tested to obtain optimised hybridisation results. Dose response range of concentration from 1 nM to 1 µM shown possible detection of PNA/DNA hybridisation, this shows that the potential change is due to the effect of successful hybridisation detected on the surface. In Figure 5-4, the overall changes of each injection of DNA concentration are plotted. Clear results showing that successful binding have negative range of potential changes, increases over the range of concentrations of the same target oligonucleotides.

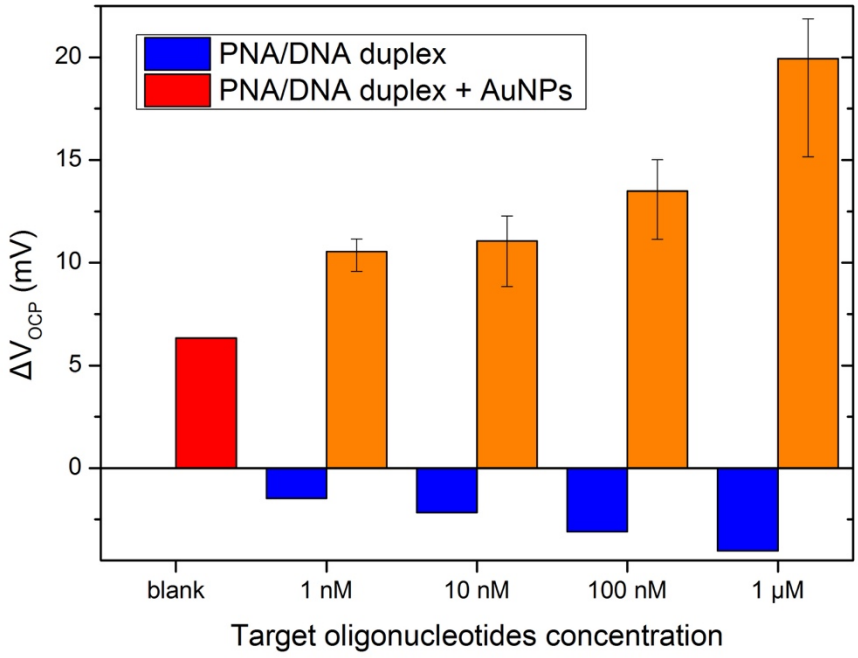

Figure 5-4 Dose response (OCP). Blue bars represent binding with target oligonucleotides, yellow bars represent AuNPs amplification, red bar represent blank upon AuNPs amplification. Error bars represents the minimum and maximum changes of OCP detected.

The hybridisation results were lower than expected, with the highest concentration of 1 µM tested showing less than -5 mV change. A likely reason is due to the presence of the long linker used on the PNA probes, which lift up the PNA probe from the surface, causing lower detection responses because of Debye length limitation. A second reason that can cause a lower potential change is because the experiment was done without a flow cell. This causes excess of target complimentary stranded DNA floating in the bulk solution, which causes a hindering effect that lowers the overall potential change.

This overall potential change of PNA/DNA hybridisation upon binding has higher potential change compared to DNA/DNA hybridisation. A clear reason here is because of PNA probes were used for the detection, which can form an uncharged surface that have a major difference with DNA probes used in the last chapter. This will be discussed before the end of the chapter.

5.2.2.1.2 Potentiometric Response of Positively Charged Gold Nanoparticle

AuNPs that are contained in 10 mM PB buffer pH 7.4 were injected after 30 minutes of PNA/DNA hybridisation. The complementary stranded DNA that has hybridised with the ssPNA probe formed a negatively charged PNA/DNA duplex. This was used to exploit the use of positive charges that are carried on the gold nanoparticles as a signal enhancement technique. The 16-base probe PNA that is used to form the SAM has a PEG linker (AEEA, $C_{21}H_{23}NO_6$) with a length of *circa* 1.4 nm and a total length of *circa* 6.7 nm. This is approximately 1/3 of the length of the 20 nm AuNPs.

By electrostatically attaching AuNPs to only PNA/DNA duplexes by the attraction of positive and negative charges, the biolayer formed a more positively charged surface, which by that gave a more positive potential change upon the attachment. Another reason for the increase was due to the disruption of the dielectric biolayer by the large amount of AuNPs attached to the biolayer, this will be shown by the result shown through a Cole-Cole plot in the validation sub-chapter. As an example, after attachment of AuNPs, there is an increase of 14.70 mV under the experiment with the injection of 100 nM DNA, which significantly enhanced the detection result. Enhancements by AuNPs in different concentrations are shown in Figure 5-4. As explained in the last sub-chapter, the same reasons that can cause hindering effect upon hybridisation, higher potential change was also observed upon injection of AuNPs to the blank test. With the current setup, although there are changes in both cases of attachment to PNA/DNA duplex and blank test, a clear difference can be distinguishable, and a baseline could be made to subtract away the noise.

To further improve the current results between hybridisation and attachment of AuNPs and blank, setup has to include rinsing steps. By adding a flow cell to the OCP system, extra rinsing steps can be made after each injection, which can rinse away the excess number of molecules floating in the solution inside the cell. By this, the background signal could be lowered, and more accurate measurements of the hybridisation and enhancement results can be obtained.

Cautions need to be taken when preparing AuNPs after sonication until injection, since aggregation may occur if the AuNPs solution is not injected straight away. A flowing

solution through the cell is also needed to prevent AuNPs sticking to the wall or sinking to the bottom of the cell or onto the electrode surface due to gravity attracting the aggregated AuNPs.

5.2.2.2 Validation of the System with Impedimetric Response of the System

To obtain the impedance data of EIS measurements, the negatively charged redox couple $[Fe(CN)_6]^{3-/4-}$ is used in solution. Although the negative charge carried by the DNA backbone isn't present on PNA, the PNA + MCH co-immobilised layer on the surface still provides a physical barrier to the redox markers hindering its charge transfer to the gold electrode. Upon hybridisation, the increase in negative charge on the biolayer by the complementary stranded DNA enhances the barrier not only with extra physical barrier, but also with an electrostatic barrier. By the increase of local cation concentration on the biolayer, resulting in an increase of the Gouy–Chapman diffuse layer capacitance, and an overall increase of capacitance, thus further reducing the charge transfer. A huge variation in the values of R_{ct} can hence be detected as a signal of DNA binding. For further amplification of the signal, AuNPs were electrostatically attached to the PNA/DNA duplexes. Upon attachment of 20 nm positively charged AuNPs, the AuNPs caused a disruption on the biolayer, which totally rearranged the biolayer and a decrease on R_{ct} was observed.

Upon hybridisation, the R_{ct} corresponds to the point in the Nyquist plot where the semi-circle crosses the Z_{real} axis, which increases from 1.3 kΩ to 12.6 kΩ. This is increased by 969% upon hybridisation as shown in Figure 5-5. This large change is mostly due to the negative charge attached to the biolayer that increased the barrier, confirming that the DNA is attached to the biolayer. This reflects that the negative shift on OCP is due to the negative charge accumulated on the biolayer.

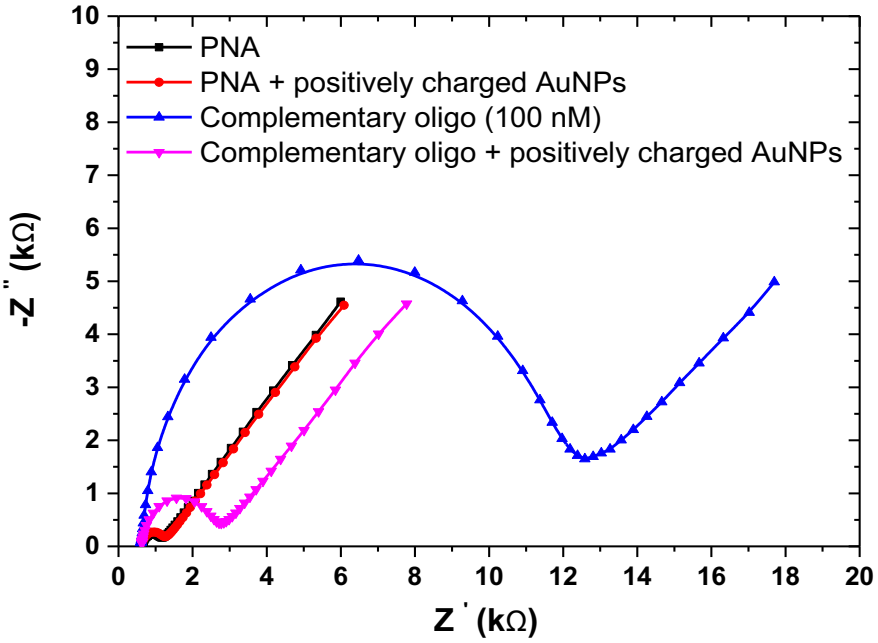

Figure 5-5 Nyquist plot represents the charge transfer resistance of the PNA – DNA system (EIS). Black curve shows PNA probes on the surface, red curve shows only a slight change when positively charged AuNPs are added to PNA probes, blue curve shows PNA/DNA duplex, pink curve shows the attachment of AuNPs to PNA/DNA duplex for signal enhancement.

Upon attachment of 20 nm positively charged AuNPs, the R_{ct} decreases from 12.6 kΩ to 2.9 kΩ. This huge drop decreased down to 23% upon attachment of AuNPs. The attachment by electrostatic force causes such a huge decrease by disrupting the whole dielectric biolayer, which makes the redox couple able to reach the gold surface. The redox couple may either directly reaches the gold surface, or mostly uses AuNP as a hoping step. This correlates to the results that the OCP signal increases because of the attachment of the excess of positive charge carried by AuNPs to the biolayer.

Under the same system report by Jolly *et al.* (2015), Cole-Cole plot was obtained to understand the capacitance change by measuring EIS with 10 mM PB pH.7.4, without the negatively charged redox couple $[Fe(CN)_6]^{3-/4-}$. In Figure 5-6, the capacitance results of DNA hybridisation and attachment of AuNPs are shown.

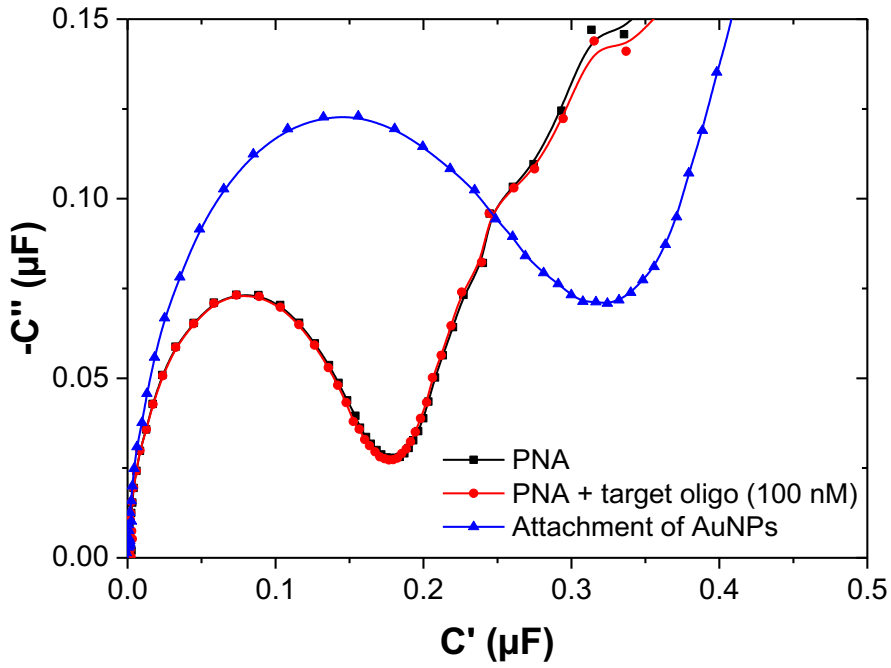

Figure 5-6 Cole-Cole plot represents the capacitance of the PNA – DNA system (EIS). Black curve shows PNA probe on the surface, red curve shows a slight decrease after PNA/DNA hybridisation, blue curve shows attachment of AuNPs for enhancement. (Adapted from Jolly *et al.* (2015))

By extracting the capacitance of the system from:

$$C^* = C' + jC'' \equiv \frac{1}{j\omega Z} = \frac{-Z''}{j\omega|Z|^2} + j\frac{-Z'}{j\omega|Z|^2} \qquad (12)$$

where C' corresponds to the real part of the capacitance, and C'' corresponds to the imaginary part of the capacitance. Z' corresponds to the real part of the impedance, and Z'' corresponds to the imaginary part of impedance, and $\omega=2\pi f$ is the angular frequency of the measurement.

Upon PNA/DNA hybridisation, there is no change or even a decrease in capacitance. A reason was suggested because of the PNA has a Polyethylene-glycol (PEG) linker (AEEA, $C_{21}H_{23}NO_6$), the binding event took place at a far for surface distance, which is above the Debye length of this system. This caused a screening of negative charges

of the DNA, which is the hindering effect that lowered the capacitance. Upon attachment of AuNPs a significant increase was observed. This is mainly due to the disruption of the biolayer, which the AuNPs are electrostatically attached to the surface, causing a huge change in the condition. With the two results from a view of capacitance of the system, this can confirm that the change of potential in OCP was due to the PNA/DNA hybridisation and attachment of AuNPs.

5.2.3 Discussion on DNA – DNA and PNA – DNA System

It is not possible to compare DNA – DNA system with PNA – DNA system under identical conditions under the current experiments. The reasons for being non-identical are because DNA and PNA each have different molecular structures, linkers, lengths, and hybridisation characteristics; all of which could cause differences in probe density on the fabricated sensor surface and hybridisation efficiency upon binding. To consider them as close as possible, same immobilisation and hybridisation protocol were used to achieve a comparison for this discussion.

With both systems using 10 mM PB buffer as the optimal buffer, range of 3 mV to 8 mV of potential changes could be detected on PNA – DNA system (1 nM to 1 μM of target oligonucleotide), while DNA – DNA system gives no or hard to distinguish potential changes. Upon adding the respective signal enhancer to each system, potential changes could be seen upon the attachment of the signal enhancer to the dsDNA and PNA/DNA duplex, thus this suggested that probes are definitely immobilised on the sensor surface by the effect of enhancement. With studies (Steel *et al.*, 1998) suggested that 100% hybridisation efficiency could be achieved by optimal mixed SAM structure with a probe density of 3×10^{12} molecules/cm^2. Hence it can be assumed that hybridisation did take place, but the signal was hindered on the DNA – DNA system. The advantage of PNA is seen not only from OCP, but also demonstrated by a large enhancement on other techniques, such as EIS. Studies (Keighley *et al.*, 2008a; Keighley *et al.*, 2008b) have shown that with both system immobilised at their optimised density, EIS have shown about 1000-fold increase of charge transfer resistance signal upon hybridisation was achieved with PNA probes.

With the current setup, PNA – DNA system is clearly showing higher changes upon hybridisation compared to DNA – DNA system with OCP. As DNA carries negative charge on the backbone, a repulsive effect based on the negative charge could affect the DNA/DNA hybridisation, and also cause a hindering effect on the surface and bulk solution. While PNA has higher bonding energy and better capability of mismatch discrimination, negative charge upon PNA/DNA hybridisation can be truly detected once attached to the biolayer. The conclusion hence can be made that under OCP, which detects the change of charges on the biolayer, a surface that changes from neutral to negative, comparing to negative to negative change, clearly gives higher potential change.

5.3 Summary

This chapter has presented the detection of PNA – DNA interaction on gold electrode through OCP, with the use of a PEI-capped AuNPs as a signal enhancer upon its attachment to dsDNA. Following the use of DNA in the previous chapter for the study of OCP detection of DNA – DNA interaction, here another DNA-based system is presented. The OCP detection of PNA – DNA interaction is presented as the third electrochemical system. With the exploitation of the inherent charge of the target oligonucleotide, the charge density at the biolayer upon target DNA hybridisation to the PNA probe has shown a change on the overall OCP that is similar to the DNA – DNA system. Although both of the systems are DNA-based, the PNA/DNA duplex comparatively, has a higher OCP signal amplitude and stability upon hybridisation. The difference of the OCP signal amplitude was due to a major difference in the structural design of the backbone. DNA has a deoxyribose sugar backbone that includes phosphate groups, while PNA is composed of repeating N-(2-aminoethyl)-glycine units linked by peptide bonds. As DNA carries negative charge on the backbone, a repulsive effect based on the negative charge could affect the DNA/DNA hybridisation, and also cause a hindering effect on the surface and bulk solution. While PNA has higher bonding energy and better capability of mismatch discrimination, negative charge upon PNA/DNA hybridisation can be truly detected once attached to the biolayer, hence its ability to achieve a higher OCP signal amplitude difference.

The characteristic of PEG-like linker (AEEA) for the enhanced anti-fouling properties was also demonstrated. With AEEA, only 2.5% of non-specific binding was observed, a much lower non-specific binding when compared to others work on non-PEG-like linker (C-6 thiol). However, because of the presence of the long linker used, lower detection responses were observed. This is due to the PNA probes being lifted up from the surface, moving towards the Debye length limitation. A second reason for the lower potential change is because the experiment was done without a flow cell. This causes excess of target complimentary stranded DNA to be present in the bulk solution, which in turn causes a hindering effect that lowers the overall potential change. Hence, a microfluidic system will be introduced into the OCP measurement system in order to achieve an automatic rising step, and to provide autonomous samples and solutions handling. Although a lower than expected potential change was observed upon hybridisation, the attachment of positively charged AuNPs gave a significant increase. This is mainly due to the disruption of the biolayer, which the AuNPs are electrostatically attached to the surface, causing a huge change in the surface condition. Validation of the OCP results was also studied with impedimetric response of the system, presented with a Nyquist plot (the charge transfer resistance) and a Cole-Cole plot (capacitance). With the two results from a view of capacitance of the system, this can confirm that the change of potential in OCP was due to the PNA/DNA hybridisation and attachment of positively charged AuNPs.

References

Bartel, D.P. 2007. Micrornas: Genomics, biogenesis, mechanism, and function (reprinted from cell, vol 116, pg 281-297, 2004). *Cell,* 131**,** 11-29.

Catuogno, S., Esposito, C.L., Quintavalle, C., Cerchia, L., Condorelli, G. & De Franciscis, V. 2011. Recent advance in biosensors for micrornas detection in cancer. *Cancers (Basel),* 3**,** 1877-98.

Chen, C.F., Ridzon, D.A., Broomer, A.J., Zhou, Z.H., Lee, D.H., Nguyen, J.T., Barbisin, M., Xu, N.L., Mahuvakar, V.R., Andersen, M.R., Lao, K.Q., Livak, K.J. & Guegler, K.J. 2005. Real-time quantification of micrornas by stem-loop rt-pcr. *Nucleic Acids Research,* 33.

Demidov, V.V., Potaman, V.N., Frankkamenetskii, M.D., Egholm, M., Buchard, O., Sonnichsen, S.H. & Nielsen, P.E. 1994. Stability of peptide nucleic-acids in human serum and cellular-extracts. *Biochemical Pharmacology,* 48**,** 1310-1313.

Elghanian, R., Storhoff, J.J., Mucic, R.C., Letsinger, R.L. & Mirkin, C.A. 1997. Selective colorimetric detection of polynucleotides based on the distance-dependent optical properties of gold nanoparticles. *Science,* 277**,** 1078-1081.

Jolly, P., Wong, L.C.C., Miodek, A., Lindsay, M.A. & Estrela, P. 2015. A simple and highly sensitive electrochemical platform for detection of micrornas. *2015 Ieee Sensors***,** 803-806.

Keighley, S.D., Estrela, P., Li, P. & Mighorato, P. 2008a. Optimization of label-free DNA detection with electrochemical impedance spectroscopy using pna probes. *Biosensors & Bioelectronics,* 24**,** 906-911.

Keighley, S.D., Li, P., Estrela, P. & Mighorato, P. 2008b. Optimization of DNA immobilization on gold electrodes for label-free detection by electrochemical impedance spectroscopy. *Biosensors & Bioelectronics,* 23**,** 1291-1297.

Kim, K., Lee, H.B., Lee, J.W., Park, H.K. & Shin, K.S. 2008. Self-assembly of poly(ethylenimine)-capped au nanoparticles at a toluene-water interface for efficient surface-enhanced raman scattering. *Langmuir,* 24**,** 7178-7183.

Lu, J., Getz, G., Miska, E.A., Alvarez-Saavedra, E., Lamb, J., Peck, D., Sweet-Cordero, A., Ebet, B.L., Mak, R.H., Ferrando, A.A., Downing, J.R., Jacks, T., Horvitz, H.R. & Golub, T.R. 2005. Microrna expression profiles classify human cancers. *Nature,* 435**,** 834-838.

Mitchell, P.S., Parkin, R.K., Kroh, E.M., Fritz, B.R., Wyman, S.K., Pogosova-Agadjanyan, E.L., Peterson, A., Noteboom, J., O'Briant, K.C., Allen, A., Lin, D.W., Urban, N., Drescher, C.W., Knudsen, B.S., Stirewalt, D.L., Gentleman, R., Vessella, R.L., Nelson, P.S., Martin, D.B. & Tewari, M. 2008. Circulating micrornas as stable blood-based markers for cancer detection. *Proceedings of the National Academy of Sciences of the United States of America,* 105**,** 10513-10518.

Ray, A. & Norden, B. 2000. Peptide nucleic acid (pna): Its medical and biotechnical applications and promise for the future. *Faseb Journal,* 14**,** 1041-1060.

Steel, A.B., Herne, T.M. & Tarlov, M.J. 1998. Electrochemical quantitation of DNA immobilized on gold. *Analytical Chemistry,* 70**,** 4670-4677.

Taton, T.A., Mirkin, C.A. & Letsinger, R.L. 2000. Scanometric DNA array detection with nanoparticle probes. *Science,* 289**,** 1757-1760.

Varallyay, E., Burgyan, J. & Havelda, Z. 2008. Microrna detection by northern blotting using locked nucleic acid probes. *Nature Protocols,* 3**,** 190-196.

Wang, J., Xu, D.K., Kawde, A.N. & Polsky, R. 2001. Metal nanoparticle-based electrochemical stripping potentiometric detection of DNA hybridization. *Analytical Chemistry,* 73**,** 5576-5581.

Zhang, J., Song, S.P., Zhang, L.Y., Wang, L.H., Wu, H.P., Pan, D. & Fan, C.H. 2006. Sequence-specific detection of femtomolar DNA via a chronocoulometric DNA sensor (cds): Effects of nanoparticle-mediated amplification and nanoscale control of DNA assembly at electrodes. *Journal of the American Chemical Society,* 128**,** 8575-8580.

CHAPTER 6.

OCP Detection of Protein Phosphorylation and Multimodal Electrochemical and Nanoplasmonic Sensing Approaches

This last experimental chapter investigates the detection of drugs that inhibit kinase activity through Open Circuit Potentiometry (OCP), with the use of an on-chip multimodal electrochemical and nanoplasmonic biosensing system. The detection of protein phosphorylation driven by kinase is discussed, with the use of ferrocene-crowned nanoparticles for signal enhancement. In addition, the use of several electrochemical techniques, namely, electrochemical impedance spectroscopy (EIS), differential pulse voltammetry (DPV), and nanoplasmonic technique, localised surface plasmon resonance (LSPR) on the same chip is presented as a multimodal approach for biosensing applications. High levels of accuracy and reliability on a single multimodal platform with OCP as one of the detection techniques is demonstrated.

The work presented in this chapter has been partly published in Formisano *et al.* (2015). The author contributed to this research on the background research, the electronic hardware design and software programming of the OCP integrated system, the design and integration of the multimodal electrochemical and nanoplasmonic sensing approaches (OCP, EIS, DPV and LSPR), the design and production of the flow cell system, the thermal evaporation process and preparation of gold working electrodes, the electrochemical characterisation measurements with OCP detection technique, and finally, the analytical study of the protein phosphorylation with OCP when compared to other detection techniques in this multimodal sensing system.

6.1 Introduction

Different electrochemical techniques have been used in the study of biomolecular interactions and on the validation of biomolecular detection. In the previous chapters, OCP has been demonstrated as a promising electrochemical detection technique, with validation from other techniques, such as EIS, DPV, CV, etc. In this last chapter, simultaneous use with other electrochemical detection techniques and the integration of automation systems and multiplexing are studied.

Complementary characterisation techniques are used in order to validate the biosensor or provide complementary information on the biological recognition system, as each electrochemical detection technique provides unique information which could be correlated and further enhance the validity of the system. Reports on integrating multiple electrochemical detection techniques on a single measurement system have been published (Bhalla *et al.*, 2015a; She *et al.*, 2015), which could be used for detecting different properties of an interaction or validate a detection of analyte. With an integrated multimodal system, a generic biosensor platform can be used for a wide range of applications, where the user is able to select the most suitable or appropriate detection techniques according to the biomolecule or the information that is required for the electrochemical system.

In this chapter, a protein phosphorylation system is examined. Diseases such as neoplasia (Parang and Sun, 2005), an abnormal growth of tissue, also known as tumour when it forms a mass, is a kind of abnormal phosphorylation of proteins interceded by kinases. Furthermore, over 400 diseases that are directly or indirectly responsible to the activity of protein kinases have been discovered (Cohen, 2002; Cohen and Alessi, 2013; ter Haar *et al.*, 2004; Weinmann and Metternich, 2005). Thus, the use of protein kinases as a source for the discovery of potential drug targets to intervene diseases could have a large area for research. As reported by the United States Food and Drug Administration in July 2015 (Roskoski Jr., 2015), there are only 30 protein kinase inhibitors approved, which shows that the drug market is still very premature. The limited approval is primarily due to time, cost, and laborious lab-based detection techniques, such as mass spectroscopy and western blot. These assays normally require the use of toxic or radioactive reagents for the labelling process, thus high-throughput applications cannot be easily achieved in these systems (Laufer *et al.*, 2005). The development of a high-throughput biosensing system for screening large libraries of kinase inhibitors has gained high interest, which could be used by the pharmaceutic industries for drug discovery applications.

OCP with other promising electrochemical and nanoplasmonic techniques have been applied for the detection of protein phosphorylation driven by kinases. As OCP could be used as a label-free technique for detection, a 'proof of concept' multimodal biosensor detection system is designed in order to screen through multiple detection targets simultaneously. In a 3-step approach, a multimodal biosensor is designed to enable parallel detection of protein phosphorylation with multiple detection techniques. Firstly, OCP is used for the monitoring of phosphorylation process in real time; followed by the use of LSPR for detecting the phosphorylated proteins after the attachment of AuNPs to the thio-phosphoryl groups (Bhalla *et al.*, 2015a; Bhalla *et al.*, 2015b); and lastly, with the use of EIS and DPV for detecting the attachment of thiolated ferrocene (Fc) that grafted onto the AuNPs.

With these techniques on a signal chip, self-validation of the results could be performed and provide effective and reliable detection. With the application of this multimodal approach in detection of protein phosphorylation, OCP is shown to be a

promising real-time detection system, and to provide useful information as a complementary detection technique to other label-free systems. With the enhancement technique shown here, not only showing how AuNPs and Fc could enhance other detection system, but also in this case, OCP could be a unique system to others that promising signal is achieved without attachment of enhancing molecules.

6.1.1 Protein Phosphorylation

Protein phosphorylation is the addition of a covalently bound phosphate group to a protein, through a post-translational modification step, which is catalysed by kinases. By phosphorylation, the structural conformation of a protein can be altered, which causes the protein to be activated, deactivated, or modifying the actual function of the protein. A schematic of a phosphorylated protein is illustrated in Figure 6-1. The first report on protein phosphorylation was in 1906 by Levene et al. with phosphorylated vitellin (Leavene and Alsberg, 1906). The most commonly known amino acids that phosphorylation is carried out are serine, threonine, tyrosine, and histidine, as they play an important role in signaling pathways and metabolism. Due to protein phosphorylation having such an important role in cell regulation, disturbance of kinase activities can cause various diseases. Thus, discovering and monitoring molecules that are able to modulate protein kinase activity and inhibit protein phosphorylation has gained high interest. By new discoveries, new drugs can be identified.

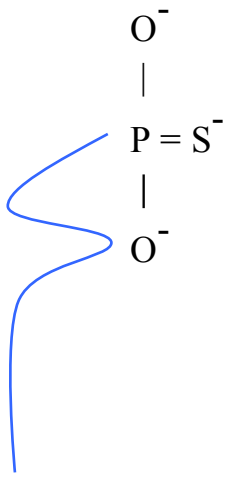

Figure 6-1 Schematic of a phosphorylated protein.

To exploit the phosphorylation biosensor for OCP, here we need to understand the characteristics of protein phosphorylation reaction. The reaction facilitated by kinase, involves the release of proton (H^+) and the transfer of a phosphate group from a donor, in this case adenosine triphosphate (ATP), which increases the negative charge on the protein structure. Hence, as the charge on the biolayer changes, the OCP of the system could be measured. Also, as ATP consists of three phosphoryl groups, the release of protons is highly attractive to OCP. The terminal phosphoryl group (gamma (γ) phosphoryl group) are transferred to the protein upon phosphorylation, hence when the γ-phosphoryl group goes through a modification, OCP and other sensing techniques can measure the changes. As an example, the modification of the γ-phosphoryl group with a sulphide bond will allow the attachment of AuNPs, which allows biosensing techniques to measure the difference.

6.1.2 Gold Nanoparticles and Ferrocene

Ferrocene (Fc) is an organic compound with the formula $Fe(C_5H_5)_2$, which is one of the prototypical metallocenes. It is a type of organometallic chemical compound (Chirik, 2010) that consists of two cyclopentadienyl anions (Cp, which is $C_5H_5^-$) rings with a metal cation atom in the center, in this case Fe, as a commonly known sandwich structure compound. A schematic of the Fc compound is illustrated in Figure 6-2.

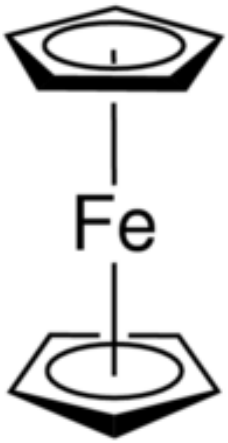

Figure 6-2 Schematic of Fc. (Adapted from Sigma-Aldrich http://www.sigmaaldrich.com/).

The Fc structure has a carbon-carbon bond distances at 1.40 Å within the five-membered rings, and with the Fe-C bond distances at 2.04 Å. Each Cp is allocated with a negative charge, bringing the number of π-electrons on each ring to six, and thus making them aromatic. With the 2 rings of the sandwich structure, the twelve electrons are then shared with the metal via covalent bonding. In addition to the six d-electrons on Fe^{2+}, the whole complex has a total of 18 electrons.

The attachment of AuNPs and Fc enabled extra sensing capabilities to the system here presented. The electrochemical detection approaches are as follows: First, attaching uncharged AuNPs only onto thio-phosphorylated protein samples. This provides a wide surface accessible for the next modification step. A modification of the biolayer is then done by the covalent grafting of thiolated ferrocene onto AuNPs. As a cation metal compound that carries positive charge, here the open circuit potential (OCP) is expected to have a potential shift towards the positive side upon attachment of Fc. Other detection techniques which harvest from the addition of AuNPs and Fc will be discussed below, including EIS, DPV and LSPR, in a multimodal biosensing approach.

6.2 Protein Phosphorylation System

Here we present the protein phosphorylation system with AuNPs and Fc, a schematic of the system is illustrated in Figure 6-3. The potentiometric responses of protein phosphorylation and the attachment of AuNPs and Fc are presented with a discussion compared with multimodal biosensing approaches.

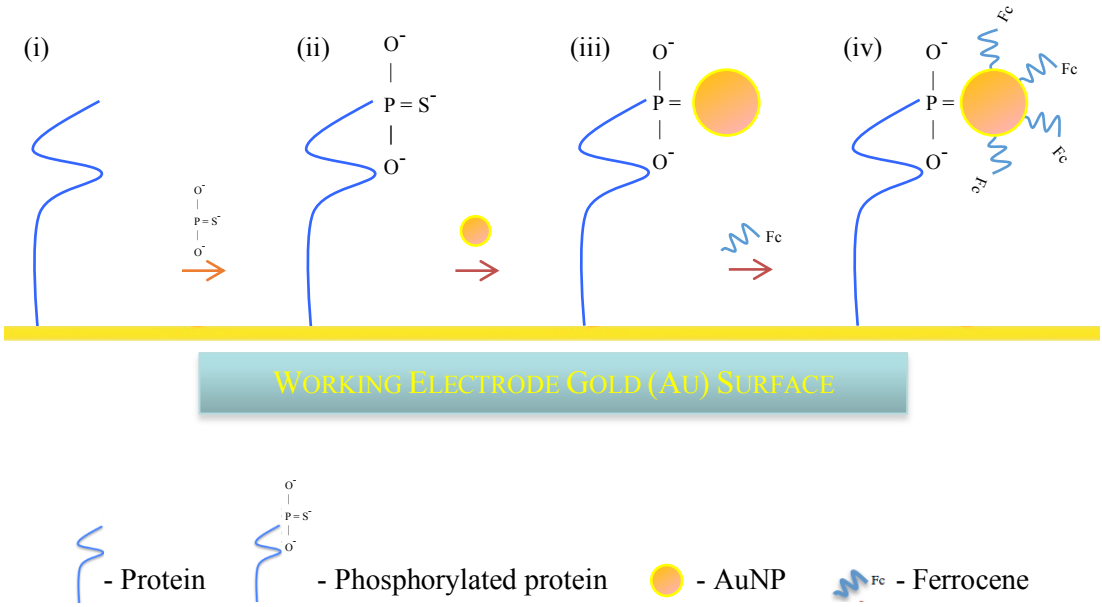

Figure 6-3 Schematic of protein phosphorylation system with AuNP and Fc. (i) Protein immobilisation. (ii) Thio-phosphorylation. (iii) Attachment of AuNP to phosphorylated protein. And finally, (iv) attachment of Fc to AuNP.

6.2.1 Experimental Preparation and Characterisation Methods

6.2.1.1 Materials

Tris base, magnesium chloride ($MgCl^2$), sodium chloride (NaCl), acetone, mercaptoundecanoic acid (MUA), 6-Mercapto-1-hexanol (97%) (MCH), ethyl-dimethylaminopropyl carbodiimide (EDC), N-hydroxysuccinimide (NHS), 6-(Ferrocenyl)hexanethiol, ethanolamine, ethanol, potassium phosphate monobasic solution (1 M), potassium phosphate dibasic solution (1 M), 3-(N-morpholino)propanesulfonic buffer (MOPS), PKC-α kinase inhibitor (GF 109203X), 5'-[γ-thio] triphosphate (ATP-S), and uncharged gold nanoparticles (20 nm average spherical diameter in 0.1 mM PBS) were purchased from Sigma-Aldrich. Dephosphorylated myelin basic protein (MBP) and PKC lipid activator were purchased from Millipore. PKC-α human recombinant kinase produced in Sf9, was procured from ProSpec-Tany TechnoGene Ltd. All aqueous solutions were prepared using 18.2 MΩ cm ultra-pure water (Millipore, Billerica, MA, USA) with a Pyrogard filter (Millipore).

6.2.1.2 Electrochemical Measurements

6.2.1.2.1 Open Circuit Potentiometry

OCP measurement on the protein phosphorylation was carried out using the custom made electronic measurement system based on INA116 ultra low input bias current instrumentation amplifier. The simultaneous measurement setup was used consisting of an in-house fabricated chip with an array of four working electrodes on a signal chip with a radius of 2.0 mm (in-house fabricated), an Ag/AgCl (3M NaCl) reference electrode (BASi, USA) placed into a salt bridge, and a platinum wire (ALS Co., Ltd, Japan) for grounding the solution in the electrochemical cell. The working electrodes chip was prepared in-house by a thermal evaporator (BOC Edwards, USA) with 20 nm Chromium (Cr) and 100 nm Gold (Au) on a glass slide. The OCP was measured in a solution of 10 mM Tris base pH 7.4 containing 6 mM NaCl, and 0.4 mM $MgCl_2$. The reference electrode was connected via a salt bridge filled with the same 10 mM Tris base pH 7.4. OCP measurement was recorded in real time and continuously starting from protein phosphorylation until the experiment finished. A maximum of four working electrodes were measured at the same time through four different channels simultaneously for the potential changes, by using a common reference electrode. The modification steps after SAM preparation were carried out under a flow rate of 100 µl/min using a peristaltic pump (323-Du, Watson Marlow) and an in-house built polytetrafluoroethylene (PTFE) flow cell with an inner chamber of approximate dimensions 25 × 8 × 5 mm^3 (length × width × height) and an internal volume of 1 ml.

6.2.1.2.2 Electrochemical Impedance Spectroscopy and Differential Pulse Voltammetry

As a multimodal biosensor, EIS was performed using a CompactStat potentiostat (Ivium Technologies, The Netherlands). A conventional three-electrode configuration was used consisting of the same working electrodes, reference electrode, and the platinum wire as a counter from the OCP cell setup, against which all potentials are quoted. The electrochemical impedance spectrum was measured in 10 mM Tris base pH 7.4. The reference electrode was connected via a salt bridge filled with 10 mM Tris

base pH 7.4. The impedance spectrum was measured over the frequency range of 100 kHz to 0.1 Hz, with a 10 mV a.c. voltage superimposed to the OCP.

The values of resistance (R_l) and capacitance (C_l) on the Cole-Cole plot were used for comparing the EIS results, in order to calculate as an ideal impedimetric sensor that measure the response at a single frequency. R_l and C_l were measured at a frequency that can minimise the imaginary response of the complex capacitance ($1/j\omega Z$); typically, the minimum C'' occurs at 1 Hz. By measuring at a single frequency, the measurement time was shortening from 3.5 minutes (scanning frequencies from 100 kHz to 0.1 Hz) to 20 seconds.

DPV was used to monitor the Fc peak as another electrochemical technique, by scanning the potentials *vs.* an Ag/AgCl reference electrode, within a 10 second time frame.

6.2.1.2.3 Localised Surface Plasmon Resonance

After obtaining the electrochemical measurement readings, LSPR was measured using an in-house built system with discrete components (Ocean Optics, USA), consisting of a reflection probe (R400-7-UV–VIS) with both detector and light source, a Tungsten Halogen source (LS-1-LL) and a spectroscope (USB4000-UV–VIS-ES). LSPR was set to measure in reflection mode. Using a cross-platform spectroscopy operation software SPECTRASUITE (Ocean Optics, USA), each measurement was recorded with a time of few seconds.

6.2.1.3 Preparation of the MUA/MCH Self-Assembled Monolayer

Four parallel gold disc working electrodes on a signal chip with a radius of 2.0 mm (in-house fabricated) were sonicated in acetone for 3 minutes, rinsed in ultra-pure water and again with ethanol to clean the gold surface properly before using. Electrodes were then rinsed with ultra-pure water, dried in a stream of nitrogen, and immobolised with mixed 1 mM MUA and 1 mM MCH in a ratio of 1:9 MUA:MCH immobilisation solution for overnight in a humidity chamber. After immobilisation,

electrodes were rinsed in ultra-pure water to remove any unattached thiols. To ensure complete thiol coverage of the gold surface and to cover possible pinholes on the gold surface, the electrodes were backfilled with mercaptohexanol (MCH) by immersion in 1 mM MCH in ultra-pure water for 1 h.

6.2.1.4 Protein Phosphorylation with Attachment of Gold Nanoparticle and Ferrocene

Careful design of the protocol to enable streamlined measurements is made to enable the multimodal approach on-chip. Before the measurements, the MUA/MCH SAM was activated by injecting 1 ml of 40 mg/ml EDC and 10 mg/ml NHS. For protein attachment, 200 µl of 156 µM MBP protein in 10 mM MOPS pH 7.0 (128 mM $MgCl_2$, 641 mM EDTA, 1.134 µg inactive lambda phosphatase, and 0.05% sodium azide) was flown into the cell. Unreacted carboxyl groups were blocked by using 500 µl of 10 mM ethanolamine pH 8.5. Phosphorylation of MBP was carried out in 10 mM Tris base pH 7.4 (6 mM NaCl, and 0.4 mM $MgCl_2$) (hereafter referred to as *reaction buffer*). The whole reaction volume was fixed to 100 µl for all replicates and their controls. 1 µM ATP-S and 4 units of PKC-α (1 unit per 25 µl) were subsequently added into the reaction buffer. To initiate the phosphorylation reaction, 5 µl of PKC lipid activator (1:20 of reaction volume), containing 0.5 mg/ml phosphatidylserine and 0.05 mg/ml diacylglycerol in 20 mM MOPS pH 7.2, 25 mM β-glycerol phosphate, 1 mM sodium orthovanadate, 1 mM dithiothreitol, and 1 mM $CaCl_2$ were added. Control reactions were performed by adding 0.1 µM PKC kinase inhibitor (GF 109203X) to the phosphorylation reaction. Enhancement of signal was performed by adding AuNPs and ferrocene subsequently with a 10 minutes step after the potential reached a stable value in OCP. Thio-ferrocene modification was done by adding 500 µl of 1 mM 6-(Ferrocenyl)hexanethiol dissolved in ethanol and diluted to 1:100 in the reaction buffer.

6.2.2 Discussion on Protein Phosphorylation with Multimodal Sensing Approaches

6.2.2.1 Potentiometric Responses of the System with Open Circuit Potentiometry

6.2.2.1.1 Potentiometric Response of Protein Phosphorylation

OCP was monitored in real time upon thio-phosphorylation of MBP immobilised on the gold surface of the array of four electrodes. Upon protein thio-phosphorylation, a potential change of -30.0 mV was shown on the sample, in comparison to -1.7 mV in the presence of PKC-α kinase inhibitor, illustrated in Figure 6-4.

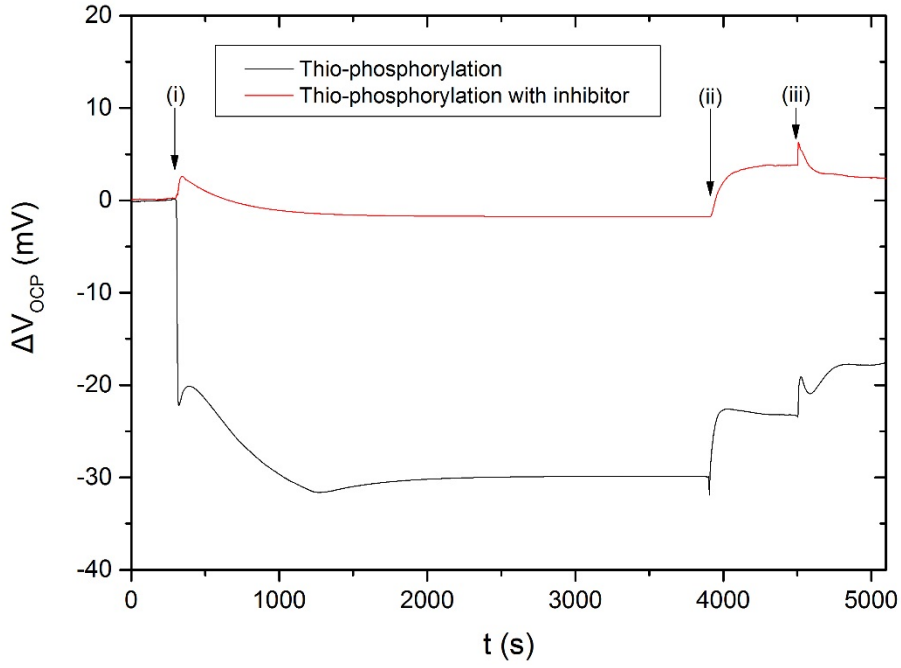

Figure 6-4 Protein phosphorylation with attachment of AuNPs and Fc (OCP). Injection of (i) ATP-S, PKC-α, and PKC lipid activator with PKC-α kinase inhibitor in one sample, (ii) AuNP, (iii) Fc.

The negative shift on the potential indicates the addition of the negatively charged phosphate groups to MBP. By using a flow cell in this experiment, the steady flow rate enhances the chance one protein to be thio-phosphorylated, thus a more rapid drop of potential was seen upon phosphorylation reaction in the early stage and a gradual

decrease rate is observed. Since a flow was used, rinsing followed the reaction and a decrease of potential change by time was observed until reaching a stable potential.

Small peaks of the potential shift were observed during thio-phosphorylation at t = 800 s. This may be due to a lower concentration of activation solution flowing through between two higher concentrations, causing a rinsing effect that affected the kinetics, thus the potential changes. Furthermore, this could be a transition state as the surface was re-organising, and the charges detected are still not in a stable state on the biolayer. The stable potential was reached after t = 2100 s.

6.2.2.1.2 Potentiometric response of Gold Nanoparticles and Ferrocene Attachment

Upon AuNP attachment, potential shifts of +6.8 mV and +5.4 are observed in the thio-phosphorylation and inhibition reactions, respectively. This similar shift is mostly attributed to the changes in buffer conditions upon introducing AuNPs in the flow cell, as the AuNPs are contained in 0.1 mM PBS, which is different to the reaction buffer mentioned above. As the AuNPs that are used in this electrochemical system are uncharged, potential changes here shouldn't be due to charges as in the positive charged AuNPs used for enhancement in the last chapter work. A further confirmation that the positive potential changes upon attachment was due to the buffer effect, which was supported with the LSPR measurements in reflection mode (Bhalla *et al.*, 2015b). The results that were observed confirm that AuNPs is only present in the thio-phosphorylation samples.

Upon addition of thiolated Fc to the system, prominent signal changes were detected. The thio-phosphorylation formed the Fc-crown-like-structure that increased the electrochemical double layer. A further potential shift of +5.3 mV was observed in the case of the thio-phosphorylated samples. However, for the control samples and those with inhibitors, the shift was lower than +1.5 mV. These results observed confirm that only a minimum amount of AuNPs is attached to those samples, since the potential change is much lower and distinguishable from the change of thio-phosphorylated samples. A comparison of signal changes of each modification step and sample are shown in Figure 6-5.

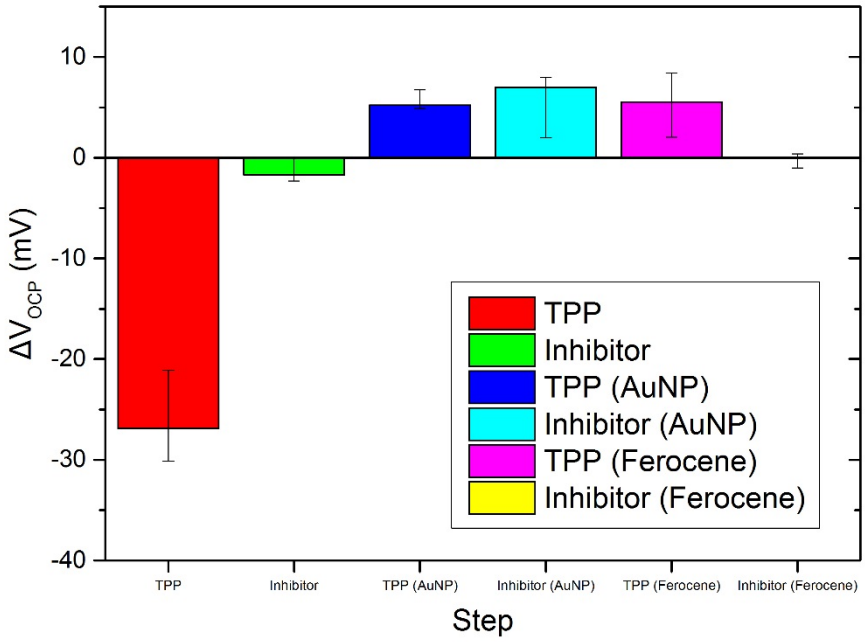

Figure 6-5 Responses from injection of each step (OCP). (i) Red bar represents thio-phosphorylation, (ii) green bar represents thio-phosphorylation with inhibitor, (iii) and (iv) blue bar and light blue bar represent attachment of AuNP to (i) and (ii) respectively, and finally, (v) and (vi) purple bar and yellow bar represent attachment of Fc to (iii) and (iv) respectively. Error bars represents the minimum and maximum changes of OCP detected.

From the design of this electrochemical system, the addition of Fc grafting onto AuNPs was designed to enhance the signal, which can then increase the signal difference for detection. However, the signal response upon attachment of Fc was not high enough to be an enhancement technique in OCP in this multimodal biosensing approach. With an average potential shift of – 26.04 ± 4.53 mV on the protein phosphorylation samples, a clear difference on the potential shift could be seen already with the protein phosphorylation samples when comparing to the samples with inhibitor.

Compared to the last two chapters on DNA-based systems where both systems had an enhancement technique to optimise the signal differences, the results from protein phosphorylation system suggest that not all electrochemical systems have the need for an enhancement technique to obtain a clear result for detection. But when combined with different electrochemical detection techniques on a signal platform for this new

multimodal biosensing approach, a platform here is demonstrated to have the potential of achieving high levels of accuracy, reliability, and validity.

6.2.2.2 Validation of the System with Multimodal Biosensing Techniques

Through the multimodal biosensing approach that was reported in Formisano *et al.* (2015), four different electrochemical measurement techniques (OCP, EIS, DPV and LSPR) were investigated; the results of which are shown in Figure 6-6 from (A) to (D) respectively. The results are illustrated for the comparison of OCP (Figure 6-6A) to the other three detection techniques, which are combined into the system from other authors that have contributed to the publication.

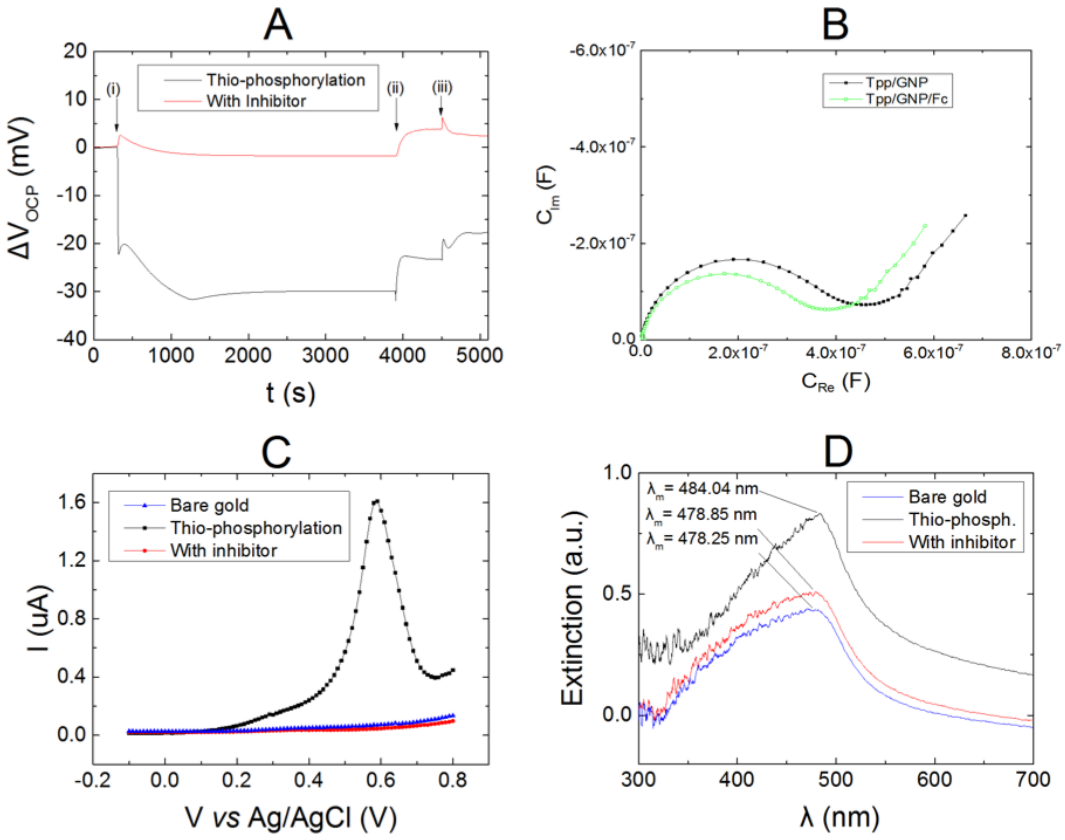

Figure 6-6 Multimodal detection of protein phosphorylation. (A) OCP. (B) Cole-Cole plot by EIS. (C) DPV. (D) LSPR. (Adapted from Formisano et al. (2015)).

The four different electrochemical measurement techniques that have been mentioned are implemented into one platform. A block diagram in Figure 6-7 is used to highlight the system elements and other sensors that have been included in this multimodal sensing system.

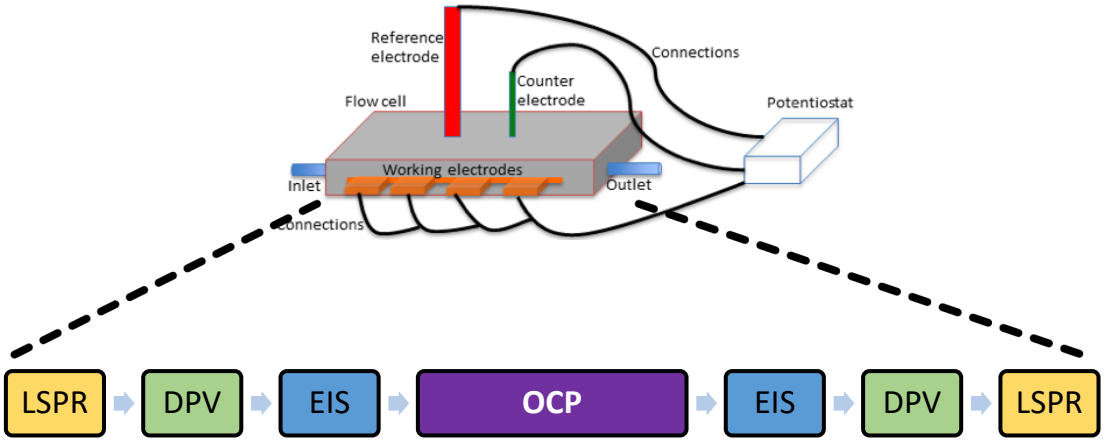

Figure 6-7 Diagram representation of the system elements and sensors of the multimodal sensing system. The flow of the multimodal biosensing approaches is included.

In the following, linkages between the systems will be drawn to validate the results of OCP, and to combine the results to provide a full picture of the electrochemical system, and finally to understand the benefits of using multichannel OCP system with other electrochemical techniques in a multimodal approach.

6.2.2.3 Plasmonic Response of the System with Localised Surface Plasmon Resonance

Measurements were done on the electrodes surface with bare gold, thio-phosphorylated sample, and thio-phosphorylated sample with inhibitor in order to observe the presence of AuNPs. A consistent red shift of 5.8 ± 0.4 nm for thio-phosphorylated sample was recorded, comparing to only 0.9 ± 0.2 nm shift for reactions with the presence of phosphorylation inhibitor in the samples, illustrated in

Figure 6-6D. These results show that the presence of AuNPs are only observed for the thio-phosphorylated samples which are without inhibitor.

By the clear results observed in reflection mode, an explanation could be drawn for the changes of potential observed in OCP upon AuNPs attachment. The main reason for the changes after injection was not because AuNPs attached to both different samples that are with and without inhibitor, but mainly due to the buffer effect when the AuNPs are injected. As AuNPs are contained in 0.1 mM PBS solution, an ionic change of measurement buffer solution from the original reaction buffer with the addition of PBS solution was introduced to the system. This was drawn as a further confirmation of AuNPs attachment, with the OCP results observed.

With the confirmation of AuNPs attachment by LSPR, the final step is to use Fc grafting onto AuNPs for allowing the detection of phosphorylation using EIS and DPV.

6.2.2.4 Impedimetric Response of the System with Electrochemical Impedance Spectroscopy

The use of EIS without the redox couple was mainly used to observe the changes of the electrochemical double layer by measuring the change of capacitance at the frequency 1 Hz due to the relative minimum imaginary part of the capacitance measured at this frequency. Impedimetric data obtained were compared upon the Fc-crowned gold nanoparticle attachment. Both R_l (Z' at 1 Hz) and C_l ($-1/2\pi f Z''$ at 1 Hz) changes were correlated to the presence and absence of kinase inhibitor, as well as where thio-phosphorylation compounds (i.e. kinase, ATP-S and kinase activator) were not used.

Here we show the results from EIS measurements in Figure 6-6B, which is after protein immobilisation but before the OCP measurement, and after the OCP measurement including all modifications, which is after the attachment of Fc. Measurements plotted for the thio-phosphorylated samples before (black dotted lines) and after (green dotted lines) Fc injection are used to observe the changes after the last

modification step on the electrodes. With EIS, the electrochemical double layer can fully explain the condition of the biolayer, this could be used to confirm that the Fc is attached to AuNPs. Further confirming the potential shift in OCP was due to the charge carried by Fc attached to the biolayer. A correlation of results were also made by DPV.

6.2.2.5 Amperometric Response of the system with Differential Pulse Voltammetry

The use of DPV was mainly used to observe the Fc peak in the electrochemical system. The AuNPs that have been attached to the protein phosphorylated samples provided a wide surface accessible for the thiolated ferrocene grafting, thus allowing the use of DPV as a powerful and convincing technique to crosscheck the thio-phosphorylation modification. A peak of 1.31 ± 0.26 μA height (using baseline subtraction) caused by Fc was detected at 0.59 V in Figure 6-6C shown with a black line, while no peak was observed for the both controls, which are the samples on bare gold and the samples on protein phosphorylation with inhibitor shown in blue and red respectively.

6.3 Discussion on Multimodal Biosensing

Designing a multimodal biosensing platform was challenging, especially with OCP monitoring real-time changes in the system. A well-designed measurement protocol with streamlined procedures enabled the proposal of the multimodal approach on-chip. OCP was designed to monitor not only protein phosphorylation, but also ferrocene-crowned nanoparticles modification. As a real-time measurement technique, other electrochemical detection techniques cannot be carried out during the live measurement of OCP. In order to fulfil a multimodal biosensing approach, the other three detection techniques, namely EIS, DPV, and LSPR, were designed to measure prior to and after the OCP measurement. With the automated system controlled by software with injection of solutions to the cell automatically during the real-time measurement, this can prevent unwanted charge or noise to the system that can affect the final measurement result.

Prior to OCP measurement, EIS and DPV were carried out. With EIS to obtain the capacitance of the system, this could be used as a reference to monitor changes of the electrochemical double layer. DPV can also be used to confirm that no unwanted redox molecules are present.

After OCP measurement, EIS, DPV, and at last, LSPR were carried out. By the detection of capacitance of the system with EIS, changes of capacitance due to the combination of protein phosphorylation with the attachment of AuNPs and Fc can be demonstrated. Followed by using DPV to observe the presence of Fc peak, a confirmation can be made by cross-checking the presence of Fc in the system, which is used to validate the thio-phosphorylation event that was achieved. And finally, LSPR is carried out after all the electrochemical detection techniques, which is used to monitor the presence of AuNPs. By detecting the presence of AuNPs in only thio-phosphorylated samples, a confirmation could be made to further validate the multimodal approach on the detection of the protein phosphorylation system.

With all the detection techniques we can observe different kinds of effects due to different modifications on the biolayer. More interestingly, by combining these techniques, not just OCP could be validated as a useful real-time technique, but a further confirmation of the results on the multimodal biosensing system could be achieved.

6.4 Summary

This chapter has presented the detection of protein phosphorylation with multimodal electrochemical and nanoplasmonic sensing approaches. The detection of protein phosphorylation was investigated with OCP and a number of electrochemical and nanoplasmonic biosensing techniques. The use of on-chip multimodal sensing approaches is very promising towards integrated biosensing systems, which measure different parameters involved in biomolecular interactions and provide automated validation of true positives. A proof of concept that enables multiple detection technologies, including OCP, EIS DPV and LSPR, for screening inhibitors of kinase

activity was developed. The original design of the electrochemical system is to have Fc attaches to the AuNPs like a crown for signal enhancement. However, from the results of thio-phosphorylation of MBP, a clear distinction and been seen between different techniques. OCP showed a change of -30.0 mV upon protein thio-phosphorylation in comparison to -1.7 mV in the presence of PKC-α kinase inhibitor. This is due to the addition of the negatively charged phosphate groups to MBP. However, prominent signal changes due to the electrochemical double layer modification were induced in electrodes where thio-phosporylation occurred by means of the Fc-crown-like-structure, benefitting EIS and DPV. By combining multiple sensing techniques on a single platform, the techniques complemented each other and achieved high levels of accuracy and reliability in the measurements.

The multimodal biosensor presented here was successfully implemented as one single biosensing system and investigated using a small array of electrodes in a flow cell with automation. With this approach, it can be used to assay activity of any kinase-protein pair in the presence of known/unknown inhibitors. This opens opportunities to develop an integrated device with multiple sensing technologies, including OCP as demonstrated, for drug discovery applications. It also demonstrated a simple and cost-effective multimodal biosensor system for screening inhibitors of kinase. To further extend the advantages, the hardware platform that has been demonstrated can be easily adapted into other biosensing applications for making other new discoveries.

References

Bhalla, N., Di Lorenzo, M., Pula, G. & Estrela, P. 2015a. Protein phosphorylation detection using dual-mode field-effect devices and nanoplasmonic sensors. *Scientific Reports,* 5.

Bhalla, N., Formisano, N., Miodek, A., Jain, A., Di Lorenzo, M., Pula, G. & Estrela, P. 2015b. Plasmonic ruler on field-effect devices for kinase drug discovery applications. *Biosensors & Bioelectronics,* 71**,** 121-128.

Chirik, P.J. 2010. Group 4 transition metal sandwich complexes: Still fresh after almost 60 years. *Organometallics,* 29**,** 1500-1517.

Cohen, P. 2002. Protein kinases - the major drug targets of the twenty-first century? *Nature Reviews Drug Discovery,* 1**,** 309-315.

Cohen, P. & Alessi, D.R. 2013. Kinase drug discovery - what's next in the field? *Acs Chemical Biology,* 8**,** 96-104.

Formisano, N., Bhalla, N., Wong, L.C.C., Di Lorenzo, M., Pula, G. & Estrela, P. 2015. Multimodal electrochemical and nanoplasmonic biosensors using ferrocene-crowned nanoparticles for kinase drug discovery applications. *Electrochemistry Communications,* 57**,** 70-73.

Laufer, S., Thuma, S., Peifer, C., Greim, C., Herweh, Y., Albrecht, A. & Dehner, F. 2005. An immunosorbent, nonradioactive p38 map kinase assay comparable to standard radioactive liquid-phase assays. *Analytical Biochemistry,* 344**,** 135-137.

Leavene, P.A. & Alsberg, C.L. 1906. The cleavage products of vitellin. *J. Biol. Chem.,* 2 (1)**,** 127-133.

Parang, K. & Sun, G.Q. 2005. Protein kinase inhibitors in drug discovery. *Drug Discovery Handbook***,** 1191-1257.

Roskoski Jr., R. 2015. Usfda approved protein kinase inhibitors.

She, Z., Topping, K., Shamsi, M.H., Wang, N., Chan, N.W.C. & Kraatz, H.B. 2015. Investigation of the utility of complementary electrochemical detection techniques to examine the in vitro affinity of bacterial flagellins for a toll-like receptor 5 biosensor. *Analytical Chemistry,* 87**,** 4218-4224.

ter Haar, E., Walters, W.P., Pazhanisamy, S., Taslimi, P., Pierce, A.C., Bemis, G.W., Salituro, F.G. & Harbeson, S.L. 2004. Kinase chemogenomics: Targeting the human

kinome for target validation and drug discovery. *Mini-Reviews in Medicinal Chemistry,* 4**,** 235-253.

Weinmann, H. & Metternich, R. 2005. Drug discovery process for kinase inhibitors. *Chembiochem,* 6**,** 455-459.

CHAPTER 7.

Conclusions

With the aim of developing a simple yet sensitive multiplexed OCP measurement system for biosensing applications, the work in this thesis serves as a potential orientation for understanding and implementing a true OCP biosensing system for multiple electrochemical systems. The potential use of OCP for biosensing applications is still developing and paving the way to become one of the mainstream electrochemical detection techniques. The simplicity and straightforward measurement of charges of biomolecules on the biolayer has become a big advantage for OCP when comparing to other electrochemical detection techniques. In this thesis, a multiplexed OCP measurement system has been investigated and demonstrated with promising results on multiple electrochemical systems.

By completing and implementing a multiplexed design for the OCP measurement system, the true OCP of multiple biosensing channels can be detected in a simultaneous approach. Such an OCP measurement system using easily accessible off-the-shelf components allows for the production of a low-cost platform for research and diagnostic use, by combining with the correct electrochemical system. In order to develop such a biosensing system for OCP, several areas surrounding the electronic measurement system have been investigated. These include the stability of the system, the design of the multichannel approach, and the ability of the system to perform analytical and selectivity performance studies. Multiplexing, miniaturisation and integration of a full biosensing system have also been achieved with the integration of software control and auto-flow system. To fulfil multiple use cases, DNA-based and protein-based electrochemical systems have been investigated and demonstrated that

OCP has the potential to become a valuable electrochemical detection technique. A case study on PSA was also investigated and demonstrates the applicability and robustness of the OCP measurement system for clinical and diagnostic uses. The studies do not just measure the charge difference on the biolayer upon preliminary binding events, but each of the systems are also attached to an optimisation or enhancement method. Since the strategies to each of the electrochemical systems are different, a number of optimisation or enhancement methods have been used and presented, including the attachment of intercalators, positively charged AuNPs, and non-charged AuNPs with Fc respectively. Using the validation from other electrochemical detection systems, it can be seen that the results obtained from OCP are promising. These wide varieties of electrochemical systems and applications would enable the development of such a biosensing platform for mass-production and give commercial feasibility.

OCP has been widely implemented into standard potentiostats, provided as one of the multiple electrochemical detection techniques in the potentiostat system. However, there are only a limited number of publications about OCP for biosensors development and an even lower number of these are specifically using OCP in a multiplexed environment for biosensing applications. In addition, OCP through standard potentiostats is not measuring the true OCP due to the electronic architecture of the system. Through a standard potentiostat, a small current is applied during the measurement of OCP and this may cause a disruption to the biolayer. The true OCP described in this thesis used an ultra-low input bias current instrumentation amplifier for the measurement, measuring the potential difference between the working electrode and reference electrode without applying any current to the electrochemical system. Although for most electrochemical systems the measurements with standard potentiostats are a good approximation, the true OCP described in this thesis is highly desirable.

The development of multichannel OCP measurement systems with the detection of prostate cancer biomarkers as a case study is presented in Chapter 3. This chapter presented and discussed the investigation of the system stability with simultaneous multichannel measurements in real time. Although optimisation of the measured OCP

was a challenge, the multiple assembly techniques used for the electronic circuitry were able to minimise the noise in the signals and perform an accurate and stable measurement. A full OCP measurement system is presented and discussed in the case study and the investigation of the sensor differentiation ability was performed.

The experimental work in this chapter was published and presented a sensitive label-free, cost-effective OCP system that can be used to develop sensitive aptasensors. The aptasensor developed for PSA using this OCP detection technique demonstrated a 600-fold increased sensitivity with similar aptasensors using EIS. The sensor displayed good selectivity when challenged with stringent control proteins. PSA was used as a case study to show the applicability of the technique and the robustness of the multichannel approach. This strategy can be easily adapted for the detection of a wide range of biomarkers in a multiplexed platform using not only aptamers but also other receptor molecules such as peptides, antibodies and lectins.

The detection of DNA – DNA interaction on gold electrode through EIS and OCP is presented in Chapter 4, with the use of a novel cobalt complex $[Co(GA)_2(aqphen)]Cl$ as a signal enhancer upon its attachment to dsDNA. The use of intrinsic charge carried by the phosphate backbone of DNA was demonstrated. It has been presented how noise in the electronic system and bad signal lines protection can affect the OCP results upon DNA hybridisation, leading to unreadable results. However, the structural change of the dsDNA with the intercalator that causes a significant potential change has been detected with OCP. A confirmation of the results for OCP has been investigated with EIS, which is a promising electrochemical technique. With the existing hardware at this stage, signal protection was shown as the main aspect that needs to be further studied. Upon finishing the study with the detection of DNA – DNA interaction, the next chapter introduced another DNA-based system, the detection of PNA – DNA interaction.

The detection of PNA – DNA interaction on gold electrode through OCP is presented in Chapter 5, with the use of a PEI-capped AuNPs as a signal enhancer upon its attachment to dsDNA. The use of the non-charged PNA shown higher bonding energy and better capability of mismatch discrimination, thus a higher change of potential

upon hybridisation. With the attachment of positively charged AuNPs, a hindering effect was observed and suggested that a rinse-off of excessive AuNPs can enhance the signal. The stirring cell used here is redesigned and replaced by a flow cell in the next electrochemical system. Validation of the OCP results was also studied with impedimetric response of the system, presented with a Nyquist plot (the charge transfer resistance) and a Cole-Cole plot (capacitance).

The detection of protein phosphorylation with multimodal electrochemical and nanoplasmonic sensing approaches is presented in Chapter 6 as the final experiment in this thesis. By comparing with the other electrochemical detection techniques (EIS, DPV) that has been implemented into the single biosensing platform, OCP has shown promising results on protein phosphorylation, without the needs for extra enhancement steps. The accuracy on the single multimodal platform with OCP as one of the detection techniques is demonstrated. This multimodal sensing approaches has fully demonstrated the uniqueness of OCP.

In conclusion, the study of multichannel OCP in biosensing applications and the development of such integrated biosensing systems are part of a highly interdisciplinary field. The investigation relies on distinct aspects such as electronic circuitry design, embedded system design, biosensing probe with respective analyte, biosensor design and fabrication, electrochemical interface, surface chemistry, microfluidics, system control, software programming, analytical techniques, etc. Using OCP and other promising biosensing techniques, several electrochemical systems were studied and paved the path for the development of a multiplexed OCP measurement system. By additional collaboration with colleagues, a simple and cost-effective multimodal biosensor was presented. These studies not only demonstrated the potential of true OCP as a complementary technique for biosensing, but also the potential of multiplexed OCP for a wide range of biosensing applications that exploit charge changes on the biolayer. Furthermore, a simultaneous parallel biosensing approach not only minimises the time and cost of a study, but also enables further analytic performance investigations such as dose response, binding kinetics, etc.

7.1 Future Work

The work presented in this thesis tackled the lack of studies on OCP and has fostered the potential use cases by OCP detection on various other electrochemical systems. In the years ahead, I expect more researches that involve the cooperation of interdisciplinary scholars can be pursued to further the findings of this thesis. The future work includes:

7.1.1 Cancer Biomarkers and Aptasensor

The OCP system showed a very successful result with the aptasensor that was developed for PSA. This development of a sensitive, label-free, cost effective OCP system that can be used to develop sensitive aptasensors, demonstrated a 600-fold increased sensitivity when compared to EIS detection technique. The sensor also displayed good selectivity when challenged with stringent control proteins. By using other cancer biomarkers in the development process, a wide range of sensitive aptasensor can be further developed with the OCP system for the detection of cancer. With this novel approach, the effectiveness of developing new sensitive cancer detection assays can be highly increased.

This strategy can be easily adopted for the detection of other biomarkers in a multiplexed approach, using not only aptamers but also other receptor molecules such as peptides, antibodies and lectins.

7.1.2 miRNA

The OCP detection of PNA/DNA interaction was demonstrated as a stepping stone experiment. With the successful use of PNA for DNA detection, the electrochemical assay was further investigated to detect miRNA by other electrochemical detection techniques in my research group. The detection of miRNA with the same assay demonstrated a limit of detection of 0.37 fM and a wide dynamic range from 1 fM to 100 nM along with clear distinction from mismatched target miRNA sequences. Since miRNAs are involved in the gene regulation of the human body and have been

reported to be linked with numerous diseases, miRNAs have the potential for further investigation in order to obtain information about the state of the progression of a disease. By detecting the expression levels, altered expression of miRNAs can act as the fingerprint and provide substantial amount of information. The research in Chapter 5 prepared the initial findings of the sensitive PNA/DNA duplex detection with OCP detection technique, enabling PNA/miRNA duplex as the future work inside the research group. Further investigation of PNA/miRNA duplex with OCP detection technique along with the development of microarray platforms is desirable.

7.1.3 Semiconductor Design of the OCP Electronic System

The achieved results in this research all lead to practical use cases of the system in future work for OCP biosensing. With the successful design by using off-the-shelf components to assemble the electronics in an efficient and cost-effective way, a miniaturise OCP system should be further investigated. To design a miniaturise OCP system, semiconductor level design is suggested in order to produce a small footprint of the circuit. The miniaturise system can then be implemented with microarrays and a microfluidic platform, and complete with an autonomous processing system.

Appendix

Appendix I. Assembly Techniques for the OCP Electronic Circuitry

In order to maximise the performance of the INA116 for the signal detection, which includes the sensitivity, accuracy and stability, a series of design criteria and assembly techniques are investigated and implemented, including circuit board layout design, circuit input protection, coaxial cable used between the signal source and circuit board, and others, to protect signals and deliver the best OCP results. The methods used are crucial to achieve a low noise electronic system (Ott, 1988) for the biosensing platform.

I.I Circuit Board Signal Routings

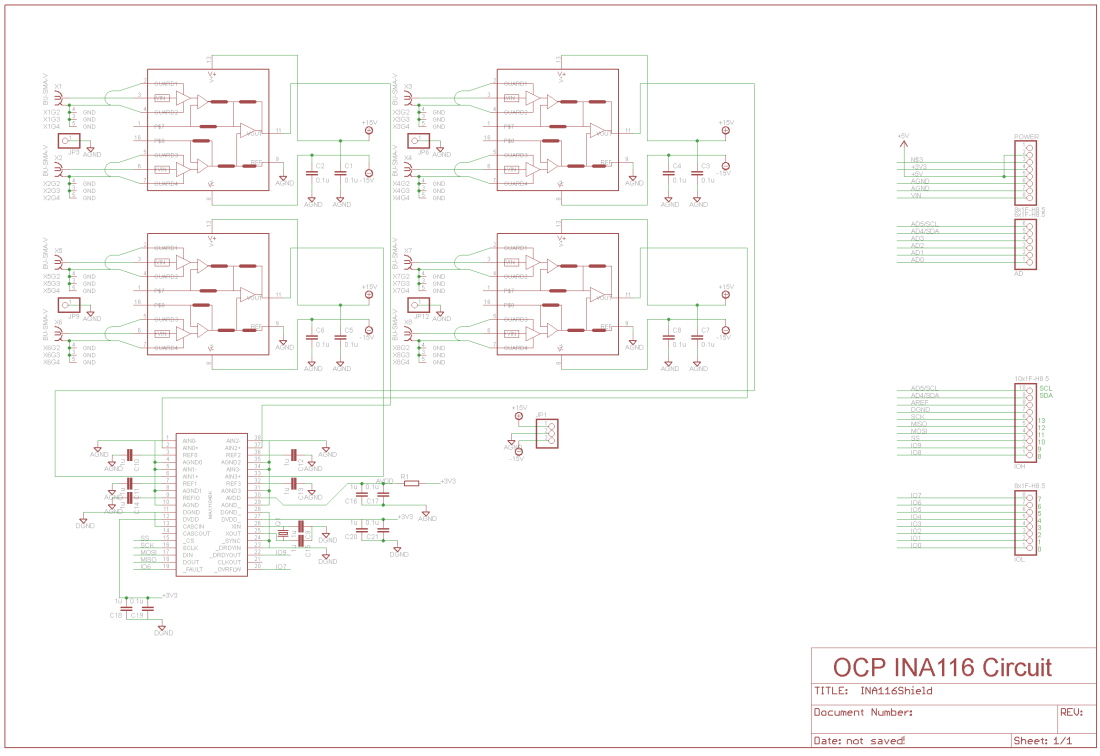

Figure I-1 PCB schematic layout including four INA116 instrumentation amplifier and a MAX11040K analog-to-digital converter.

A printed circuit board (PCB) was designed and printed through an in-house printing unit. The PCB schematic layout, illustrated in Figure I-1 (see Appendix IV for a large-scale schematic).

The PCB schematic layout including four INA116 instrumentation amplifier and a MAX11040K analog-to-digital converter. According to the components used, a well-thought PCB design layout of the INA116 circuit was printed by a LPKF PCB prototyping machine. This is printed and processed according to the instrumentation amplifiers guideline (Burr-Brown, 1995) in order to assemble a high sensitivity circuit. To prevent noise from both positive and negative power lines, both of them are routed from the top and bottom layer of the PCB layout respectively as seen in Figure I-2.

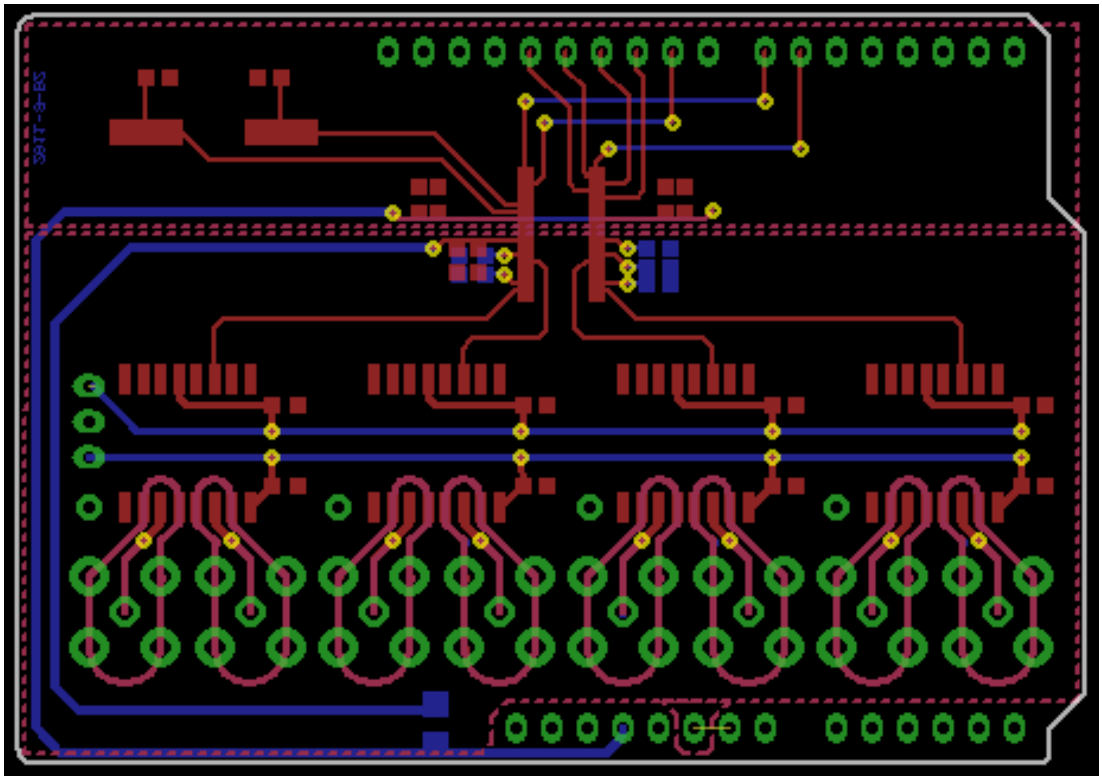

Figure I-2 PCB routing including 4 INA116 instrumentation amplifier (centre) and MAX11040K analog-to-digital converter (top centre). (Red represents top layer, blue represents bottom layer, black represents ground plane)

On the top layer, analog signals and digital signals are separated by the MAX11040K into two main areas. The empty spaces (blackout area) are then covered with ground planes to further improve the separation of the signals, with separate ground planes for both analog and digital areas. SMA connectors made with brass/gold materials are used. The SMA connector used for coaxial cable has a minimal connector interface, which should provide a good protection for the signal from the electrodes to the input of INA116 instrumentation amplifiers.

I.II Circuit Input Protection

To achieve the exceptionally low input bias current performance of the INA116 instrumentation amplifier, a careful circuit board layout and assembly techniques are needed in order to build the circuit on a PCB. On the INA116, terminals 2, 4, 5 and 7 that are adjacent to the input pins 3 and 6 provided a guarding path for the top and the bottom of the input pins, illustrated in Figure I-3. Both sides of the circuit board have been guarded even when only one side has input terminal conductor. All the time varying signals have been routed away from all the input terminal conductor to prevent cross-talk, and all solder masks have not covered the guard traces to prevent increase of leakage and noise on the original signals, which have been described in the previous sub-chapter I.I Circuit Board Signal Routings.

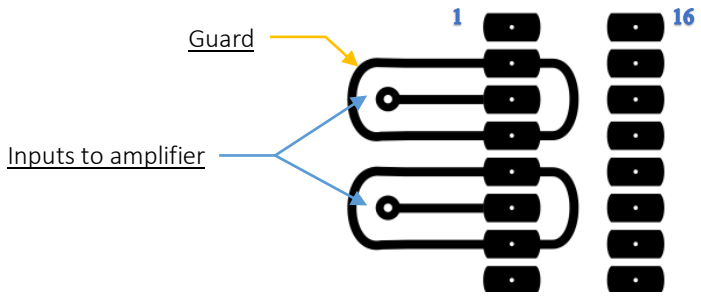

Figure I-3 Suggestion of circuit board guard layout by manufacturer. (Adapted from Burr-Brown (1995))

Through the investigation of input protection methods, the circuit board guard layout suggested by Burr-Brown INA116 data sheet (Burr-Brown, 1995) was amended to fit the SMA connector components that have been used and implemented to achieve the performance of the low input bias current. The amended circuit guard layout is illustrated through the PCB routing in Figure I-2.

To increase the accuracy, low leakage current assembly method is used by bending the input pins outwards and soldering the input connections directly together. This assembly method is used to avoid any contacts with the circuit board, which could induce noise to the amplifier from the circuit rails. The technique is more useful when compared with other wiring techniques as this can prevent the most leakage that can affect the performance of the amplifier. However, this is not a practical method for the production period, as a solid mechanical assembly method is required to gain a good result in production.

Placing a Faraday shield around the amplifier and input connection assembly is highly recommended to eliminate stray fields and keeping plastic away to prevent static charges due to any motion or vibration on the system. Being extremely careful with static charges is needed, as charges may lead to continuous shift in the measurement, resulting in incorrect data.

I.III Transmission Lines - Coaxial Inputs

To provide protected conducting paths as the transmission lines for the signals between the electrodes of the biosensor system and the PCB input connections, coaxial cables are used in the system. The whole conducting pathway is designed to be a Faraday shielded pathway, which the protection is extended from the circuit board guard layout to the electrode. Figure I-4 shows an illustration of the coaxial cable structure.

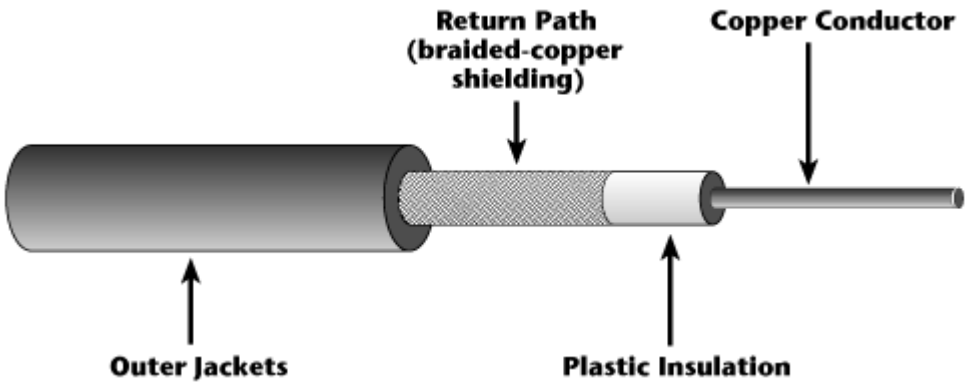

Figure I-4 Illustration of a coaxial cable.

The copper conductor in the centre is surrounded by plastic insulation, which helps filter out extraneous interference. The plastic insulation is covered by the return path, which is usually braided-copper shielding. Outer jackets form a protective covering for the whole coaxial cable structure.

As the OCP biosensing application is a type of high impedance input connection; the input should be guarded all the way to the signal source, i.e. the electrode. The guarding of the pathway ensures there is low leakage from the whole system. As the signal from the electrochemical system is a slow (low frequencies) input signal, the internal guard output of the INA116 instrumentation amplifier can drive the cable shield directly, providing necessary and adequate protection for the signalling path. This guard drive output current of the INA116 is limited to approximately +2 mA / – 50 μA.

Signal processing is a key part of the biosensor detecting circuitry. A proper design from electronic circuit to the overall system is especially important when signals are small and electronic noise can be higher than the detected signal from the biosensor (Spieler, 2003a; Spieler, 2003b). A well-handled analog signal would be an advantage for the following conversion steps in the system.

References

Burr-Brown 1995. Ultra low input bias current instrumentation amplifier. *INA116 datasheet.* Burr-Brown.

Ott, H.W. 1988. *Noise reduction techniques in electronic systems,* New York: Wiley.

Spieler, H. 2003a. Analog and digital electronics for detectors. *In:* ICFA Instrumentation School, 8-19 Dec 2003, Itacuruca, Rio de Janeiro, Brazil. 1-43.

Spieler, H. 2003b. Front-end electronics and signal processing. *Instrumentation in Elementary Particle Physics,* 674**,** 76-100.

Appendix II. Data for Figure 5-4

Table II-1 Data for Figure 5-4

Concentration	PNA/DNA + AuNPs			PNA/DNA
	ΔV_{OCP} (V)	yEr (V)	yEr (V)	ΔV_{OCP} (V)
blank	0.00634	--	--	0.00000
1 nM	0.01055	6.02E-04	-9.73E-04	-0.00147
10 nM	0.01106	1.23E-03	-2.21E-03	-0.00216
100 nM	0.01349	1.54E-03	-2.35E-03	-0.00310
1 µM	0.01993	1.93E-03	-4.77E-03	-0.00403

Appendix III. Data for Figure 6-5

Table III-1 Data for Figure 6-5

Step	ΔV_{OCP} (mV)	yEr (mV)	yEr (mV)
TPP	-26.88	5.79	-3.27
Inhibitor	-1.70	1.70	-0.60
TPP (AuNP)	5.23	1.53	-0.33
Inhibitor (AuNP)	7.00	1.00	-5.00
TPP (Ferocene)	5.55	2.83	-3.53
Inhibitor (Ferocene)	0.00	0.40	-1.00